PHOTOINDUCED NON-EQUILIBRIUM PHASE TRANSITIONS IN CUPRATE SUPERCONDUCTORS

Ivan Madan

Doctoral Dissertation
Jožef Stefan International Postgraduate School
Ljubljana, Slovenia

Supervisor: Prof. Dr. Dragan Mihailović, Jožef Stefan Institute, Ljubljana, Slovenia

Evaluation Board:
Asst. Prof. Tomaž Mertelj, Chair, Jožef Stefan Institute, Ljubljana, Slovenia
Prof. Dr. Viktor Kabanov, Member, Jožef Stefan Institute, Ljubljana, Slovenia
Prof. Dr. Steven Johnson, Member, ETH, Zürich, Switzerland

MEDNARODNA PODIPLOMSKA ŠOLA JOŽEFA STEFANA
JOŽEF STEFAN INTERNATIONAL POSTGRADUATE SCHOOL



Ivan Madan

PHOTOINDUCED NON-EQUILIBRIUM PHASE TRANSITIONS IN CUPRATE SUPERCONDUCTORS

Doctoral Dissertation

FOTOINDUCIRANI NERAVNOVESNI FAZNI PREHODI V KUPRATNIH SUPERPREVODNIKIH

Doktorska disertacija

Supervisor: Prof. Dr. Dragan Mihailović

Ljubljana, Slovenia, August 2015

Acknowledgments

First I would like to thank my supervisor professor Dragan Mihailović for providing me the opportunity to join his group and for his patient guidance and valuable ideas. I thank Tomaž Mertelj for introducing me to the lab and for involved discussions of the experimental results. I would also like to thank Viktor Kabanov for providing me deeper and clearer insight into the theoretical concepts. I thank the students with whom I was lucky to work with - Jure Novak, Jan Gospodarič and Alfredas Kiudys. Special thanks goes to everyone in the Department for Complex Matter for their help and support as well as a good mood along these years. My sincere thanks goes to my brother for reading the first draft. I express my endless gratitude to Anna who has always supported me on the way. I acknowledge the Javni Sklad Republike Slovenije za Razvoj Kadrov in Štipendije for covering the school and living costs (scholarship number 11011-21/2011) as well as the department for Complex Matter for hosting me and creating the perfect working conditions in social and scientific regards.

Abstract

This thesis is dedicated to the study of non-equilibrium phase transition occurring in the cuprate superconductors. Since the characteristic time-scale of elementary processes involved in the transitions is in the femtosecond range, the main measuring technique employed is the ultrafast femtosecond optical spectroscopy. Most of the results presented here involve application of the novel 3 pulse technique, specially developed for the study of non-equilibrium phase transitions. In this technique the first strong pulse destroys the ordered state, the second pump pulse serves as a small perturbation of the transient state which is reflected in the change of the optical constants probed by the third pulse.

There are two ordered phases of interest in the cuprates - the pseudogap and the superconducting state. Starting from the previous results that both of them can be destroyed by an ultrashort laser pulse we study the process of destruction in more detail. The major part of the thesis is dedicated to the study of the recovery of these states supported by numerical modeling within time-dependent Ginzburg Landau (TDGL) framework. In particular we firmly establish the non-equilibrium nature of the transition, i.e. that the transition is defined by the evolution of the order parameter in the formed potential landscape rather than the dynamics of the equilibrium order parameter which is defined by the evolution of the potential landscape (quasi-equilibrium case). We establish the importance of fluctuations as they provide the seed for the order parameter growth and show possibility of a description of the non-equilibrium phase transition with the TDGL theory.

Separately we present the first attempt to experimentally detect the response due to the superconducting fluctuations in pump-probe measurements far above T_c. The comparison of the optical response with the THz conductivity measurements previously reported in literature uncovered a difference in the critical behaviour of the phase and amplitude of the order parameter, and consequently a different microscopic nature of the relaxation for these physical quantities. Fits of the critical behavior revealed that the phase relaxation is governed by dynamical critical exponents predicted by Gaussian description of fluctuations, whereas the amplitude relaxation exhibits a shallower power law behavior.

Three pulse experiments conducted in the pseudogap region far above T_c have revealed the short range nature of the pseudogap state and individual character of the state formation. Experimental examination of the pseudogap destruction energy shows linear dependence on doping and no dependence on temperature. This can be explained when energy losses to subgap phonons are considered.

Povzetek

Doktorsko delo obravnava neravnovesne fazne prehode v kupratnih superprevodnikih. Tipični karakteristični čas urejanja elektronov je nekaj femtosekund, zato za opazovanje pojavov uporabljamo femtosekundno optično spektroskopijo. Večino rezultatov smo pridobili z uporabo nove trisunkovne tehnike, namenjene preučevanju neravnovesnih prehodov. Pri eksperimentu s prvim močnim sunkom uničimo urejeno stanje in z drugim šibko vzbudimo nastajajoče stanje. Tretji sunek, ki ga zajamemo, meri spremembo optičnih konstant.

V doktorskem delu raziskujemo dve urejeni stanji v kupratih - stanje psevdoreže in superprevodno stanje. Predstavimo sistematične meritve uničenja stanja psevdoreže in superprevodnega stanja. V glavnem delu doktorata obravnavamo raziskave pojavov obeh stanj ter numerično modeliranje z neravnovesno teorijo Ginzburg-Landaua (NTGL). Še posebej izpostavimo neravnovesno naravo prehoda. Prehod torej ni določen kot evolucija ravnovesnega parametra reda, ki je definiran s časovno odvisnim potencialom (kvazi-ravnovesje), temveč z evolucijo parametra reda v nastalem potencialu. Ugotovili smo, da so fluktuacije izredno pomembne, saj služijo kot izvor rasti parametra reda. Pokazali smo možnost opisa prehoda z NTGL.

Predstavljamo tudi prvo eksperimentalno ločitev odziva superprevodnih fluktuacij nad kritično temperaturo v pump-probe eksperimentih. Primerjava z objavljenimi THz podatki pokaže, da imata relaksacija amplitude in faze različno kritično vedenje, kar je dokaz za obstoj različnih mikroskopskih mehanizmov relaksacije.

Trisunkovne meritve v stanju psevdoreže so pokazale kratek korelacijski doseg dinamičnega stanja in individualne značilnosti relaksacije kvazidelcev. Energija, potrebna za netermalno uničenje psevdoreže, je linearno odvisna od širine reže. To pojasnimo z upoštevanjem generacije fononov z energijo, manjšo od psevdoreže.

Contents

List of Figures **xiii**

List of Tables **xv**

Abbreviations **xvii**

1 Introduction **1**
1.1 Physical Properties of Cuprate Superconductors 2
1.1.1 Structural properties and charge ordering 2
1.1.2 Electronic properties and phase diagram 3
1.1.3 Microscopical models of high temperature superconductivity . . 6
1.2 Dynamic Properties of High-T_c Materials 7
1.2.1 Characteristic features of the pump-probe response in different phases 7
1.2.2 Relaxation in the metallic state 8
1.2.3 Quasiparticle relaxation in the gapped systems: bottleneck model 10
1.2.4 Fluence dependence of the pump-probe response 13
1.3 Non-Equilibrium Symmetry Breaking Transitions 14
1.3.1 Landau theory of phase transitions. Ginzburg-Landau theory . 14
1.3.2 The time-dependent Ginzburg-Landau theory 16
1.3.3 Dynamics through the phase transition - Kibble-Zurek description 17

2 Experimental Details and Methods **19**
2.1 Femtosecond Time-Resolved Optical Spectroscopy 19
2.2 Description of the Detection Scheme and Lock-In Detection 21
2.3 The 3 Pulse Experiment: Signal Simulation and Data Analysis 22
2.4 Description of the Ultrafast Response in Terms of Raman Susceptibilities and Polarization Selective Detection 26
2.5 Fitting procedure 29
2.6 Samples 30

3 Pseudogap State Response, Photodestruction and Recovery **33**
3.1 Pseudogap: General Overview 33
3.2 Pump-probe Response in BSCCO: Temperature and Polarization Study 36
3.3 Photodestruction of the Pseudogap State 42
3.4 Recovery of the Pseudogap State 44
3.4.1 Comments and remarks 47
3.5 Polaronic Interpretation of the Long-Lived Response 48
3.5.1 Evidence for multi-scale behavior from near-IR pump-probe experiments 49

4 Normal-to-Superconducting Phase Transition **53**
4.1 Response Function 53
4.2 Destruction of the Superconducting Condensate in LSCO and BSCCO 54
4.3 Recovery of the Superconducting Condensate in LSCO 57
4.3.1 Experimental 57
4.3.2 TDGL modeling 59
4.4 Recovery of the Superconducting Condensate in BSCCO 64
4.5 Criticism 69

5 Superconducting Fluctuations **73**
5.1 Superconducting Fluctuations: General Overview 73
5.2 Observation of Superconducting Response above T_c by Three Pulse Technique 76
5.2.1 Results 77
5.2.2 Discussion 80

6 Pump-probe Characterization of $HgBa_2CuO_{4+\delta}$ **83**

7 Conclusions and Outlook **89**

Appendix A Material Constants **91**

References **93**

Bibliography **113**

List of Figures

Figure 1.1: Crystal structure of LSCO-214 (a) and BSCCO-2212 (b) crystals 3
Figure 1.2: Schematic phase diagram of the cuprate superconductors 5
Figure 1.3: Fermi surface of the cuprates 6
Figure 1.4: Temperature dependence of the pump-probe response for UD BSCCO sample. 8
Figure 1.5: Temperature dependence of the superconducting and pseudogap components 12
Figure 1.6: Temperature dependence of the relaxation time of the superconducting and pseudogap components. 13
Figure 1.7: Schematic representation of topological defects formation in the course of a non-equilibrium phase transition 18

Figure 2.1: A schematic of the pump-probe setup 20
Figure 2.2: Lock-in detection principle 21
Figure 2.3: A schematic of the three-pulse pump-probe experiment with the sequence of pulses and notation of delays. 23
Figure 2.4: Pump-induced transient reflectivity in a three pulse experiment . 24
Figure 2.5: Simulation of the pump-probe response in the 3 pulse experiments 25
Figure 2.6: Comparison of different approaches to the data analysis. 26
Figure 2.7: Spectral shape of the response in the cuprates 27
Figure 2.8: Description of the balanced detection scheme 28
Figure 2.9: SEM image of the BSCCO surface 30

Figure 3.1: Pseudogap and superconducting energy scales for a number of cuprates 34
Figure 3.2: Schematic weighting of the RS transition 35
Figure 3.3: ARPES data on superconducting gap and pseudogap 36
Figure 3.4: Schematic representation of the two possible mechanisms of quasiparticle excitation 37
Figure 3.5: Probe polarization dependence for different pump polarizations . 37
Figure 3.6: The probe-polarization dependence under 400 nm excitation . . . 38
Figure 3.7: The probe-polarization dependence under 800 nm excitation . . . 39
Figure 3.8: Temperature dependence of the non-symmetric components . . . 40
Figure 3.9: Temperature dependence of the amplitudes of the non-symmetric components 41
Figure 3.10: Pseudogap response as a function of fluence 43
Figure 3.11: Typical result of the three pulse experiment 44
Figure 3.12: Evolution of the pseudogap resonse amplitude and the QP relaxation time 45

Figure 3.13: Recovery of the PG state after destruction by a laser pulse as a function of fluence at different temperatures 46
Figure 3.14: Mid-IR polaronic feature in photoinduced conductivity 48
Figure 3.15: Polaronic Mid-IR features in transient reflectivity response 49
Figure 3.16: Comparison of the sub-ps and nanosecond transient responses . . 50

Figure 4.1: The response function 54
Figure 4.2: The superconducting condensate photodestruction in LSCO . . . 55
Figure 4.3: Superconducting condensate photodestruction in BSCCO 56
Figure 4.4: Recovery of the superconducting response in LSCO 58
Figure 4.5: The results of the simulation by the two-temperature model . . . 60
Figure 4.6: Dependence of the TDGL equations solution on τ_{GL} 61
Figure 4.7: Results of the numerical simulation of the TDGL equations . . . 62
Figure 4.8: Initial conditions used with TDGL equation 63
Figure 4.9: Recovery of the superconducting response in BSCCO 64
Figure 4.10: Evolution of the superconducting component in BSCCO 65
Figure 4.11: A typical result of the balanced 3 pulse experiment 66
Figure 4.12: Evolution of the superconducting component from balanced experiment 67
Figure 4.13: Recovery time of the superconducting component 68
Figure 4.14: Evolution of the quasiparticle relaxation rate and amplitude of the superconducting component measured in balanced experiment 69
Figure 4.15: The response function with BCS gap dependence 70

Figure 5.1: The specific heat of the representatives for different classes of superconductors 74
Figure 5.2: Description of the 3 pulse method and pump-probe signals. 78
Figure 5.3: Comparison of pairing amplitude and phase coherence dynamics . 79
Figure 5.4: Dynamical critical behavior for different doping levels 80

Figure 6.1: Temperature dependence of the pump probe response in HBCO . 83
Figure 6.2: The amplitude and relaxation time of the superconducting component for the UD and OP HBCO samples. 84
Figure 6.3: Probe polarization dependence of the pseudogap and superconducting responses 85
Figure 6.4: Fluence dependence of the pseudogap and superconducting responses 86
Figure 6.5: Evolution of the transient reflectivity response in HBCO 87

List of Tables

Table 2.1: Samples under investigation and their critical temperatures. 30

Table A.1: Material specific constants of the samples under investigation. . . . 92

Abbreviations

2D	two-dimensional
3D	three-dimensional
AF	antiferromagnetic
AOM	acousto-optic modulator
ARPES	angle-resolved photoemission spectroscopy
BBO	beta barium borate
BCS	Bardeen-Cooper-Schrieffer
BEC	Bose-Einstein-Condensate
Bi2212	$Bi_2Sr_2CaCu_2O_{8+\delta}$
BKT	Berezinski-Kosterlitz-Thouless
BSCCO	$Bi_2Sr_2CaCu_2O_{8+\delta}$
CDW	charge density wave
DE	dissipative excitation
FS	Fermi surface
GL	Ginzburg-Landau
HBCO	$HgBa_2CuO_{4+\delta}$
HFP	high frequency phonon
Hg1201	$HgBa_2CuO_{4+\delta}$
IE	impulsive excitation
IR	infra-red
JDOS	joint density of states
KZ	Kibble-Zurek
LCO	La_2CuO_4
LSCO	$La_{2-x}Sr_xCuO_4$
LTT	low temperature tetragonal
MF	mean field
NMR	nuclear magnetic resonance
OD	over-doped
OP	optimally-doped
OPA	Optical Parametric Amplifier
PG	pseudogap
PIA	photoinduced absorption
QP	quasiparticle
RS	Raman spectroscopy
RT	Rothwarf-Taylor
RVB	resonating valence bond
SDW	spin density wave
SQUID	superconductive quantum interference device
SRS	stimulated Raman scattering

STS	scanning tunneling spectroscopy
TDGL	time-dependent Ginzburg-Landau
Tl2201	$Tl_2Ba_2CuO_{6+\delta}$
TTM	two-temperature model
UD	under-doped
Y123	$YBa_2Cu_3O_{7-x}$
YBCO	$YBa_2Cu_3O_{7-x}$ or $YBa_2Cu_4O_y$

Chapter 1

Introduction

The cuprate superconductors attracted grand attention ever since their discovery in 1986[1]. A substantial effort[2] had been put into revealing the microscopic mechanism of the superconductivity as well as understanding normal state properties. The latter, which are rather different from the normal metals, are quite similar across all cuprate families. Most of the unsolved problems of the physics of the cuprates were formulated in the first several years after the discovery. Only with accumulation of reliable experimental data the fog has slowly began to lift. Here we will post some of these problems, with more detailed explanation given further in this chapter: - what is the nature of the pseudogap state, how is it related to superconductivity and charge and spin orders observed in some experiments? - what is the "pairing glue" in the cuprate superconductors and particularly is it dominated by spin fluctuations or phonons, or is the "glue" itself an inappropriate concept? - what is the symmetry of the order parameter, and particularly is it the same for electron and hole doped samples? - are there a quantum critical points under the superconducting dome? - is there a Fermi surface reconstruction and how is it related to emergent phenomena? From all these questions only the d-wave symmetry of the order parameter is more or less settled and even in this topic discussion is not over. Other problems have their supporters and opponents. Though we will go along these questions and discuss our results in the context of the mentioned problems, the central issue considered in this thesis - the physics of non-equilibrium phase transitions - is more general than the physics of cuprates. However, in our experiments it is inseparable from the discussion on the physics of superconductivity in cuprates. In this section we will provide a general introduction into the related aspects of physical properties of the cuprate superconductors followed by a description of the Ginzburg-Landau approach. This approach will be used as a basic model for the description of the non-equilibrium phase transition following early works by Kibble and Zurek[3]–[5].

The amount of experimental data available for cuprate high-T_c superconductors is vast.[6]–[15] The quality of experimental data is improving in the course of time due to both, an improved samples quality and development of new techniques, which has been advanced also mainly due to problems formulated within the field. One of such techniques is the time-resolved optical spectroscopy, which being an independent experimental tool, nowadays gives birth to ultrafast extension of the classical techniques: X-ray and electron diffraction, near field and electron microscopies, angle-resolved photoemission spectroscopy. The all-optical technique remains the most sensitive tool, with a wide range of control parameters: the temperature of a sample, polarization, fluence and wavelengths of the excitation and the probing

beams. A more detailed description of the technique will be given in 2.

1.1 Physical Properties of Cuprate Superconductors

A proper description of the superconducting properties in the cuprates has to be accompanied by a discussion of structural, magnetic and normal state electronic properties due to their intimate relationship. Where applicable we will try to draw the parallels between the properties of the cuprates and other known classes of unconventional superconductors, with particular focus on the trendy pnictide superconductors. The following discussion should be considered as introductory and its goal is to facilitate the entrance into the field rather than give a complete overview of the problem, for the deeper overview we refer the reader to recent books[16], [17] and review articles [2], [9], [13], [18]–[20].

1.1.1 Structural properties and charge ordering

All cuprates are layered perovskite-like materials, meaning that all contain one (like $La_{2-x}Sr_xCuO_4$ (LSCO)see Fig. 1.1) or several [two in the case of $Bi_2Sr_2CaCu_2O_{8+\delta}$ (BSCCO)] perovskite-like CuO_2 planes separated by charge reservoirs layers. In the multilayer compounds the CuO_2 planes are separated by a cation layer, and are electronically strongly coupled whereas the neighboring groups of CuO_2 planes are separated by oxides of typically rare-earth or heavy metal ions. The chemical doping happens in this charge reservoir layers and can be realized either by a substitution of the trivalent ions with divalent ones, as in the case of LSCO, or by an introduction of oxygen as in the case of BSCCO. These two examples are very representative doping options though do not cover all the possibilities. A Cu atom in the CuO_2 plane can be either in a four-(in plane), five-(pyramid) or six-(octahedron) fold coordination due to a variety of possible different crystal structures. Most of the cuprates have tetragonal crystal structure at high temperatures with a structural transition to the orthorhombic structure at temperatures reasonably above the superconducting temperature[17]. Some of the members of La-based compounds also exhibit an orthorhombic to low temperature tetragonal (LTT) transition with a larger unit cell. Hg-based compounds do not have an orthorhombic distortion which is believed to be a reason for their record high critical temperatures.

Presence of the aforementioned low temperature tetragonal phase in $La_{2-x}Ba_xCuO_4$ seems to be of extreme importance for stabilization of the unique form of a charge and spin modulation referred to as *stripes*[9], [21], [22]. The stripe order is a phase separated state where holes condense into one dimensional[1] metallic stripes of a single site width separated by antiferromagnetic (AF) hole poor regions 3-site wide. This state seems to compete with superconductivity and is the reason for the so-called *1/8 anomaly* - suppression of the critical temperature at holes concentration equal to 1/8 holes per Cu doping (i.e. 1 hole per stripe charge period, doping level required for maximum stripe stability). Similar although much weaker suppression is observed in YBCO (the SC region shown in Fig. 1.2) that does not have an LTT phase, suggesting that charge order might be universal. The reconstruction of the Fermi surface (described below) deduced from quantum oscillations experiments in YBCO[23] and HBCO[24] cuprates was suggested to be caused by the presence of

[1] when 2D copper-oxygen planes are discussed

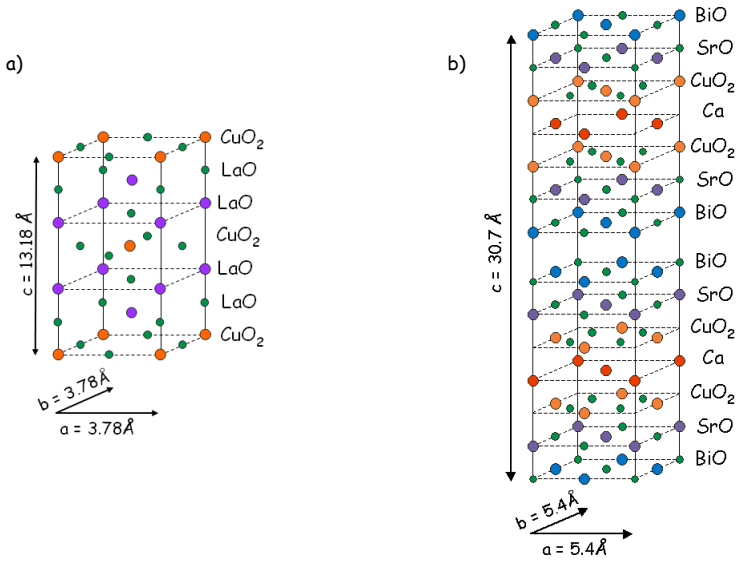


Figure 1.1: Crystal structure of LSCO-214 (a) and BSCCO-2212 (b) crystals. Note the cleaving plane that lies between two Bi-O layers. Pictures are adopted from http://hoffman.physics.harvard.edu/.

the fluctuating charge order. Recent developments in hard X-ray scattering and resonant techniques allowed to show that the fluctuating short-range charge order is a universal feature that happens in all cuprate families[25], [26]. This is however different from the static stripes picture, as the 2-fold ratio between magnetic and charge modulation wavevectors is not preserved as well as wavevector doping dependence has opposite trend. In BSCCO, which we mostly concentrate on, most recent results suggest that this short-range order is related to the pseudogap phase[26], described in Chapter 3.

Apart from the charge modulation in the Cu-O planes other charge-density waves were observed in Bi-O and Cu-O chains in the case of BSCCO[27] and YBCO[28] correspondingly. These have smaller influence on superconducting properties but can complicate a data analysis. Though in principle in BSCCO these modulations can be suppressed by Pb or Y doping, our samples are pristine and we analyze our data taking the presence of charge density modulation into account.

1.1.2 Electronic properties and phase diagram

In this subsection we discuss the phase diagram of the cuprates and describe the underlying electronic structure in different phases.

Let us start from parent undoped compounds. Electronic bands of the cuprate superconductors originate from energetically close $3d^9$ levels of Cu^{2+} and $2p^6$ levels of O^{2-} ions. In an octahedral crystal field these split into an e_g doublet and a t_g triplet for Cu^{2+}, with further Jahn-Teller splitting which gives a high energy half occupied $b_{1g}\{d(x^2-y^2)\}$ orbital (x and y are in-plane directed along Cu-O bond). This orbital is responsible for formation of σ-bonding with the oxygen $p(x)$ and $p(y)$ orbitals, resulting in a deep lying occupied bonding and half-occupied antibonding $pd\sigma$-bands. The latter define the electronic properties of the cuprates that we are interested in. As a half-filled band it should be metallic, however, the electronic

correlations (on-site Coulomb repulsion) in the cuprates are very strong ($U = 8 - 10$ eV) and are significantly higher than the bandwidth ($W \sim$ 3 eV) resulting in an insulating Mott state.[17] The presence of two distinct kinds of ions in the cuprate plane make these materials different from the model Mott-Hubbard insulator. In the Hubbard model the lowest possible excitation energy would correspond to the transition to the upper Hubbard band and is defined by U whereas in the cuprates the charge transfer transition from the copper to the oxygen atom has a significantly lower energy of the order of 2 eV. The material still remains insulating and due to the superexchange it exhibits antiferromagnetic spin ordering. It should be stressed that electronic properties are highly two-dimensional both due to the structural anisotropy and two-dimensionality of the orbitals involved in the formation of $pd\sigma$ band.

The superconductivity in these compounds appears upon doping above the threshold of around 0.05 holes/Cu, where the insulator-to-metal Mott transition occurs (see Fig. 1.2). Superconductivity appears upon cooling from an anomalous metallic state that has the following peculiar properties. Even though the temperature dependence of the in-plane conductivity has the metallic response, the resistivity is linear with temperature contrary to the expected T^2 behavior in Fermi-liquid theory at low temperatures. Search for an explanation of this behaviour resulted in various theories, most prominent of them are the quantum critical point theory[29], where excitations of both close ground states of different symmetries define the properties at nonzero temperatures, and the unusual Fermi-liquid theories (see for example [30])[2]. Moreover the system exhibits a so-called pseudogap, the suppression in the density of states at the Fermi energy. It gradually appears below a certain temperature denoted as T^* that linearly decreases with increasing doping (Fig. 1.2). To the best of our knowledge there is no thermodynamic evidence for a phase transition into the pseudogap phase (so the notation "phase" itself is not strictly applicable, but commonly used) though the time-reversal, rotational, and particle-hole symmetries breaking below T^* have been reported [31]–[36]. Most illustratively the pseudogap is seen in Angle-resolved photoemission spectroscopy (ARPES) measurements[7], but also the in nuclear magnetic resonance (NMR) where it was observed for the first time[37] indicating that it is also a spin gap, and other techniques such as the optical conductivity[12], Raman, tunneling[14] and pump-probe spectroscopy[38].

It is instructive to explore the Fermi-surface evolution across the phase diagram. In Fig. 1.3 the antiferromagnetic zone boundary is shown by the gray line. As the transition to metal occurs the density of states at the Fermi level becomes nonzero. In the underdoped region below T^* however states appear (or, more precisely, are observed) only on the Fermi arcs marked by the dark dashed lines. Above T^* the Fermi surface measured by ARPES is continuous and closed.[31] Edges of the Fermi arcs, so-called hot spots, are rigorous with T down to the onset of the superconducting fluctuations. For a while it was believed that the position of the hot spots is defined by the crossing of the Fermi surface (FS) with the AF zone boundary - as electrons with the AF wavevector are subjected to strong scattering which leads to the opening of the gap. Recent results[26], [39] suggest that the position of the edges of the Fermi arcs is defined by the wavevector of a fluctuating charge order H_{CDW}, which causes a reconstruction of the Fermi-surface to the small pockets, shown as filled areas in Fig. 1.3. The gap associated with the charge density wave (CDW)

[2]The strong argument in defense of the Fermi-liquid description is the observation of quantum oscillations in different families and at different dopings.[23], [24]

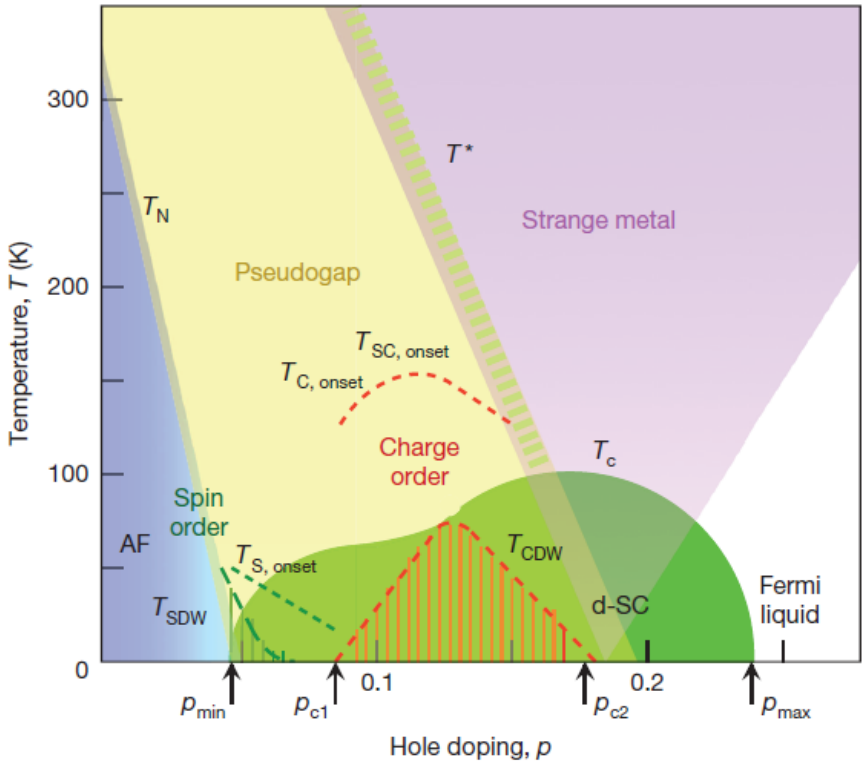


Figure 1.2: Schematic phase diagram of the cuprate superconductors. T_N, T_c, T_{CDW}, T_{SDW} - are the Neel, superconducting, CDW (only under high magnetic field) and spin density wave (SDW) transition temperatures respectively. The subscript 'onset' marks the temperature at which the corresponding fluctuating response is observed (see Chapter 3 for the discussion on the charge order). T^* is the pseudogap onset temperature. Depending on the compound some phases are not observed, or only short range correlations are present. Adopted from [6].

in this picture is then a natural candidate for the pseudogap (PG). With further increase of doping in the overdoped samples a large hole Fermi surface is observed even at low temperatures[40].

Pseudogap is not unique to the cuprates but is also seen in other strongly correlated materials such as manganites[41], [42]. Nevertheless there are strong arguments that favor an intimate relation between the superconductivity and the pseudogap. Such is particularly the *d*-wave symmetry of the pseudogap and absence of cuprates which would exhibit the superconductivity without the pseudogap.[3] Most closely the two phenomena are linked in the model where the pseudogap is considered to be due to the preformed pairs (or dynamically fluctuating clusters of (bi-)polarons) which acquire macroscopic phase coherence through the percolation when the temperature is lowered to T_c. A lot of authors[43]–[45] however consider the pseudogap as the state competing to the superconducting order, but this issue can hardly be considered as settled. It is safer to state that the pseudogap coexists with supercon-

[3]Here an important remark must be made: the hole and electron doped cuprates have several distinctions, one of which is that it is doubtful that the pseudogap is present in the electron doped cuprates. Most of the literature however covers only the hole-doped materials due to accessibility of samples and higher critical temperatures. If not stated otherwise our discussion pertains to the hole-doped cuprates.

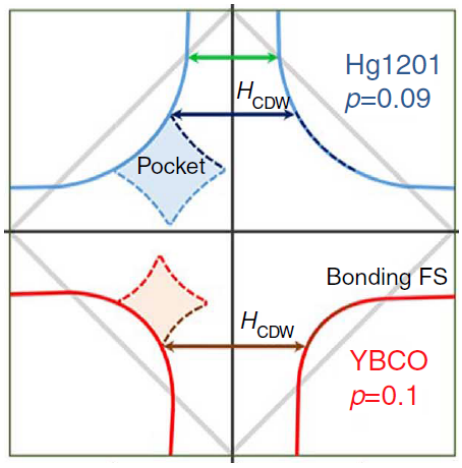


Figure 1.3: Fermi surface of the cuprates. The reconstruction is caused by a dynamic CDW at the wavevector H_{CDW}. Solid line shows the metallic Fermi surface as can be seen in ARPES above T^*, the filled area corresponds to the pockets observed in quantum oscillations. The top and the bottom semiplane correspond to different doping levels of HBCO and YBCO correspondingly and reveals inverse dependence between H_{CDW} and pocket size. Grey line is the AF Brillouin zone. Figure is adopted from [39].

ductivity which has been confirmed also by the time-resolved techniques[46].

1.1.3 Microscopical models of high temperature superconductivity

The nature of the superconducting state remains an unsettled issue even thirty years after their discovery. In this subsection we briefly discuss the main theories that attempt to explain the high temperature superconductivity. A more detailed description of the models can be found in [17], [18].

The aforementioned bipolaronic model developed by A. A. Alexandrov[47]–[49] is based on the assignation of the pseudogap to the binding of small polarons into the bipolarons. The corresponding binding energy would correspond to the pseudogap energy, which is temperature independent but reduces as screening increases with doping. At T_c bipolarons form a Bose-Einstein condensate(BEC), which is superconducting. Conceptually close to the bipolaron model is a fluctuating stripe superconductivity. In this theory competing Coulomb repulsion and lattice distortion lead to the formation of charge inhomogeneities[50] which acquire a macroscopic phase coherence at T_c via Josephson coupling.

As superconductivity develops from the antiferromagnetic insulator and since the magnetic excitations play an important role in the normal state properties of doped cuprates several models based on magnetism driven superconductivity were proposed.

The resonating valence bond (RVB) theory by P. W. Anderson[51] is describing Heisenberg antiferromagnet with a destroyed long-range order due to low dimensionality and doped holes. Nevertheless electrons pair via exchange interaction into singlet dimers called RVB (more precisely it is the superposition of all possible singlets). Upon doping or excitation a spin-charge separation occurs [52] so that holons (spinless charged particles) can form a coherent superconducting state.

Spin fluctuation pairing is a model that resembles concept of the Bardeen-

Cooper-Schrieffer (BCS) superconductivity with an antiferromagnetic paramagnon instead of phonon acting as the coupling boson. It was first proposed for the heavy fermion systems[53], [54] and then adopted for the cuprates. In this case pairing occurs in the $d-$channel and is maximally efficient at the antiferromagnetic wavevector $Q = (\pi/a, \pi/a)$.

1.2 Dynamic Properties of High-T_c Materials

In this section we discuss the dynamical electronic properties for metallic and gapped systems relevant to the cuprates. First we present typical example of the pump probe response at different temperatures which correspond to different states in the phase diagram. Then we present different theoretical approaches which are typically used to discuss the pump-probe data.

1.2.1 Characteristic features of the pump-probe response in different phases

Here we briefly introduce the characteristic pump-probe response in the metallic, pseudogap and superconducting state of cuprate superconductors, emphasizing on the characteristic features of each phase. The description of the experimental technique as well as the description of the data analysis are presented in Chapter 2.

In Fig. 1.4 the pump-probe response of the UD BSCCO sample at different temperatures is presented. In the temperature region 200 - 300 K, i.e. above the T^*, the system exhibits metallic behavior (the strange metal phase in the phase diagram in Fig. 1.2). The response is characterized by the two exponential decays and a long-lived component. The fast sub-100 fs component corresponds to the energy loss by high energy electrons discussed in details in the following subsection. The vast phenomenological description of this metallic response for different cuprates is given in [55], [56]. The slower component correspond to the energy exchange between phonons that are strongly coupled to electrons and remnant lattice[57]. The long-lived plateau is attributed to heating.

Below the T^* temperature negative response starts to dominate. This response is attributed to the relaxation of the quasiparticle response across the pseudogap. It is characterized by the negative sign, sub-ps relaxation time and gradual appearance on top of the metallic response indicating their coexistence. The coexistence has been further confirmed by the wavelength and polarization study.[59] These experiments have shown that firstly the metallic response is nearly independent on temperature, and secondly that the pseudogap response gradually grows with cooling and it's characteristic time is very weakly temperature dependent in the whole temperature range of the experiment (down to 4 K). The amplitude and sign of the response depend on probe polarization and wavelength. The systematic study of the wavelength dependent of the pump-probe response at different temperatures has been reported by Giannetti et al.[60] while the systematic polarization study is presented in Chapter 3. The theory of the temperature dependence of the pseudogap response is presented in Subsection 1.2.3.

Already above T_c the positive component with picosecond relaxation time starts to appear, growing significantly as $T \to T_c$ and further with cooling. This component has been previously attributed to the quasiparticle relaxation across the superconducting gap[38], [61]–[63]. The relaxation time of this component exhibits

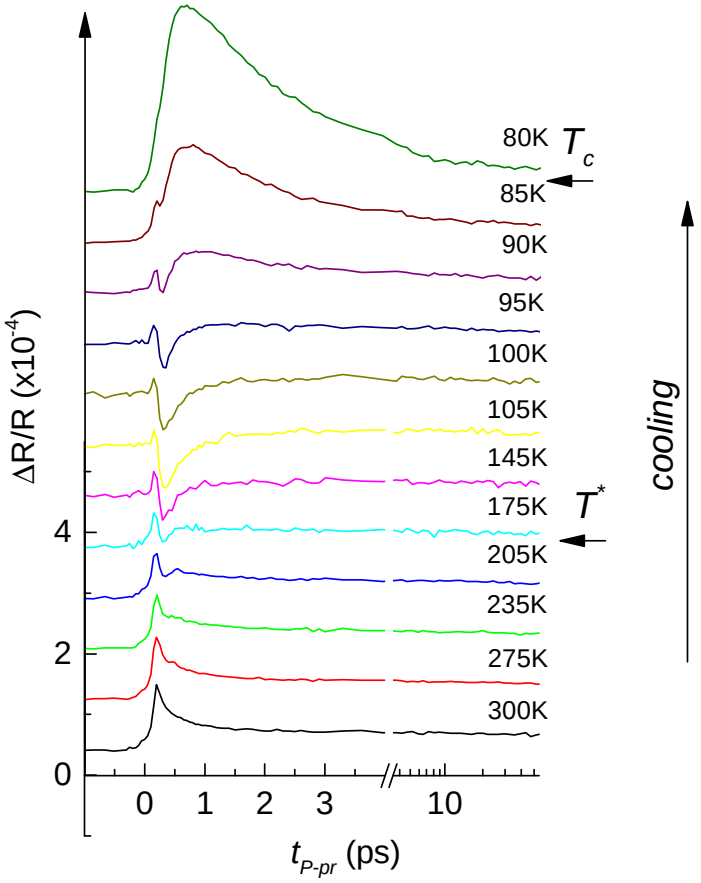


Figure 1.4: Temperature dependence of the pump-probe response for UD BSCCO sample. T_c measured by SQUID and T^* estimated from literature[58] are marked by arrows. Pump fluence is $\mathcal{F} = 9\,\mu\mathrm{J/cm}^2$.

divergence-like feature when the critical temperature is approached from either side. With cooling the relaxation time first decreases but then (below approximately 2/3 of T_c) increases significantly in the samples with low defect concentration. This low-T divergence is pronounced in LSCO[62] and BSCCO[59] but is nearly absent in YBCO[38] samples.

The theory developed by Kabanov et al.[64] presented in Subsection 1.2.3 quantitatively allows to ascribe different components to the quasiparticle relaxation across the superconducting and pseudo- gaps on the basis of temperature dependence of the response. Essential features of the theory are the gaps size and temperature dependence, which have been shown to agree with the more direct experimental measurements.[59], [62], [64]

1.2.2 Relaxation in the metallic state

The term "normal state" implies absence of the superconductivity. In cuprates as we have seen there are quite distinct states which fall into this description. The term metallic state would imply that we are discussing temperatures above T^*. Our experience, which also follows other observations, tells us that there is no clear

transition at T^* and the signatures of the pseudogap state are observable way above this temperature. They however become negligibly small when approaching room temperature and overdoped region of doping from below. We should remark that this metallic state is often called strange metal in contrast to the Fermi-liquid metal observed in strongly overdoped regime. In the ensuing paragraphs we introduce models that describe ultrafast dynamics in elemental metal, but are often applied to superconductors as well. In cuprates the metallic relaxation is also observed under the T^* temperature. In later chapters for accuracy we will use the term hot electron energy relaxation.

The two-temperature model is a revision by Allen[65] of the original idea proposed by Kaganov, Lifshitz and Tantarov[66]. It describes the evolution of the metal after excitation with an ultrashort pump pulse. The photons predominantly couple to the electronic degrees of freedom without any significant excitation of the lattice (and in a general case spin) subsystems. The crucial assumption that lies at the base of the two-temperature model is that the electrons thermalize faster than the energy transfer to phonons occurs, thus making it possible to describe the kinetics of the system in terms of the electronic and the lattice temperatures:

$$C_{\mathrm{el}}\frac{\partial T_{\mathrm{el}}}{\partial t} = -\gamma(T_{\mathrm{el}} - T_{\mathrm{lat}}) + P(t), \tag{1.1}$$

$$C_{\mathrm{lat}}\frac{\partial T_{\mathrm{lat}}}{\partial t} = \gamma(T_{\mathrm{el}} - T_{\mathrm{lat}}). \tag{1.2}$$

Here $P(t)$ would correspond to the initial heating of electrons with a laser pulse (for the description of the relaxation only the initial electronic temperature is important). Allen's result is the derivation of the connection between the temperature relaxation rate $\gamma_{\mathrm{T}} = \gamma/C_{\mathrm{el}}$ and the second moment of the Eliashberg function[4] $\lambda\langle\omega^2\rangle = 2\int_0^\infty d\Omega[\alpha^2F(\Omega)/\Omega]\Omega^2$ in the form of

$$\gamma_{\mathrm{T}} = (3\hbar\lambda\langle\omega^2\rangle/\pi k_{\mathrm{B}}T_{\mathrm{el}})(1 - \hbar^2\langle\omega^4\rangle/12\langle\omega^2\rangle k_{\mathrm{B}}^2T_{\mathrm{e}}T_{\mathrm{L}} + ...), \tag{1.3}$$

(in the real experimental conditions the second and higher terms in parenthesis are typically small and thus are neglected). This allows one to estimate the electron phonon coupling constant λ which enters the Eliashberg-Migdal theory[67] of superconductivity and particularly the McMillan's formula for $T_{\mathrm{c}} = \frac{\Theta_D}{1.45}exp[-\frac{1.04(1+\lambda)}{\lambda-\mu^*(1+0.62\lambda)}]$ [68]. This estimation is based on the approximation that the second moment of the Eliashberg function $\lambda\langle\omega^2\rangle$ is roughly equal to the product of electron phonon coupling constant λ and square of effective phonon frequency ω_0^2.

The evolution of the temperature in real systems is extracted from the transient reflectivity measurements. Typically a linear relation between the changes in temperature and reflectivity is assumed. When applied to the cuprates the two-temperature model often does not provide a reliable approximation and is quite often extended to the so-called three[11] or even five[69]temperature models. The additional temperatures correspond to separation of lattice into strongly or weakly coupled phonons or introducing other degrees of freedom such as magnons.

Even though the temperature-based models have become widely used particularly in the field of the high-temperature superconductors the systematic study has

[4]The Eliashberg spectral function $\alpha^2F(\Omega)$ defines the total transition probability for the electron by coupling to a boson of frequency Ω.

shown some disagreement of the predictions of the model with the experiments. Particularly the temperature relaxation time is expected to be strongly dependent on the initial electron temperature i.e. pump fluence as can be seen from Eq. (1.3). This strong dependence has never been observed[56]. This inconsistency has led to the development of the so-called non-equilibrium model[70], [71], which disregards the main assumption of Allen that the electron-electron thermalization time is much faster than that of the electron-phonon thermalization. Instead authors solve the Boltzmann kinetic equation with the main result (for the room-temperature region) given by:

$$\gamma_{\mathrm{T}} = \frac{3\hbar\lambda < \omega^2 >}{2\pi k_{\mathrm{B}} T_{\mathrm{lat}}}, \tag{1.4}$$

Here the relaxation rate is defined by the lattice temperature which due to the large lattice heat capacity changes negligibly with the laser fluence.

1.2.3 Quasiparticle relaxation in the gapped systems: bottleneck model

Here we briefly discuss the model which is widely used for the description of the temperature dependence of the amplitude and the relaxation times of the transient reflectivity response associated with superconducting and pseudogap state in cuprates and other gapped systems.[38], [59], [62], [72]–[77] If other is not stated we assume that the transient reflectivity is proportional to the number of photoexcited quasiparticles.

When the system exhibits a gap in the single-particle spectrum the relaxation dynamics is subjected to the so-called bottleneck process: slowing down of the relaxation due to the reexcitation of quasiparticles by the high frequency phonons. Let us consider in more detail the relaxation process after absorption of a photon. Absorption of a photon (typically 1.5 eV) excites a carrier from below the Fermi energy to the states far above the Fermi energy (in cuprates these are aforementioned charge transfer excitations). Even though the initial excitation is interband the optical conductivity in the cuprates reveals a significant ingap joint density of states (JDOS)[12] which allows to describe this relaxation stage as metallic, described in the previous section. Then, in the prebottleneck stage, above-the-gap quasiparticle excitations reach a quasi-equilibrium with the high frequency phonons (HFPs) $\hbar\Omega \geq \Delta$. The formation of a superconducting pair leads to the emission of a HFP which in turn can either be absorbed by a superconducting pair forming a pair of quasiparticles or release the energy either via an anharmonic decay into the subgap phonons or just escape from the excitation volume. If absorption by a superconducting pair is dominant we say that the relaxation is subject to a strong bottleneck, otherwise a weak bottleneck is in place.

Authors of [64] deduce the expression for the photoinduced quasiparticle density dependence on temperature from the energy balance between the quasiparticle and HFPs , which is defined by the gap properties. In the original article the case of nodeless gap and gap with nodes were considered as well as temperature independent and temperature dependent gaps. For the cuprates the pseudogap response temperature dependence is typically well approximated by the *temperature independent nodeless gap* model [38], [62], [73], [74], [78], [79]:

$$n_{\mathrm{pe}} = \frac{E_{\mathrm{I}}/\Delta}{1 + \frac{2\nu}{N(0)\hbar\Omega_c} exp[-\Delta/k_B T]}, \tag{1.5}$$

here ν is the number of HFPs and Ω_c is phonon cutoff frequency, $N(0)$ is the density of states at the fermi level.

The superconducting response can be reproduced with the BCS-like *temperature dependent nodeless gap* model[38], [62], [73], [74], [78], [79]:

$$n_{\rm pe} = \frac{E_{\rm I}/(\Delta(T) + k_{\rm B}T/2)}{1 + \frac{2\nu}{N(0)\hbar\Omega_c}\sqrt{\frac{2k_BT}{\pi\Delta(T)}}exp[-\Delta(T)/k_{\rm B}T]}. \tag{1.6}$$

As an example of application of these models we present the data for BSCCO[79] shown in Fig. 1.5. Typically $N(0)$ and Ω_c can be estimated from other experiments, whereas ν and $\Delta(0)$ are left as the fit parameters. Usually there is only few phonons strongly interacting with quasiparticles, and $\Delta(0)$ is in a reasonable agreement with other experiments. This observation allowed to confirm the validity of the bottleneck model in the weak excitation regime. A peculiar result coming out of the original consideration is that better fit is obtained with the model which assumes nodeless gaps for both the SC and the PG excitations[64] which is in apparent contradiction to the d-wave symmetry of the gap that was unambiguously confirmed by ARPES. There are two possibilities to reconcile these results. First, the gaps can have $d+s$-wave symmetry and the s component will be definitive for the pump-probe observation as proposed recently by Sakai et al.[80] The second possibility is that the momentum scattering which is expected to be more effective than the energy relaxation is reduced due to some reason (e.g. reduced phase space for scattering, as illustrated in [61]) as it was observed in time-resolved ARPES experiments[81].

In the high excitation limit all Cooper pairs are excited and the change of reflectivity is described by the Mattis-Bardeen formula[82], [83]:

$$\left(\frac{\Delta R}{R}\right)_{\rm SC}^{total} \propto \left(\frac{\Delta_{\rm SC}(T)}{\hbar\omega}\right)^2 ln(\frac{3.3\hbar\omega}{\Delta_{\rm SC}(T)}), \tag{1.7}$$

where ω corresponds to the frequency of the light (probe). The comparison of the high and low excitation regimes is also given in Fig. 1.5 .

In the following paragraphs we consider the temperature dependence of the quasiparticle relaxation time.

In the previously mentioned work [64] Kabanov et al. calculated the phonon relaxation time by solving the kinetic Boltzmann equations in the approximation that the phonon-phonon scattering processes are dominant and other energy relaxation channels are ignored. The final result is:

$$\frac{1}{\tau_{\rm ph}} = \frac{12\Gamma_\omega\Delta(T)^2}{\hbar\omega^2 ln(1/\{E_I/2N(0)\Delta(0)^2 + exp[-\Delta(T)/k_{\rm B}T]\})}, \tag{1.8}$$

where ω is the phonon frequency and Γ_ω is the Raman phonon line-width. There are two remarkable features of this function. Firstly, in the limit $T \to T_c$ the relaxation time diverges $\tau_{\rm ph} = \frac{1}{\Delta(T)}$. Secondly, when the energy per pulse is reduced at low temperatures, the relaxation time is inversely proportional to the temperature $\tau_{\rm ph} \propto 1/T$ (even though the formula is derived in the high T approximation). Note that the strongest effect on the relaxation time comes from the temperature dependence of the gap. In the case of the temperature independent gap a very weak T dependence is still expected.

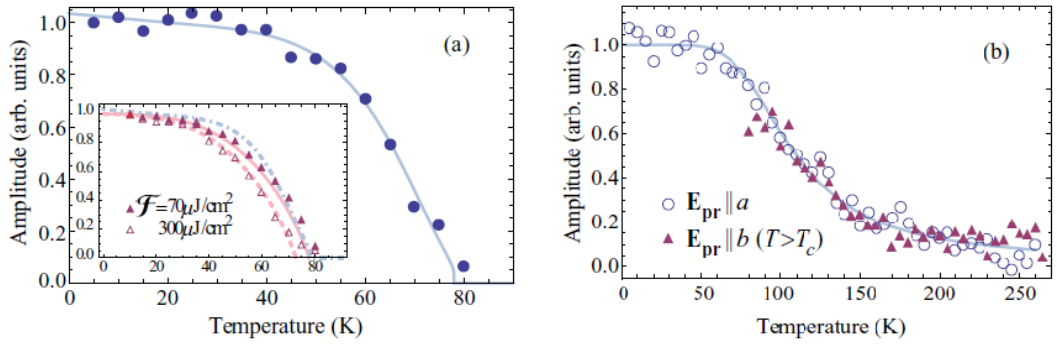


Figure 1.5: Temperature dependence of the superconducting (a) and pseudogap (b) components of the transient reflectivity signal and fits by equations (1.6) and (1.5), correspondingly. In the inset high (open triangles) and low (full triangles) excitation regimes are compared. The fit in the high excitation regime (red dashed line) takes into account the continuous heating ($\sim$ 5 K). The actual T-dependence with the heating correction is shown by the blue dashed line. Figure is adopted from [79].

The dynamics of the quasiparticle relaxation in the nonequilibrium superconductor has been initially considered within the phenomenological Rothwarf-Taylor (RT) model[84], which postulates a system of differential equations that describes the evolution of the quasiparticle N and the phonon N_ω populations[5]:

$$dN/dt = \beta N_\omega - RN^2, \tag{1.9}$$

$$dN_\omega/dt = \frac{RN^2}{2} - \beta\frac{N_\omega}{2} - (N_\omega - N_{\omega \mathrm{T}})\gamma. \tag{1.10}$$

The number of quasiparticles can be increased as a result of the phonon absorption by a Cooper pair with probability β or decreased due to the formation of a Cooper pair *by two quasiparticles* with the emission of a high frequency phonon. The phonon population is changed in the same processes or due to the anharmonic decay or diffusive transport of the phonons out of the excitation volume (both of these processes are included in the third term of Eq. (1.10) and typically considered separately in the limiting cases). If the third term is small a quasi-equilibrium is reached and the bottleneck conditions are satisfied. By setting the time derivatives and the third term of Eq. (1.10) to zero we find that the quasi-equilibrium is reached when $N_\omega = \frac{R}{\beta}N^2$.

Consideration of the prebottleneck dynamics is important and cannot be omitted from the discussion. Typically it is assumed that in the result of hot electron scattering after the initial photon absorption large number of quasiparticles is produced which further relax toward the quasiequilibrium with HFPs. The opposite situation when initial relaxation results in excitation of high-frequency phonons is also possible (see references in [85]). In *prebottleneck* stage quasiparticle relaxation rate is dependent on the quasiparticle density implying bimolecular kinetics of the relaxation. This behavior was experimentally observed at low temperatures and fluences so it was interpreted as *prebottleneck* quasiparticle thermalization with HFP

[5]We use different notation than above to avoid ambiguity in the discussion. The RT model is a simpler model which addresses the dynamic behaviour, but does not take into account gap variations. Note that N is the total number of quasiparticles so that $N = n_{\mathrm{pe}} + N_{\mathrm{T}}$.

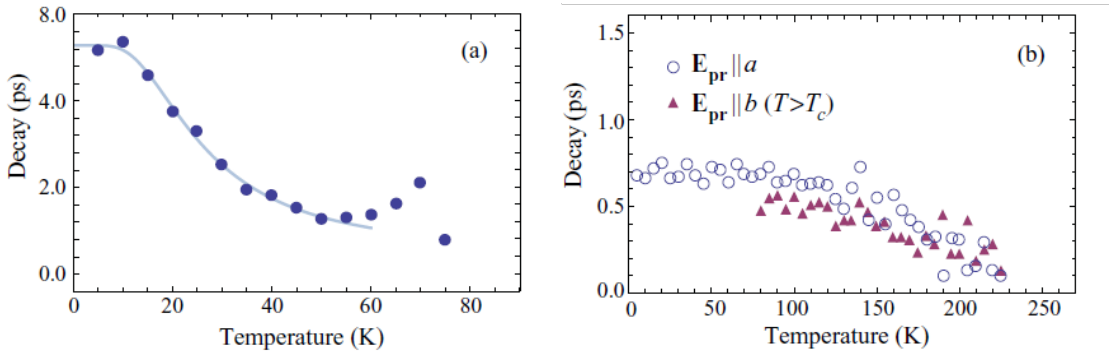


Figure 1.6: Temperature dependence of the relaxation time of the superconducting and pseudogap components. Solid line is the fit by Eq.(1.12). Figure is adopted from [79].

rather than the recombination in the condensate (bottleneck).[61], [73], [86] This latter interpretation was further disproved [85], [87] with an important note that observed fluence dependence of the relaxation time is also expected in the *bottleneck* case: in the low temperature limit the quasiparticle relaxation is described by[85]

$$q = q_T + \frac{2q_T(q_s - q_T)exp(-\theta/\tau_T)}{(q_s + q_T) - (q_s - q_T)exp(-\theta/\tau_T)}, \tag{1.11}$$

where $q = \frac{R}{\beta}N$ is the dimensionless quasiparticles concentration, $q_s = \frac{1}{4}\sqrt{1 + 16p_0 + 8q_0} - 1$ is the quasistationary value of the quasiparticles concentration preceding the relaxation (q_0 and p_0 - are the initial concentrations of quasiparticles and phonons correspondingly) and q_T is the concentration at the bath temperature T, $\theta = \beta t$ is the dimensionless time and $\tau_T^{-1} = 4\gamma q_T/\beta$ is the relaxation rate which is strongly reduced by the temperature dependent factor q_T.

At early times $\theta/\tau_T < 1$ Eq. (1.11) reduces to a hyperbolic form $q(\theta) = q_s/(1 + 2q_s\gamma\theta/\beta)$ identical to the one expected in the *prebottleneck* regime. The initial relaxation rate in this case is defined as:

$$\tau^{-1} = 2(q_s + q_T)\gamma/\beta, \tag{1.12}$$

This formula reproduces the divergence of the relaxation with decrease of both, the temperature and the fluence observed experimentally[59] (Figure (1.6)).

1.2.4 Fluence dependence of the pump-probe response

As we have already mentioned the pump-probe response is believed to be proportional to the number of the photoexcited quasiparticles. This is confirmed not only by the presented models but also by a direct comparison with the THz data[11], [88]. Taking the beam profile into account we can write:

$$\Delta R/R \propto \int_0^\infty \int_0^\infty exp(-2z/\lambda_{op})exp(-r^2/\rho_{pr}^2)n_{pe}d^2rdz. \tag{1.13}$$

The simplest model that describes the fluence dependence of the pump-probe response assumes that the number of photoexcited quasiparticles is directly proportional to the number of absorbed photons (i.e. fluence $\mathcal{F}$) up to the moment when all of the carriers forming the state are excited ($\mathcal{F} = \mathcal{F}_{th}$):

$$n_{\mathrm{pe}} \propto \begin{cases} n_{\mathrm{s}}\mathcal{F}(r,z)/\mathcal{F}_{\mathrm{th}} & \mathcal{F}(r,z) < \mathcal{F}_{\mathrm{th}}, \\ n_{\mathrm{s}} & \mathcal{F}(x) \geq \mathcal{F}_{\mathrm{th}}. \end{cases} \tag{1.14}$$

Here the depth dependence of the absorbed energy density $\mathcal{F}(z) = \mathcal{F}_0 exp(-z/\lambda_{\mathrm{op}}) exp(-r^2/\rho_{\mathrm{p}}^2)$ must be taken into account.

After the integration of the Eq. (1.13) and normalization to the saturated value[89] the expression for the transient reflectivity reads:

$$\Delta R_{\mathrm{s}}/\Delta R = \frac{3}{2} f/(1+\rho^{-2}), \quad \text{for } \mathcal{F} < \mathcal{F}_{\mathrm{th}}, \tag{1.15}$$

and

$$\Delta R_{\mathrm{s}}/\Delta R = \left[1 - f^2 + \frac{2(f\rho^2 - f^2)}{\rho^2 - 2} + \frac{6f\rho^2/(1+\rho^{-2}) - 2f^2\rho^2}{6 - 3\rho^2}\right]^{-1}, \quad \text{for } \mathcal{F} > \mathcal{F}_{\mathrm{th}}, \tag{1.16}$$

here $\rho = \rho_{\mathrm{p}}/\rho_{\mathrm{pr}}$ and $f = \mathcal{F}_{\mathrm{th}}/\mathcal{F}_0$.

Additionally, the linear with fluence term is typically added to describe other contributions to the transient reflectivity which do not saturate or saturate at higher fluences.

This model has been proposed by Kusar et al.[89] and consequently used to describe the fluence dependence for a number of superconducting and CDW systems, summarized in the article by Stojchevska et al.[90] The shape of the curve appears to be universal whereas quantitatively the energy density required to destroy the *superconducting state* appeared to be significantly larger than the condensation energy. The reason for the discrepancy lies in the indirect nature of the photodestruction - the superconducting state is destroyed only by the phonons which have $\hbar\Omega > \Delta$, the energy transferred to the subgap phonons during the initial relaxation of hot electrons is lost and forms the difference between the condensation and the photodestruction energies.

1.3 Non-Equilibrium Symmetry Breaking Transitions

Within this chapter we will introduce a theoretical framework in which the non-equilibrium phase transitions are described. We start from a general introduction of the Landau theory of phase transitions and present how it can be extended to describe the dynamics of the superconductors in general (time-dependent Ginzburg Landau theory) and the formation of the superconducting phase in a nonequilibrium phase transition (Kibble-Zurek (KZ) mechanism) particularly when the transition is inhomogeneous - the case which we will study in this thesis.

1.3.1 Landau theory of phase transitions. Ginzburg-Landau theory

The Ginzburg-Landau theory is an obligatory chapter of the general books on superconductivity [91], [92]. In the following we will briefly cover the main parts important for our further consideration.

The Landau theory of phase transition[93] implements the concept of symmetry in physics. Application of this approach has resulted in enourmous development in the condensed matter and the elementary particles physics.[94] The transition

between two phases is considered as a transition from the disordered state of high symmetry to the ordered state in which a certain symmetry is broken. The way in which a particular symmetry is broken is typically (in the absence of external field) random so the phenomenon is called a spontaneous symmetry breaking. In the normal to superconducting phase transition the gauge symmetry becomes violated: the macroscopic quantum-mechanical phase of superconducting condensate is sensitive to gauge transformations. The amplitude of the collective superconducting wave-function serves as a quantitative measure of symmetry violation and can be defined as the order parameter.

The Landau theory approximates the free energy as the Taylor expansion in terms of powers of the order parameter. From the symmetry considerations in the continuous (i.e. 2nd order) phase transitions[93], [95] odd powers are omitted. Expansion up to the fourth power captures the main properties of the phenomenon:

$$F = \alpha|\psi|^2 + \frac{\beta}{2}|\psi|^4. \tag{1.17}$$

The temperature effects are described to the lowest order by a linear dependence of the leading term $\alpha = a(T - T_c)$. Above T_c $\alpha > 0$ and the free energy has a single minimum $\psi = 0$, below T_c $\alpha < 0$ and the equilibrium is reached when $\psi = \sqrt{\alpha/\beta}$. It is sufficient to set β as a positive constant which is independent of temperature.

For a superconductor the order parameter is the wave-function of the superconducting condensate, the square of its amplitude defines the Cooper pairs density:

$$|\psi|^2 = \frac{n_s}{2}. \tag{1.18}$$

The Ginzburg-Landau theory is an extension of the aforementioned theory for the case of an inhomogeneous superconductor in the external field. In this case the total Gibbs free energy is

$$G = G_n + \int \left(\alpha|\psi|^2 + \frac{\beta}{2}|\psi|^4 + \frac{1}{4m}|-i\hbar\nabla\psi - \frac{2e}{c}\mathbf{A}\psi|^2 + \frac{(\mathrm{curl}\mathbf{A})^2}{8\pi} - \frac{\mathrm{curl}\mathbf{A}\cdot\mathbf{H_0}}{4\pi} \right) dV, \tag{1.19}$$

here G_n is the free energy of the normal state, the term $\frac{1}{4m}|-i\hbar\nabla\psi - \frac{2e}{c}\mathbf{A}\psi|^2$ is the gauge invariant kinetic energy, the fourth term under the integral is the energy of the magnetic field and the last term is the magnetic coupling to the external field $\mathbf{H_0}$.

Minimization of the free energy with regards to the order parameter and vector potential results in the two Ginzburg Landau equations (see for instance[91])

$$\alpha\psi + \beta\psi|\psi|^2 + \frac{1}{4m}\left(i\hbar\nabla + \frac{2e}{c}\mathbf{A}\right)^2\psi = 0, \tag{1.20}$$

$$-\frac{i\hbar e}{2m}\left(\psi^*\nabla\psi - \psi\nabla\psi^*\right) - \frac{2e^2}{mc}|\psi|^2\mathbf{A} = \frac{c}{4\pi}\mathrm{curlcurl}\mathbf{A} = \mathbf{J_s}, \tag{1.21}$$

and the de Gennes boundary condition

$$\left(i\hbar\nabla\psi + \frac{2e}{c}\mathbf{A}\psi\right)\cdot\mathbf{n} = 0. \tag{1.22}$$

Here **n** is the vector normal to the surface. De Gennes boundary condition is correct in the case of a superconducting-insulator interface. The superconducting coherence length and the London penetration depth can be expressed as $\xi = \sqrt{\frac{\hbar^2}{4m|\alpha|}}$ and $\lambda_{\mathrm{L}} = \sqrt{\frac{mc^2\beta}{8\pi e^2|\alpha|}}$, respectively.

1.3.2 The time-dependent Ginzburg-Landau theory

The obtained equations describe a non-homogeneous superconductor at equilibrium. Here we will consider how the Ginzburg-Landau theory has to be modified to describe dynamic phenomena. The pioneering works on expanding the Ginzburg-Landau theory to include time-depended phenomena have been done in 1966[96], [97]. A detailed review can be found in [98], [99] and, on a more advanced level, in [100].

By a definition, the system reaches the equilibrium when

$$\frac{\delta F}{\delta \psi^*} = 0. \tag{1.23}$$

The main assumption of the out-of-equilibrium description is that the rate at which system relaxes towards the equilibrium is proportional to its deviation:

$$-\gamma\hbar\frac{\partial\psi}{\partial t} = \frac{\delta F}{\delta\psi^*}, \tag{1.24}$$

where γ is a positive constant and t is the time. Equation in this form does not preserve the gauge invariance, so it should be corrected accordingly:

$$-\gamma\left(\hbar\frac{\partial\psi}{\partial t} + 2ie\chi\psi\right) = \frac{\delta F}{\delta\psi^*}, \tag{1.25}$$

where χ is the electrostatic potential.

We notice that the right-hand side of Eq. (1.25) is the formulation of the first Ginzburg-Landau (GL) equation ((1.20)), i.e.

$$-\gamma\left(\hbar\frac{\partial\psi}{\partial t} + 2ie\chi\psi\right) = \alpha\psi + \beta\psi|\psi|^2 + \frac{1}{4m}\left(i\hbar\nabla + \frac{2e}{c}\mathbf{A}\right)^2\psi. \tag{1.26}$$

The second GL equation ((1.21)) is modified due to the possibility of the normal current $\mathbf{J_n}$ in the non-equilibrium case.

$$\frac{c}{4\pi}\mathrm{curlcurl}\mathbf{A} = \mathbf{J} = \mathbf{J_s} + \mathbf{J_n}, \tag{1.27}$$

$$\mathbf{J}_s = -\frac{i\hbar e}{2m}\left(\psi^*\nabla\psi - \psi\nabla\psi^*\right) - \frac{4e^2}{mc}|\psi|^2\mathbf{A}, \tag{1.28}$$

$$\mathbf{J_n} = -\sigma_{\mathrm{n}}\left(\frac{1}{c}\frac{\partial\mathbf{A}}{\partial t} + \nabla\chi\right). \tag{1.29}$$

The total current also obeys the continuity equation

$$\mathrm{div}\mathbf{J} + \frac{e\partial n_{\mathrm{e}}}{\partial t} = 0. \tag{1.30}$$

To describe the dynamics of the system Equations (1.26)-(1.30) must be solved simultaneously. We note here that due to gauge invariance of the equations the solution of the stationary homogeneous problem can be selected to be real.

In this thesis we will solve the equations in the constant phase approximation, i.e. ignoring currents in the system (we will discuss all approximations in Chapter 4). In the constant phase approximation the equation is reduced to

$$-\gamma\hbar\frac{\partial\psi}{\partial t} = \alpha\psi + \beta\psi|\psi|^2 + \frac{1}{4m}\left(i\hbar\nabla\right)^2\psi. \tag{1.31}$$

An important prediction of this theory is the presence of the critical slowing down of the order parameter dynamics as $T \to T_c$. This can be seen from Eq. (1.24) - in the vicinity of the transition the second order term of the free energy expansion vanishes so the $\frac{\delta F}{\delta\psi^*} \to 0$. The strict theory of the critical slowing down is explained in [101].

1.3.3 Dynamics through the phase transition - Kibble-Zurek description

Let us now consider a phase transition that is happening at some finite cooling rate[5]

$$\frac{T(t) - T_{\mathrm{c}}}{T_{\mathrm{c}}} = \epsilon = t/\tau_{\mathrm{Q}}, \tag{1.32}$$

here t is the time, and τ_{Q} is the characteristic time constant of the transition which we will call the "quench time". The original discussion of this problem[3] comes from the elementary particle physics and suggestion that electromagnetic, weak and strong gauge fields restore the global symmetry at a certain temperature in a very similar way the superconducting materials restore the gauge symmetry in the normal state. As the cooling after the Big Bang occurred the symmetries became broken but the configuration of the broken-symmetry phase is selected randomly and not necessarily homogeneously in space. T. W. Kibble[3] was looking for the signatures of the transition that are left in the aftermath that would allow to devise information about the transition itself.

Consider the normal-to-superconducting state transition. The phase of the order parameter is uniquely defined at each point but differs across the sample unless the transition has occurred infinitesimally slowly. This is simply due to the reason that the information about the phase choice cannot propagate at an infinite velocity but is limited by the order parameter dynamics (in a more general case the limiting speed is the speed of light). This leads to inhomogeneous domains with randomly selected phases and domain walls in-between. As the system evolves the phase relaxes and an equilibrium configuration is achieved, which would appear as a continuous (in space) order parameter with a slowly varying phase and a number of topological defects (Abrikosov vortices) incorporated. Due to the phase continuity of the order parameter topological defect cannot disappear unless it is annihilated with the topological defect of the opposite sign (vortex of the opposite direction) or it diffuses out of the superconducting boundary. It should be noted that the stable topological defect configuration and sequential dynamical properties are defined by the space and order parameter dimensionality. For vortices to appear the space should be three dimensional with a complex order parameter[3].

To estimate the density of topological defects let us consider the evolution of the order parameter characteristics - the coherence length ξ and the relaxation time

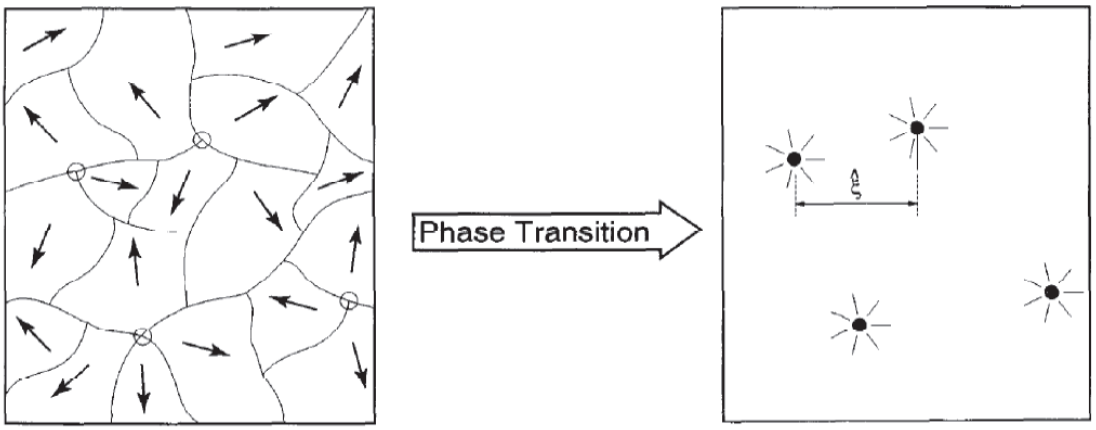


Figure 1.7: Schematic representation of topological defects formation in the course of a non-equilibrium phase transition. Arrows directions represent the phase of the order parameter, and solid circles are vortices. Picture is adopted from [5].

τ along the quench. At high temperatures rapid short-range fluctuations of the order parameter exist and both ξ and τ are defined by the instantaneous value of temperature ϵ. As the system approaches the critical temperature the relaxation time diverges as $\tau = \tau_0/|\epsilon|$ and $\xi = \xi_0/|\epsilon|^\nu$(in the GL theory $\nu = 1/2$). In the direct vicinity of the phase transition the relaxation time becomes so large that the system cannot adopt to the varying temperature and becomes effectively frozen. In this impulsive regime the system passes the transition and enters the broken symmetry phase. When the temperature, at which the relaxation time is reduced sufficiently to adiabatically follow ϵ, is achieved, the order parameter starts to grow. The phase configuration of the system is defined above T_c at the "freezing" time t_Z. This is given by the condition $\tau(t = t_\mathrm{Z}) = \tau_\mathrm{Q}$, which together with equation (1.32) gives $t_\mathrm{Z} = \sqrt{\tau_0\tau_\mathrm{Q}}$. This consideration was originally set forth by Zurek [4] and t_Z is called Zurek time. The corresponding relative temperature is defined as $\epsilon = \sqrt{\tau_0/\tau_\mathrm{Q}}$. The value of the correlation length at the "freezing" temperature defines the density of topological defects: $l_0 \approx \xi_0^{-2}(\tau_0/\tau_\mathrm{Q})^\nu$.

Now one can estimate the initial order parameter which acts as a seed for further growth when the system has "frozen-out". The correlation length at the freezing temperature is given by $\xi_\mathrm{Z} = l_0^{-1}$. The energy of the fluctuations in the volume ξ_Z^3 is given by $\xi_\mathrm{Z}^3\Delta_\mathrm{fluc}^2 N_\mathrm{F}$, where N_F is the density of states at the Fermi level. This energy should be equated to $T_\mathrm{Z} \sim T_\mathrm{c}$, which, taking into account $\xi_0 = \frac{\hbar v_\mathrm{F}}{\Delta_\mathrm{eq}}$ and $\nu = 1/2$ gives:[6]

$$\frac{\Delta_\mathrm{fluc}}{\Delta_\mathrm{eq}} \sim \left(\frac{\tau_0}{\tau_\mathrm{Q}}\right)^{3/8} \frac{T_\mathrm{c}}{E_\mathrm{F}}. \tag{1.33}$$

As one can see the faster the quench occurs the higher is the density of the topological defects and, somewhat counterintuitively, the larger is the seed for the emerging order.

[6] In the original article[102] the misprint occurred - power of the characteristic times ratio is mistakenly written as 1/8 instead of 3/8.

Chapter 2

Experimental Details and Methods

In this chapter we will focus on the experimental techniques applied and sample growth and preparation. We will describe the laser source, non-linear processes used for the photon frequency transformation, detection principles and data analysis.

2.1 Femtosecond Time-Resolved Optical Spectroscopy

The main component of the experimental setup is a femtosecond laser source. Here we will briefly introduce the laser system and the concept of ultrashort pulses generation. The schematics of the set-up has been described previously in [103] and is presented in Fig. 2.1. For the technical documentation on the laser system the reader is referred to [104] and for a general introduction in the pump-probe techniques the following literature is recommended[105], [106].

The pump-probe setup can be divided into two blocks (Fig. 2.1): 1) a pulse generation block, which includes an oscillator, a pulse stretcher/compressor and a regenerative amplifier and 2) an experimental block or more precisely the beam parameters transformation block, which can include an Optical Parametric Amplifier (OPA), beam splitters, telescope systems, delay lines, non-linear optics, polarization control optics and other elements. Whereas the first block remains practically unchangeable during the whole life-time of the laser (excluding maintaining operations) the second block is partially, sometimes completely, modified for each particular experimental cycle. In our laboratory up to three experiments can run simultaneously using the same pulse generation block. At Complex Matter department currently there are two separate femtosecond laboratories each of them has similar pulse generation blocks, based on *Coherent* femtosecond lasers. Further we will refer to these blocks as a *RegA* system.

The heart of the RegA system is a Ti:Sapphire oscillator (models *Mira*[107] or *Vitara*[108]), which produces ~ 50 fs pulses at 80 MHz repetition rate with energy per pulse up to ~ 4 nJ and the central wavelength $\lambda = 800$ nm. The oscillator itself can serve as the light source for experiments and it is mostly suitable for a low energy-per-pulse application. For the superconducting response under strong excitations, which we are interested in, this high repetition rate would lead to a significant heat pile-up which would obscure experimental data. Utilization of a regenerative amplifier in combination with an oscillator laser allows to reduce the repetition rate. Another experimental need for the use of regenerative amplifiers are their high pulse energies up to $\sim 6\mu$J, which are crucial for the non-linear processes further involved, as well as the initiation of the photoinduced phase transition. For

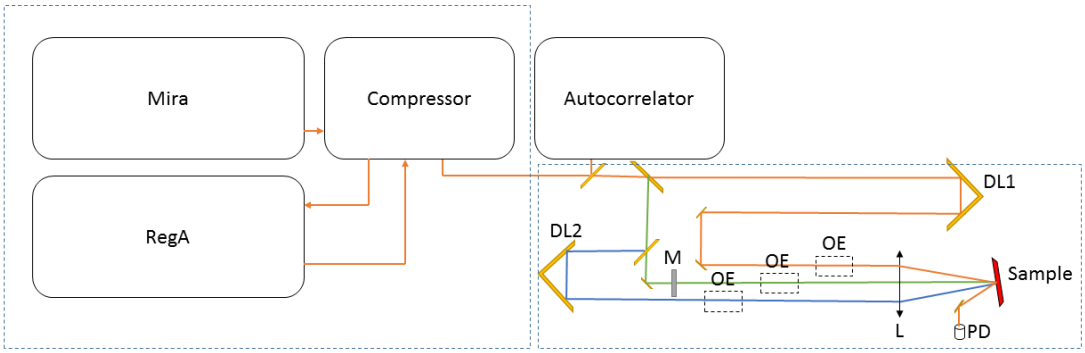


Figure 2.1: A schematic of the pump-probe setup. The dashed line marks out the pulse generation and experimental blocks discussed in text. Notation: DL1-2 - remotely controlled delay lines, M - modulator, OE - optional elements (Non-linear crystals, attenuators, $\lambda/2$ plates, polarizers), L - lens (shared or separate for each beam), PD - photodetector. Probe, pump and destruction beams are schematically colored in orange, green and blue.

Coherent RegA amplifiers the repetition rate is variable between 100 and 750 KHz. All conducted experiments were performed in the 250 KHz configuration.

Without detailing on the particular system we would like to introduce the concept of phase locking (or mode-locking) and regenerative amplification. The way ultrashort pulses are achieved is called mode-locking, meaning that a large number of modes of the resonator are set to propagate in phase. Consequently in the place where the waves are in phase modes interference constructively whereas due to the frequency difference between the modes away from this point a destructive interference takes place resulting in a narrow pulse. The mode-locking in our case is achieved by Kerr-lensing.[106]

The power of the pulses is physically limited by the damage threshold energy density of Ti:Sapphire. This is why regenerative amplifiers are employed. The output pulses of the oscillator are stretched to 50 ps. and sent on the input of a RegA. A single pulse from the pulse train is picked by an acousto-optic modulator (AOM) and passed a couple dozen times through the active media. It is then ejected from the cavity by the AOM and compressed down to $\sim$ 50 fs in a compressor. The process is repeated at a 250 KHz repetition rate.

In further the pulse train is split with beam splitters in three beams of different purpose: the destruction (D) beam meant to destroy the ordered state, the modulated pump (P) beam which acts as a small perturbation of the emerging state and the probe (pr) beam which due to a lock-in detection (explained further) is sensitive *only* to those changes in the reflectivity which are induced by the pump. A significant amount of data further presented was accumulated in classical two-pulse experiment, namely polarization, fluence and temperature dependence studies. In these studies the D pulse was simply blocked.

For some of the experiments the wavelength of the pump beam has been doubled in a non-linear (beta barium borate) BBO crystal. This allows to reduce scattering of the pump onto the detector (with use of the bandpass filters).

2.2 Description of the Detection Scheme and Lock-In Detection

The changes of the reflectivity induced by the excitation of the superconducting condensate are typically lower than 0.1 %, which is an order of magnitude less than the low frequency laser noise (the so-called pink noise the power spectral density of which is inversely proportional to the frequency is typically the main contribution). This is why the direct measurements of the reflectivity change is impossible and lock-in technique is employed, the technique which implies modulation of the signal at certain frequency with further application of the mathematical procedure which resembles the effect of a band-pass filter. Modulation of the signal is realized via modulation of the pump beam (modulation frequency in the range from 2 to 5 KHz was used). To achieve this mechanical chopping or acousto-optical modulation are typically employed.

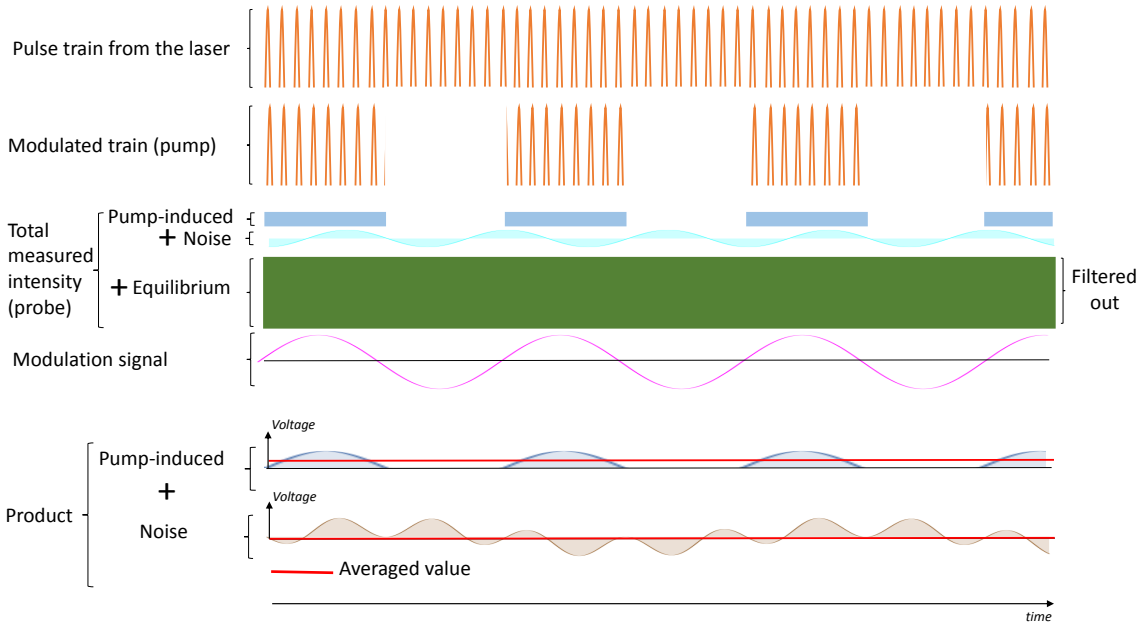


Figure 2.2: Simplified illustration of lock-in detection principle. The pulse train from the laser is modulated in the pump channel by a square function on the modulation frequency (In our case approximately 100 pulses per modulation period). Total intensity of the reflected probe beam consist of three component: time-independent large component which corresponds to the intensity in the case of non-modulated reflectivity(green), change in the intensity due to the modulation of the reflectivity(blue) and noise of the different origin at various frequencies(cyan). The constant component is typically filtered by a high pass electrical filter (20 Hz). The signal is then multiplied by a sinusoidal modulation signal(pink) in the lock-in amplifier. The pump-induced modulated part of the response results in a positive component(blue) while the noise contribution on the frequency different from the modulation frequency produces sign-changing contribution(brown). The product is subsequently averaged with a given time-constant (typically 1000 modulation periods) so that sign-changing contribution are averaged-out to zero while the pump-induced response results in a non-zero value which is saved as a data-point(average values are designated by red lines in both cases).

To understand further processing of the signal let us refer to Fig. 2.2. The intensity of the reflected probe beam can be represented as the sum of the three components with different time-dependence: the time-independent component which corresponds to the intensity of the probe beam in the absence of excitation, the square-shaped periodic component due to the pump-induced changes of the reflectivity of the sample and the noise component at different frequencies (for the sake of presentation we show a single monochromatic contribution). The current from the photodiode is converted into voltage and is split into two channels: one detects the d.c. voltage which corresponds to the total reflectivity and the other which, after filtering out the d.c. component, is sent to the input of a lock-in amplifier (*EG&G Instruments*). In the amplifier the signal is digitized and multiplied by a sinusoidal modulation signal. As can be seen from Fig. 2.2 the signal at the modulation frequency results in a constant-sign component whereas the noise produces equal contribution of both signs. After averaging over a large number of time cycles (given by a preset integration time constant) the sign-changing contributions are averaged out to zero, whereas the signal at the modulation frequency results in a non-zero average value which is recorded as a data point. The phase of the modulation signal can be adjusted automatically by the amplifier. For setting the phase scattering of the pump beam is typically used and the probe beam is blocked. Signal from pump-scattering is nearly always present except for the multi-wavelength experiments. For samples with good surface quality it can be increased by slight detuning of the polarizer. The scattering of the pump beam is delay independent and in the experiments it is subtracted by setting the offset of the amplifier when probe beam is blocked.

For each value of the pump-probe delay the signal is accumulated during the integration time-constant of the lock-in amplifier. The number of data points and the time constant are chosen to keep the measurement time in a reasonable frame.

We emphasize that in the three-pulse experiment there are large changes in the reflectivity induced by the destruction pulse and much weaker changes induced by the pump pulse. As the D beam is not modulated the corresponding change in the reflectivity is not recorder and only the pump-induced changes are saved.

2.3 The 3 Pulse Experiment: Signal Simulation and Data Analysis

The significant amount of the physical problems considered in the thesis are approached by means of the three pulse technique, already mentioned in previous sections. Here we shall exemplify the results as well as describe the approach to the data analysis.

In Fig. 2.3 we schematically represent the pulse order in the conventional 3 pulse experiments as well as notation of the delays between the pulses. In most of the experiments a single wavelength was used for all the pulses and the polarization of the pump beam was always orthogonal to that of the probe beam. This allows to minimize the contribution from the scattered pump light by setting the analyzer in front of the detector into the position parallel to the probe beam polarization. In the case of a balanced 3 pulse experiment, described further in text, the 400 nm pump was used and the scattering was cut off by a bandpass filter. The polarization of the destruction beam was set to be parallel to the polarization of the pump beam.

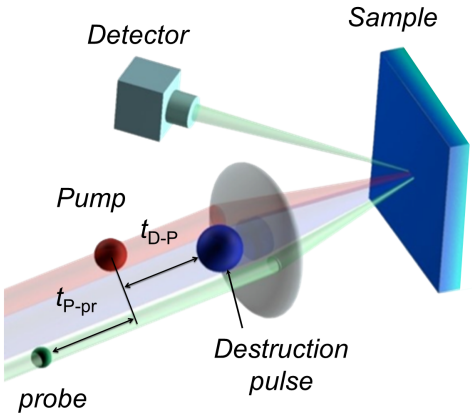


Figure 2.3: A schematic of the three-pulse pump-probe experiment with the sequence of pulses and notation of delays. Colors of the pulses do not correspond to their photon energy.

To ensure the alignment of the destruction beam the standard two-pulse experiment was conducted with the pump beam blocked and modulated destruction beam. As a useful crosscheck the power dependence of the response in this regime was measured so that the photodestruction power is estimated directly in the very same experiment.

The 3 pulse experiment can be imagined as a set of the pump-probe experiments at different values of the destruction-pump delays.[1] By providing a relation between the amplitude of the pump-probe response and the order parameter, which we will refer to as a response function, one expect to obtain the information on the dynamics of the order parameter by measuring the amplitude of the response as the $t_{\mathrm{D-P}}$ increases. The consideration regarding the response function are provided in Section 4.1. For the moment we limit ourself to the lowest order expansion of the dielectric constant in terms of the order parameter $\Delta R \sim \Delta\varepsilon \sim |\psi|^2$. The linear term does not enter the expansion as in the case of the complex order parameter it breaks the gauge invariance which should be preserved for observable quantities.[109]

In Fig. 2.4 the typical result of the superconducting response in the three pulse experiment is presented (note logarithmic scale). The number of pump-probe traces at different $t_{\mathrm{D-P}}$ are shown. The amplitude of the signal recovers with $t_{\mathrm{D-P}}$, but the shape of the response varies significantly during the recovery.

To better understand the response, take into account the evolution of the order parameter during the pump-probe scans and develop a convenient way to extract the order parameter from measured data we provide a numerical simulation of the signal measured in a 3 pulse experiment. We base our simulation on the assumptions that the photoinduced transient reflectivity is proportional to $|\psi(t_{\mathrm{D-pr}})|^2$ and the relaxation is given by the order parameter dependent quasiparticle relaxation time $\tau = \tau_{\mathrm{QP}}/|\psi(t_{\mathrm{D-pr}})|$, here τ_{QP} is the absolute minimum value of the quasiparticle relaxation in equilibrium experiment (i.e. in the absence of the D pulse)[2]. This particular shape of the divergence has been observed in the experiments[64], [77]

[1] This drastically increases time of the experiment, so the special care should be taken to control long-term drifts of the laser power.

[2] This takes into account divergence close to the critical region but ignores the temperature and fluence contributions described by Eq. (1.12) , which are valid at low T.

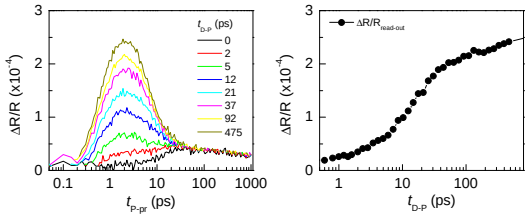


Figure 2.4: Left panel: Pump-induced transient reflectivity in a three pulse experiment in the superconducting state at different delays between the D and P pulses. Pseudogap component is subtracted (See Chapter 4 for discussion). Data for LSCO sample at 4 K $\mathcal{F}_{\rm D} = 18\ \mu{\rm J/cm}^2$.Right panel: read out of the amplitude of the pump-probe response from the left panel at $t_{\rm P-pr} = 2$ ps.

and theoretically described in [64], [100] (See also Section 1.2.3)[3]. The expression for transient reflectivity is:

$$\Delta R/R = |\psi(t_{\rm D-pr})|^2 \exp(-t_{\rm P-pr}/(\tau_{\rm QP}\,|\psi(t_{\rm D-pr})|))(1-\exp(-t/\tau_{\rm rise})), \qquad (2.1)$$

where $\tau_{\rm rise}$ is the order parameter independent rise time of the response. Though the exact shape of the $\psi(t_{\rm D-pr})$ is unknown we can approximate it with a solution of the TDGL equation if all but the lowest term in the right-hand side of the equation 1.31 are ignored. In this case the recovery of the order parameter has a simple exponential shape $\psi(t_{\rm D-pr}) = (1-\exp(-t/\tau_{\rm GL}))$.

As $\tau_{\rm GL}$ and $\tau_{\rm QP}$ can in principle differ[100] we consider several representative case: a) $\tau_{\rm GL} < \tau_{\rm QP}$, b) $\tau_{\rm GL} = \tau_{\rm QP}$ and c) $\tau_{\rm GL} = \tau_{\rm QP}$, but the gap dependence of the quasiparticle relaxation time is ignored. The last case is rather special as it does not correspond to the continuous phase transition but can take place in some special cases considered in Chapter 3. The results of the simulation are presented in Fig. 2.5 in solid lines [time is measured in numerical units (n.u.)]. To illustrate the effect of the change in the quasiparticle relaxation time we also plot quasiparticle response ignoring the gap dependence of the amplitude (shown with dashed lines), i.e.

$$\Delta R/R = \exp(-t_{\rm P-pr}/(\tau_{\rm QP}\,|\psi(t_{\rm D-pr})|))(1-\exp(-t/\tau_{\rm rise})). \qquad (2.2)$$

For the case c) these curves overlap so we plot them as a thick dashed line. The true trajectory $|\psi(t_{\rm D-pr})|^2$ is shown for comparison in blue dots. For all three cases the recovery of the amplitude at long delays ("hump" feature) observed experimentally (Fig. 2.4) is reproduced, moreover the amplitude of the "hump" is larger for faster recovery. After the peak of the hump the curves converge, but in the case c), in which the quasiparticle relaxation time is independent on the order parameter, the convergence is less pronounced. From the comparison of the simulation with the experimental data we conclude that the case b) is the most reliable approximation.

We proceed by formulating the inverse problem: how to extract the order parameter evolution from the measured data? To investigate this problem we compare two approaches to the extraction of the order parameter trajectory from the simulated data and compare them with the input trajectory. The first approach is the readout of the signal magnitude at a fixed early delay $\rm A_{read-out}$ (represented in Fig. 2.6 a)

[3]Here it's assumes that the the order parameter is proportional to the gap [91].

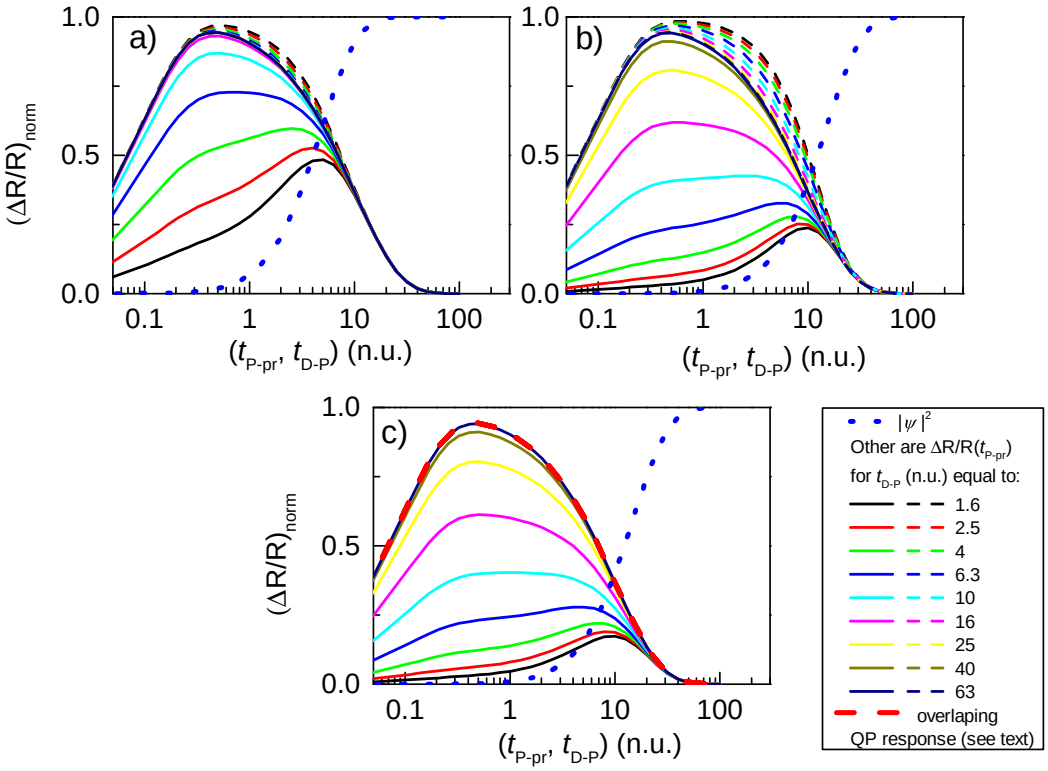


Figure 2.5: Simulation of the pump-probe response in the 3 pulse experiments. The quasiparticle response for a number of $t_{\mathrm{D-P}}$ delays is represented by solid lines (the abscissa is $t_{\mathrm{P-pr}}$). The quasiparticle response ignoring the gap dependence of the amplitude(See text) is represented by the dashed lines. Panels a)-c) correspond to the following cases: a) $\tau_{\mathrm{rec}} = 3.3$ n.u., $\tau_{\mathrm{QP}} = 10$ n.u., b) $\tau_{\mathrm{rec}} = \tau_{\mathrm{QP}} = 10$ n.u. and c) $\tau_{\mathrm{rec}} = \tau_{\mathrm{QP(eq.)}} = 10$ n.u. with relaxation time independent on $|\psi(t_{\mathrm{D-pr}})|$. In panel c) dashed lines overlap and are thus replaced by a single thick dashed red line. In every the panel recovery of the order parameter is shown with blue dots (the abscissa is $t_{\mathrm{D-P}}$). Time is measured in numerical units (n.u.).

by open blue squares). This approach gives excellent results as long as the readout delay is small in comparison to the order parameter recovery time. The second approach is to plot the maximum of the quasiparticle response $\mathrm{A_{max}}$ as a function of $t_{\mathrm{D-P}}$ [shown with black circles in Fig. 2.6 a)]. This approach is more definitive as it does not involve freedom of choice in delay selection. However it gives an erroneous result when compared to the true trajectory $|\psi(t_{\mathrm{D-pr}})|^2$ (black line). We also scale and shift both datasets from 0 to 1 to compare the characteristic recovery time. The resulting curves (shown with red crosses and black stars in Fig. 2.6 b) for the first and the second approach respectively) differ significantly. The read-out approach again shows much closer correspondence to the input trajectory.

In this section we investigated certain features of the three pulse experiment results. We however didn't considered inhomogeneities which are essential for the pump-probe experiments. More accurate simulations which take into account the inhomogeneities as well as other terms in the TDGL equations will be presented in Chapter 4.

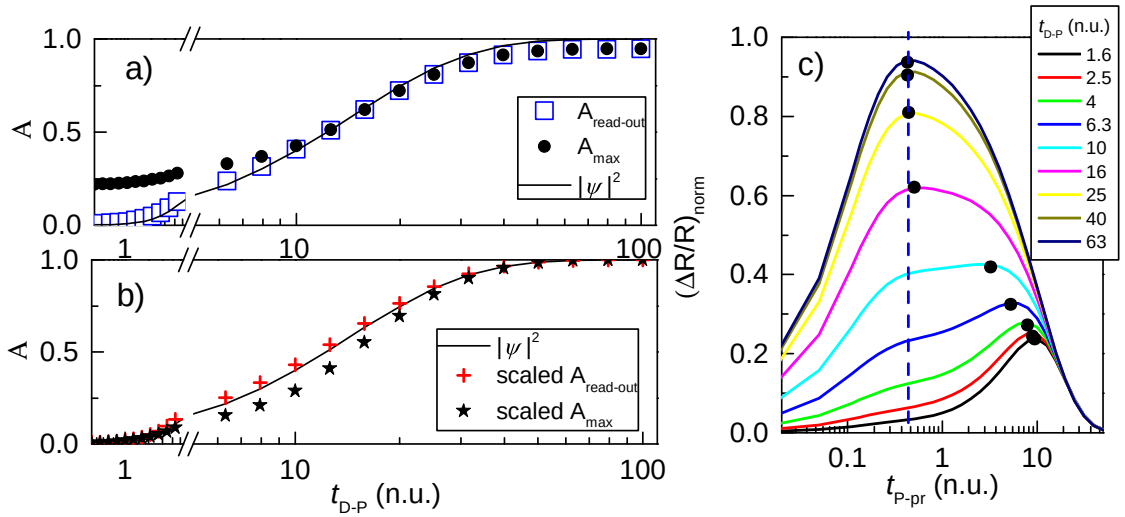


Figure 2.6: Comparison of different approaches to the data analysis. a) Analysis of the simulated data shown in panel c). The black circles are the maximum values of quasiparticle response A_{max} (shown with black circles in right panel) as a function of t_{D-P}. The open blue squares are the result of the read-out at 0.5 n.u. $A_{read-out}$ (shown as dashed blue vertical line in panel c) as a function of t_{D-P}. b) Scaled and shifted A_{max} and $A_{read-out}$ shown in black stars and red crosses respectively. The input trajectory $|\psi|^2$ is shown in black line in a) and b). c) The quasiparticle response for a number of t_{D-P} which corresponds to the case $\tau_{rec} = \tau_{QP} = 10$ n.u. Time is measured in numerical units (n.u.). $\tau_{GL} = 10$ n.u.

2.4 Description of the Ultrafast Response in Terms of Raman Susceptibilities and Polarization Selective Detection

In this section we will discuss how the pump-probe response can be described by means of Raman tensors. This knowledge is necessary for the description of the polarization dependence of the pump-probe response given in Section 3.2 and for understanding how the balanced detection scheme described further in this section allows to experimentally separate response of certain non-symmetric excitations.

Pump-probe experiments can be described as a two-step process (the pump excitation and the probe). In the first step, the *pump* pulse excitation can be divided into two processes: a dissipative excitation process (DE)[4] and an impulsive excitation (IE) process[110], [111]. The DE process is valid only after a real photon absorption has occurred, which results in a generation of a high energy photo-excited carriers. In following the carriers scatter amongst themselves and rapidly release their energy to the lattice within tens of fs, resulting in a transient nonequilibrium population of electrons, phonons, magnons, etc. The memory of the initial electron (or hole) momenta is assumed to be lost in the process.[5] If the excitation is not too intense, the DE process can be considered as a weak coherent perturbation of the QP density n_q near the Fermi level which does not cause a significant renormalization of

[4]This should not be confused with the displacive excitation of coherent phonons. Even though the two processes are close in the case of DE we do not talk about coherence.

[5]This assumption is rather safe for the metals, but might always hold.

the electronic structure. As a scalar n_q can linearly couple (only) to the symmetric A_g excitations. Which modes are excited in the IE process is determined by the opaque-media Raman tensor $\pi^R \sim \left(\frac{d\mathrm{Re}(\epsilon)}{d\omega} + 2i\mathrm{Im}(\epsilon)/\Omega\right)$[110], [111].[6] The off-diagonal terms can also cause non-A_g (non-symmetric) modes to be excited. In the pseudo-tetragonal (D_{4h}) symmetry, usually considered as appropriate for the parent structure in cuprates, for polarizations in the ab plane, A_{1g}, A_{2g} as well as B_{1g} and B_{2g} excitations can be excited. In this case the pump polarization defines which excitations will be excited.

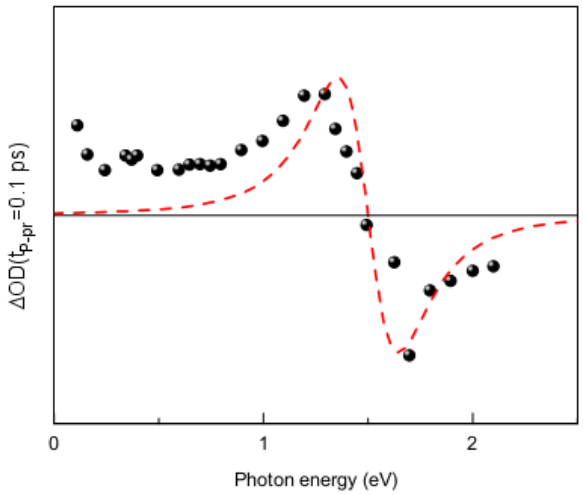


Figure 2.7: Spectral shape of the response in the cuprate Nd_2CuO_4. The wavelength dependence of the pump probe response (dots) compared to the derivative of the Lorentzian function corresponding to charge transfer transition at 1.5 eV. The data for $\Delta(OD)$ are from [112].

In the second step, i.e. the *probe* experiment, the transient change of reflectivity is recorded, which can also be described either as photoinduced absorption (PIA) or as an stimulated Raman scattering (SRS) process[110], [111]. In the former case the dielectric tensor defines the polarization selection rules. In the SRS process the polarization P_k due to a pump-induced change of n_q is given by: $P_k = \sum_l \mathcal{R}_{kl} E_l n_q$, where $\mathcal{R}_{kl} = \frac{\partial \epsilon_{kl}}{\partial n_q}$ is the Raman-like tensor, ϵ_{kl} is the complex dielectric tensor, and E_l is the l-th component of the electric field. In general the symmetry of the $\mathcal{R}_{kl}$ tensor is defined by the symmetry of the excitation produced by pump. In the following chapter we will also consider the possibility of a non-trivial symmetry of the $\mathcal{R}_{kl}$ even for the scalar excitation. We stress here that the treatment of the pump-probe response in terms of Raman susceptibility is not yet common. It is however highly probable to be applicable particularly because of the spectral shape of the response in cuprates. In the case of the resonant Raman processes involving long-live states

[6] Note that the first term in parenthesis describes the Raman process in the transparent media, whereas the second term sets in close to the absorption resonances. The second term is displacive in its principle but different form conventional displacive mechanism as in the impulsive case the excitations couple to the charge density in the excited state far away from the Fermi level.

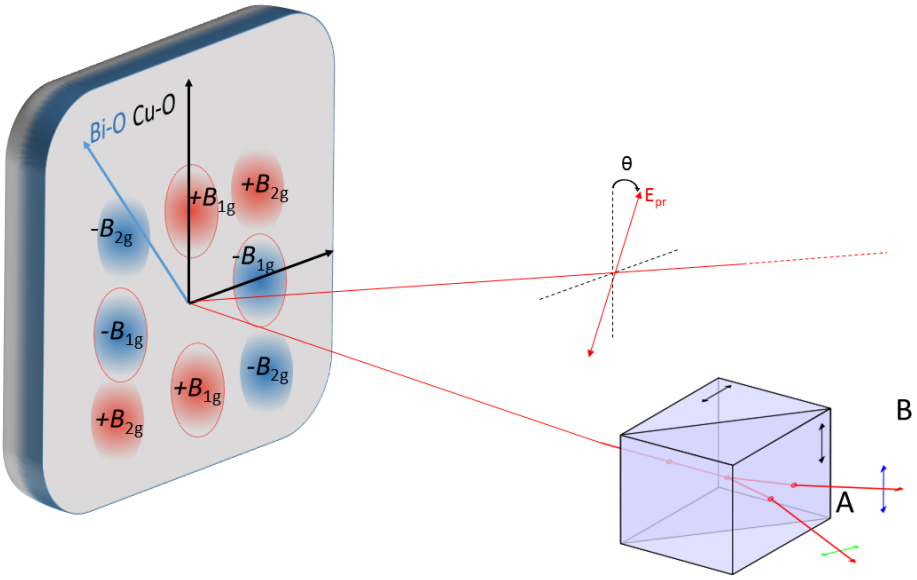


Figure 2.8: Description of the balanced detection scheme. The setup allows to directly measure different non-symmetric components. The Wollaston prism separates orthogonal component of the polarization into two different detectors (marked as A and B). The angle convention for BSCCO sample is given. Angles at which different contributions dominate are shown in colors (red and blue for positive and negative respectively). The B_{2g} regions are marked out by a red dashed circles.

the Raman tensor can be presented in the following form $\mathcal{R}_{kl} = (\frac{d\mathrm{Re}(\epsilon)}{d\omega} + i\frac{d\mathrm{Im}(\epsilon)}{d\omega})$. This has been shown to produce reliable description for the pump-probe response in semicnductors[111]. In Fig. 2.7 we compare the ultrafast response of the insulating Nd_2CuO_4 sample to the derivative over energy of the Lorentzian function which corresponds to the charge transfer transition at 1.5 eV (parameters of the Lorentzian were manually adjusted). A reliable overlap between the two is observed. We must note that this is not a proof of the Raman origin of the reseponse, but rather an indication of the option which is often omitted (alternatively, a similar line-shape of the response is expected due to the band shift in the result of heating).

Disregarding the excitation mechanism let us assume that modes of different symmetry are excited. Here we show how one can experimentally separate them out.

In the case of the D_{4h} point group the observable excitations are A_{1g}, B_{1g}, B_{2g} and A_{2g}. The dielectric tensor takes form:

$$\boldsymbol{\varepsilon_0}+\boldsymbol{\Delta\varepsilon}+\boldsymbol{c.c.} = \begin{pmatrix} \varepsilon_0 + \Delta\varepsilon(A_{1g}) + \Delta\varepsilon(B_{1g}) + c.c. & \Delta\varepsilon(A_{2g}) + \Delta\varepsilon(B_{2g}) + c.c. \\ -\Delta\varepsilon(A_{2g}) + \Delta\varepsilon(B_{2g}) + c.c. & \varepsilon_0 + \Delta\varepsilon(A_{1g}) - \Delta\varepsilon(B_{1g}) + c.c. \end{pmatrix}, \tag{2.3}$$

and the change in the reflectivity can be written as:

$$\Delta R/R \sim \frac{((\boldsymbol{\varepsilon_0} + \boldsymbol{\Delta\varepsilon} + \boldsymbol{c.c.}) \cdot \boldsymbol{E}(\theta)) \cdot ((\boldsymbol{\varepsilon_0} + \boldsymbol{\Delta\varepsilon} + \boldsymbol{c.c.}) \cdot \boldsymbol{E}(\theta))^*}{(\boldsymbol{\varepsilon_0} + \boldsymbol{c.c.})^2} - 1. \tag{2.4}$$

Writing the probe field as $\boldsymbol{E} = E_0 \begin{pmatrix} \cos\theta \\ \sin\theta \end{pmatrix}$ (θ is the angle between the laser light polarization and the Cu-O axis measured in the direction towards the a-sxis of the crystal (which is orthogonal to the Bi-O chains b-axis), as shown in Fig. 2.8) and expanding equation 2.4 the reflectivity change angular dependence reads:

$$\Delta R(\theta) = \Delta R_{A_{1g}} + \Delta R_{B_{1g}} \cos(2\theta) + \Delta R_{B_{2g}} \sin(2\theta), \tag{2.5}$$

the A_{2g} terms enters only in the second order and are thus omitted. As different components are orthogonal one can experimentally single them out. For this purpose we use a Wollaston prism based balanced detector schematically represented in Fig. 2.8. We schematically represent symmetry of the B_{1g} and B_{2g} modes in accordance to equation 2.5, blue and red color depict negative and positive contribution to the reflectivity respectively.

Let us assume that we want to single-out the $\Delta R_{B_{1g}}$. For this we set the θ to -45 deg so that the probe polarization is aligned along the $Bi-O$ direction. Further we rotate the Wollaston prism around the beam axis so that the intensity in both A and B diodes is equal. In this case we will detect in the B detector the light with the polarization component along the "vertical" (in the figure) $Cu-O$ direction and the orthogonal to it "horizontal" component in the A detector. The subtraction of two results in doubled $\Delta R_{B_{1g}}$ component, while B_{2g} and A_{1g} components are canceled. To single out B_{2g} component one needs to rotate the polarization by 45 degrees, and repeat the procedure: balance intensities by rotating the prism and subtract the signal.

The difficulty of this technique is in accurate alignment of the probe polarization with respect to the crystal axis. In practice we used following protocol. The temperature of the sample was set to the value where searched contribution, for instance $\Delta R_{B_{1g}}$, was absent (this information we've obtained from measurements polarization dependence at different temperatures). Then the polarization was roughly set to the proper direction. Fine adjustment was done by measuring the balanced response at different angles of the probe beam. The angle at which the response disappears corresponds to the desired orientation. Subsequently the temperature has been set to the desired value and experiment was conducted.

2.5 Fitting procedure

In the thesis we reported the values of the amplitudes and relaxation times extracted from fitting procedures. The amplitudes of the response are typically estimated from fitting several points in the vicinity of the peak by a parabolic function, the ordinate of the vertex of the parabola is then reported as the value of the amplitude. The values of the amplitudes are typically given without the error bars. The relaxation times are obtained from exponential fits, or fits of the sum of exponential functions if many components are present. For fitting (regresion analysis) and some of the data plots *Origin Pro* software was used. This software uses iterative algorithms (Levenberg-Marquardt) for the sum of squared residuals minimization. The error bars thus are the standard errors of the locally linearized non-linear fit.

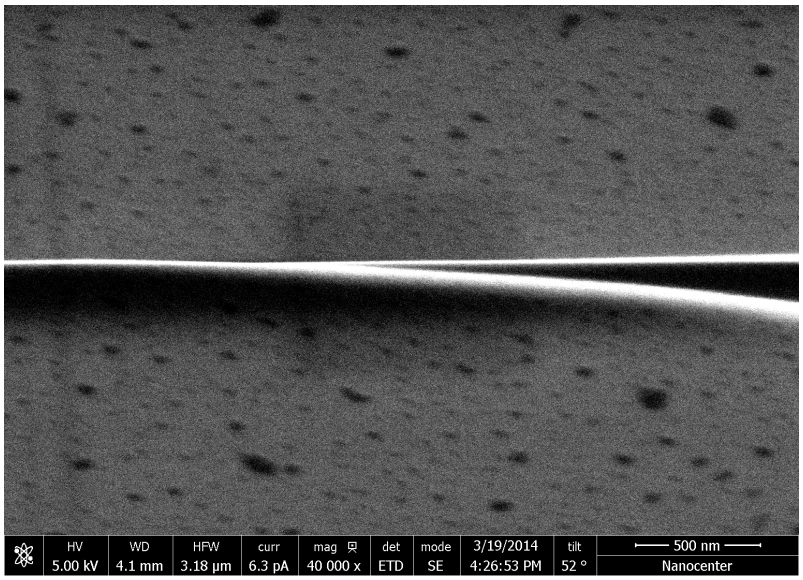


Figure 2.9: SEM image of the BSCCO surface after several months storage in the exicator. Note dark spots - products of degradation. The bright white lines are the edges of the separate flakes of the material

2.6 Samples

In the presented studies three families of cuprates were under investigation: $Bi_2Sr_2CaCu_2O_{8+\delta}$ (Bi2212 or BSCCO) with different dopings, $La_{1.9}Sr_{0.1}CuO_4$(LSCO) and $HgBa_2CuO_{4+\delta}$ (Hg1201 or HBCO) with different dopings synthesized, respectively, in Prof. M.Oda's (Hokkaido University) group by traveling solvent floating zone method, Prof S.Sugai's (Nagoya University) group by melting in the optical furnace, and Prof J.Karpinski's (ETH Zurich) and Prof. A. Sacuto (University of Paris Diderot) groups by gas media high pressure synthesis[113]. Samples were stored in the exicators. Before the measurements BSCCO and LSCO samples were cleaved by scotch tape or a sharp knife respectively. Optimally doped HBCO samples were impossible to cleave because of their small size ~100 μm and absence of a cleaving plane so they natural surface was measured. Underdoped Hg1201 surface has been polished with a 0.3 μm grain sandpaper. The necessity of the cleaving procedure is defined by the reactivity of the surface, in the case of BSCCO oxidation takes place and nanostructures are formed on the surface as can be seen in Figure 2.9.

Material	UD LSCO	BSCCO			HBCO		
		UD	OP	OD	UD	UD	OP
T_c(K)	28	81	85	80	68	79	90

Table 2.1: Samples under investigation and their critical temperatures.

The critical temperature of the samples was measured by means of the superconducting quantum interference device (SQUID) magnetometry by the synthesis groups. For optimally doped HBCO the magnetization data were not available and, as the samples were already mounted and thus unaccessible for SQUID, we estimated T_c from the temperature behavior of the quasiparticle relaxation time(see Chapter

6). The doping levels and the pseudogap temperatures were estimated from values given in literature[58].

For the polarization analysis the orientation of the sample is crucial. Polarization measurements on BSCCO sample in blue-red (400 nm pump and 800 nm probe) configuration were conducted by Prof. Toda (Hokkaido University). The satellite peaks of the Bi-O supermodulation in the X-ray diffraction pattern were used to identify the crystal orientation. Polarization measurements on BSCCO sample in red-red (800 nm pump and 800 nm probe) configuration conducted by the author. The samples were oriented in accordance to the natural cracking lines (which coincide with Cu-O directions) and further compared for consistency with the X-ray oriented samples. The results of the polarization measurements on HBCO are presented without independent X-Ray determination of the crystal orientation.

The material specific constant used in the thesis are presented in Appendix A.

Chapter 3

Pseudogap State Response, Photodestruction and Recovery

In this chapter we consider the ultrafast experiment in the high excitation regime in the pseudogap state in BSCCO sample. We start the chapter with a general overview of the experimental manifestations of the pseudogap and also give main theoretical approaches, this section will also cover observation of the charge order and its relation to the pseudogap phase. We present polarization studies of the pump-probe response with an emphasis on the symmetry breaking associated with different regions of the phase diagram and systematically study photodestruction of the pseudogap state. Here we will also cover polarization analysis in the metallic and superconducting state. Finally we examine the recovery of the pseudogap response and make conclusions about the spatial extent of the pseudogap order.

We cover only the issues necessary for further discussion. An interested reader is referred to reviews dedicated specifically to the pseudogap topic[13], [14], [114] and some which cover extensively the pseudogap within a more general consideration[7], [9], [20], [115].

3.1 Pseudogap: General Overview

The term "pseudogap" was introduced by Mott[116] to describe a state of matter which has a minimum in the density of states at the Fermi level, deep enough for the states to become localized. In further consideration, especially with regard to the cuprates, the localization aspect was put aside, although in our opinion it is still relevant. The pseudogap can arise either from the Coulomb repulsion between electrons, and/or an incipient charge or spin order, or be an indication of the electron pairing in the form of bipolaron or Cooper pairs[6], [13], [117]–[119]. Each of this scenarios is giving different relation to the superconducting order.

Even though pseudogap manifests itself in a vast number of experiments, the transition from the normal to the pseudogap state (if any exist) is broad, so that the onset temperature T^* , and the gap size Δ_{PG} defined by different techniques differ significantly reaching a factor of 2 difference (see Fig. 3.1). This leads to the still open discussion on the pseudogap in the overdoped region where the gap size and the onset temperature are approximately equal to those of the superconducting phase so that the two become hardly distinguishable, and thus it is not clear if the pseudogap onsets always above T_c or T^* crosses through the superconducting dome.

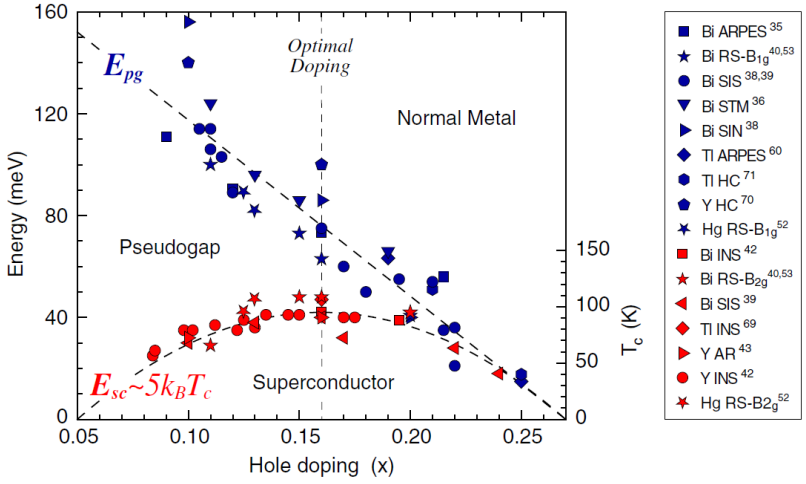


Figure 3.1: Pseudogap and superconducting energy scales for a number of cuprates. Compounds have similar $T_c^{max} \sim 95$K (Bi for Bi2212, Y for Y123, Hg for Hg1201 and Tl for Tl2201). The legend indicates the material, technique and the reference according to the bibliography of ref. [114]. Adopted from [114].

Some authors advocate that one of this scenarios is valid for the gap size whereas the other stands for the onset temperature behavior.[120]

Most of the experimental probes do not have the wavevector resolution. In this sense Raman spectroscopy (RS) and even more ARPES significantly advanced the phenomenology of the pseudogap. RS response has selection rules with regards to different regions of the Brillouin zone schematically represented in Figure 3.2. For the light polarization which transforms as B_{1g} charge excitations corresponding to the antinodal regions of the Fermi surface are probed, whereas when the scattered and incident light are transformed as B_{2g} light couples predominantly to the excitations of the nodal region. From the doping dependence of the Raman peaks seen in the corresponding symmetry channels one can attribute the pseudogap gap to the antinodal and the superconducting gap to the nodal parts of the Fermi surface. In the recent report[80] Sakai et al. suggest the presence of pseudogap response also in the B_{2g} channel which can be considered as a signature of the s-wave nature of the PG state. This last observation contradicts the prevailing view but indicates that the issue has not been settled so far.

ARPES gives the most pictorial representation of the pseudogap on the Fermi surface. As can be seen in Fig. 3.3 c) the pseudogap has the $k-$dependence similar to the superconducting gap: the gap increases towards the antinodes and has a comparable amplitude. The important difference however is that the superconducting gap goes to zero in the four points of the Fermi surface whereas in the pseudogap state there is a continuous $(\pi/2, \pi/2)$ centered zero gap region - the Fermi-arc. The presence of the arc has been interpreted as an indication of non-Fermi-liquid behaviour[7], [122], or contrary the Fermi surface exist in the form of small hole pockets due to Fermi-surface reconstruction and arcs "illusion" is just the consequence of the matrix-element sensitivity to this region of the Fermi surface[123]. Recently Reber et al.[124] pointed out that the analysis of the ARPES data and consequent representation can lead to significantly different conclusions, they argued that the Fermi-arcs appear due to the spectral weight shift from the initial d-wave gap due

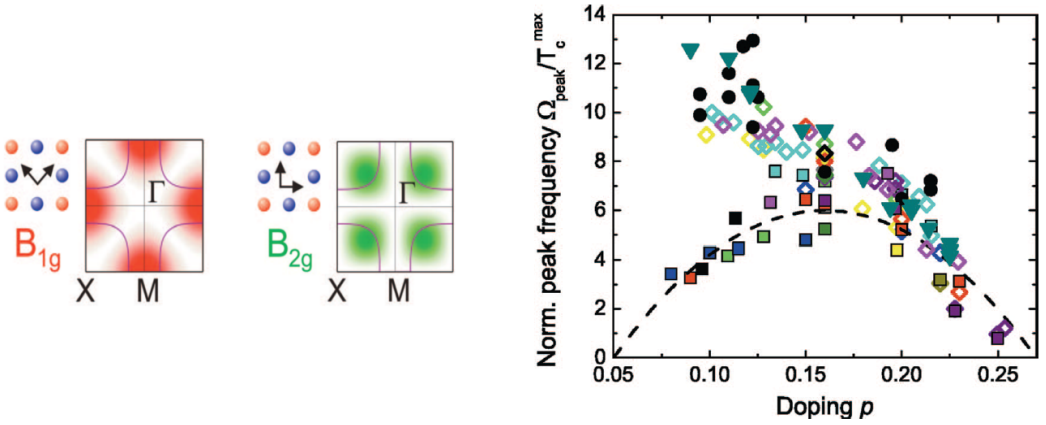


Figure 3.2: Schematic weighting of the RS transition for a polarization orientations transforming as B_{1g} and B_{2g} representation. Solid line represents the Fermi surface of the cuprates. On the right panel the scattering peak energy as a function of doping for a number of materials is presented, diamonds and squares correspond to the B_{1g} and B_{2g} channels, respectively. For comparison ARPES (circles) and the peak-to-peak energy in the tunneling differential conductance measurements (triangles) are shown. Figures are adopted from [121].

to pair breaking processes. A full gap by their opinion exists also in the pseudogap state and corresponds to the preformed pairs.

As we have already mentioned in Introduction there is no thermodynamic evidence of the phase transition, i.e. the thermodynamic potentials together with their first and second derivatives are continuous, at T^* (see for instance [125]). The absence of such phase transition seemingly contradicts the observation of broken symmetry states of different kinds: broken rotational and translational symmetries observed in scanning tunneling spectroscopy (STS) experiments[33], [126](see also the following section for the pump-probe symmetry analysis) and the time-reversal symmetry breaking observed in measurements of the Kerr effect[31]. The STS results already hint that the order lacks long-range order, which might explain the thermodynamic results. This conclusion is however not solid as the STS technique is surface sensitive and also obviously measures the pinned order only. The fluctuating order in the bulk, however, can develop correlations long enough to produce collective modes[127] but can be easily missed by the static techniques. The question of a charge density wave order as an origin of the pseudogap phenomenon was recently reinvigorated by resonant X-ray scattering data, which confirmed bulk nature of the charge modulation observed by STS and showed that their onset temperature follows the PG onset T^*[25], [26], while previously the charge order was believed to onset below T^* and was attributed to the 1/8 anomaly (see for instance the phase diagram in Fig. 1.2 adopted from [6]). In the Section 3.4 we will discuss how the pump-probe experiments can contribute to the discussion of the spatial extent of the pseudogap state.

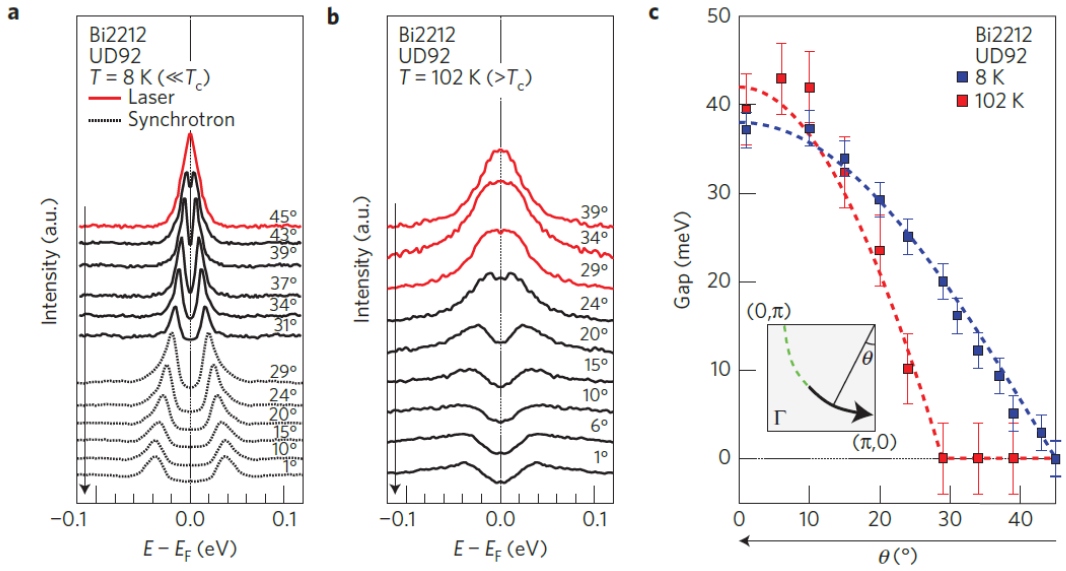


Figure 3.3: ARPES data on superconducting gap and pseudogap in the underdoped BSCCO sample (T_c=92 K). a) and b) Symmetrized spectra at the number of different cuts of the Fermi surface (see inset to c) for angle notation) in the superconducting and pseudogap state respectively. c) Gap magnitude obtained from data shown in a) and b). The figure is adopted from [7].

3.2 Pump-probe Response in BSCCO: Temperature and Polarization Study

In this section we present our study of the temperature dependence of the pump-probe response with an emphasis on the polarization properties. Discussion of the pump-probe response in terms of the Raman tensors can be found in Section 2.4. Discussion of this section extends beyond the pseudogap topic of the chapter and also covers polarization analysis of superconducting response. The fluence dependence will not be covered here but is discussed in corresponding further sections.

With regards to polarization selection rules it is important to discriminate two possible mechanisms of the quasiparticle excitation: a) The impulsive stimulated Raman scattering [111] and b) the dissipative excitation (Fig. 3.4).[1] The former process is coherent thus in the case of the excitation of the non-symmetric modes the pump-probe response should be dependent on polarizations of both the pump and the probe. If the dissipative mechanism (which was assumed implicitly in our previous discussion) is the dominant channel of the quasiparticle excitation there is no expected dependence on the pump polarization.

In Fig. 3.5 we present the result of the probe polarization dependence for different orientations of the pump polarization. No change in the probe response anysotropy

[1]Typically the Raman scattering cross-section ($\sim 10^{-12}$) is too low to be detectable with pump-probe sensitivity ($\sim 10^{-6}$) however stimulated processes are non-linear and therefore can be in principle observed, the cross-section is further increased as the excitation wavelength (1.55 eV) approaches the charge-transfer gap, so that scattering becomes resonant. In order to have stimulated process photons of energies which differ by the excitation energy (the gap energy for electronic RS) must be simultaneously present. This condition is typically satisfied for pulses from Ti:Sapphire sources ($\Delta E_{\mathrm{FWHM}} \sim 80$ meV), and the pseudogap energies ($E_{\mathrm{PG}}^{\mathrm{opt.doping}} \sim 40$ meV).

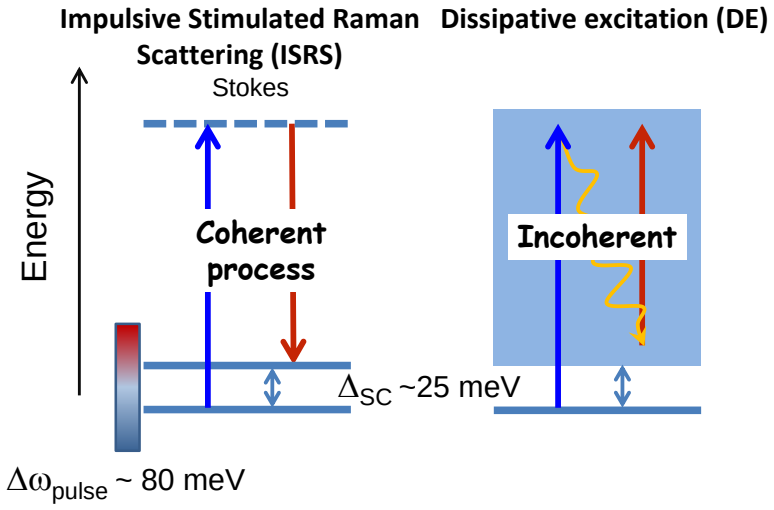


Figure 3.4: Schematic representation of the two possible mechanisms of quasiparticle excitation. Impulsive stimulated Raman Scattering is possible because the ultrafast pulse spectral width is broader than the excitation energy.

is observed indicating that dissipative mechanism is dominant.

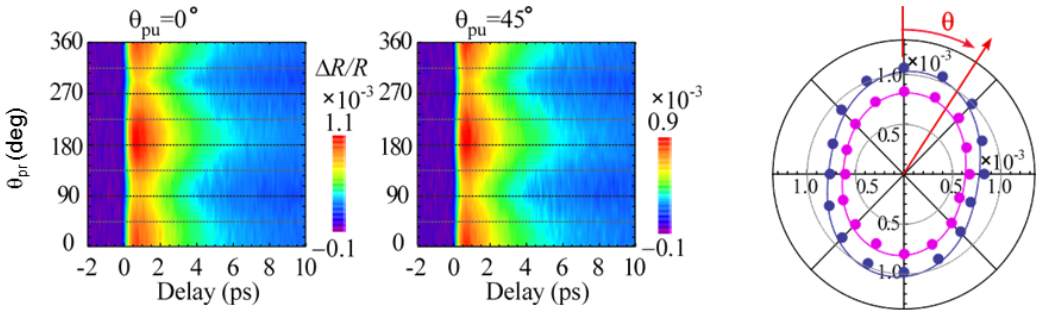


Figure 3.5: The probe polarization dependence for pump polarizations rotated by 45 deg (pump wavelength is 400 nm) at 10 K. No change in the anisotropy is observed. The variation in the intensity are due to the difference in the transmitivity of dichroic elements for different polarizations. In polar plot maximum value of the $\Delta R/R(\times 10^{-4})$ as a function of probe polarization angle is shown.

Let us discuss the dependence of the pump-probe response on the polarization of the probe beam. In the dissipative mechanism excitations of different symmetries are created stochastically and their effect on the dielectric tensor is averaged out, at

the same time the system is characterized by the time-dependent scalar densities of different excitations which can couple only to the totally symmetric representation of the dielectric tensor. In the case of the cuprates the CuO_2 planes possess the D_{4h} point symmetry and thus no dependence on the probe polarization is expected. In experiments however we clearly observe such dependence with characteristic time and temperature evolutions, which, as we will elaborately discuss below, can be explained by the reduction of the parent D_{4h} symmetry. For the description of the experimental data in order to keep agreement with Raman experiments we will use the convention of the D_{4h} group, and discuss the relation with lower symmetry groups where necessary.

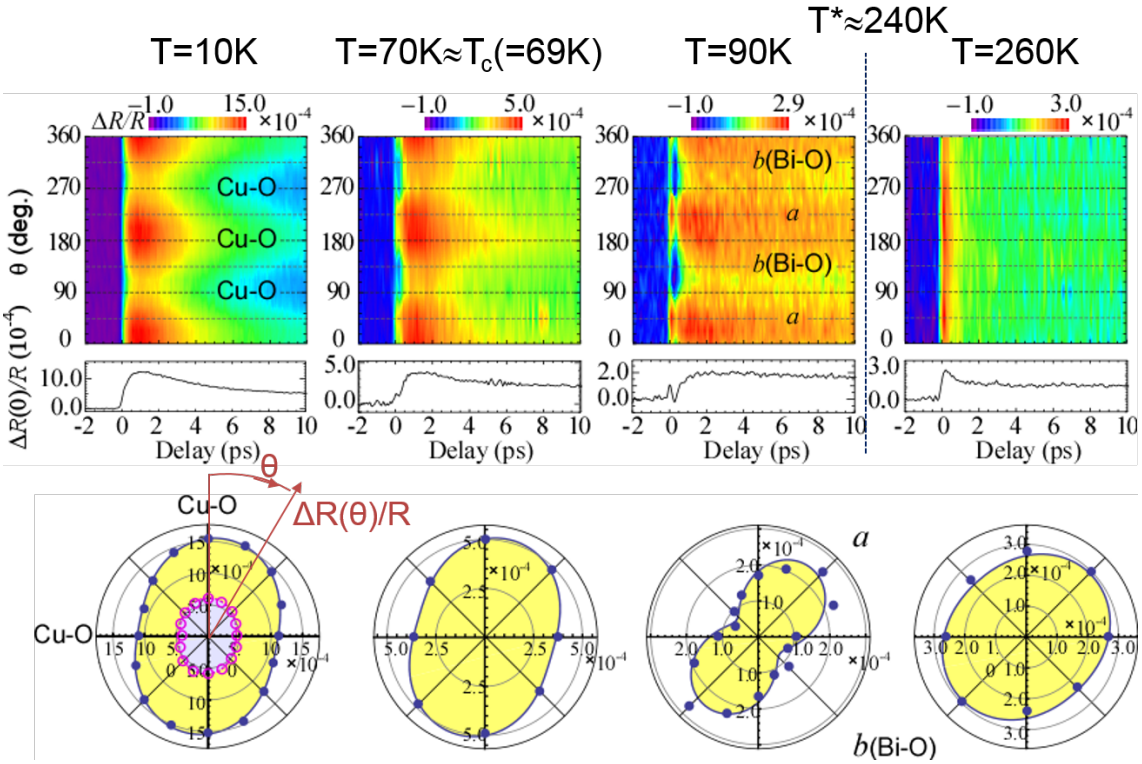


Figure 3.6: The probe-polarization dependence under excitation with 400 nm pump. The measurements are conducted in the superconducting state (T=10 K), just above T_c (T=70 K), in the pseudogap state (T=90K) and in the normal state. T_c = 69 K. Polar plots show maximum value of the $\Delta R/R(\times 10^{-4})$. The crystal axis as well as Cu-O direction and angle convention are designated.

It was previously shown[111] that the pump-probe response can be described with a Raman-like tensor $R^{\mathbf{q}}_{kl}$ (see Section 2.4 for detailed discussion). Indeed, the polarization of the medium when the distribution function has been changed by the pump pulse by $\delta f(q)$ (we consider a general case of a q-dependent change to the distribution function) is given by $P_k = \Sigma R^{\mathbf{q}}_{kl} E_l \delta f(\mathbf{q})$, where E_l is the l-th component of the probe pulse electric field and $R^{\mathbf{q}}_{kl} = \frac{\delta \epsilon_{kl}}{\delta f(\mathbf{q})}$ by definition. In the D_{4h} symmetry changes to the dielectric tensor can be decomposed into

$$\Delta\epsilon = \begin{bmatrix} \Delta\epsilon^{A_{1g}} & \\ & \Delta\epsilon^{A_{1g}} \end{bmatrix} + \begin{bmatrix} \Delta\epsilon^{B_{1g}} & \\ & -\Delta\epsilon^{B_{1g}} \end{bmatrix} + \begin{bmatrix} & \Delta\epsilon^{B_{2g}} \\ \Delta\epsilon^{B_{2g}} & \end{bmatrix} + ..., \quad (3.1)$$

Writing the probe field as $E = E_0 \begin{pmatrix} cos\theta \\ sin\theta \end{pmatrix}$ (see Fig. 3.6 for angle convention) the change in the reflectivity reduces to

$$\Delta R(\theta) = \frac{\partial R}{\partial \epsilon_1}(\Delta\epsilon_1^{A_{1g}} + \Delta\epsilon_1^{B_{1g}} cos(2\theta) + \Delta\epsilon_1^{B_{2g}} sin(2\theta)) +$$
$$+\frac{\partial R}{\partial \epsilon_2}(\Delta\epsilon_2^{A_{1g}} + \Delta\epsilon_2^{B_{1g}} cos(2\theta) + \Delta\epsilon_2^{B_{2g}} sin(2\theta)) = \quad (3.2)$$
$$= \Delta R_{A_{1g}} + \Delta R_{B_{1g}} cos(2\theta) + \Delta R_{B_{2g}} sin(2\theta). \quad (3.3)$$

The expression above gives the possibility to discriminate excitations of different symmetry by decomposing the angular dependence of the pump-probe response into orthogonal components.

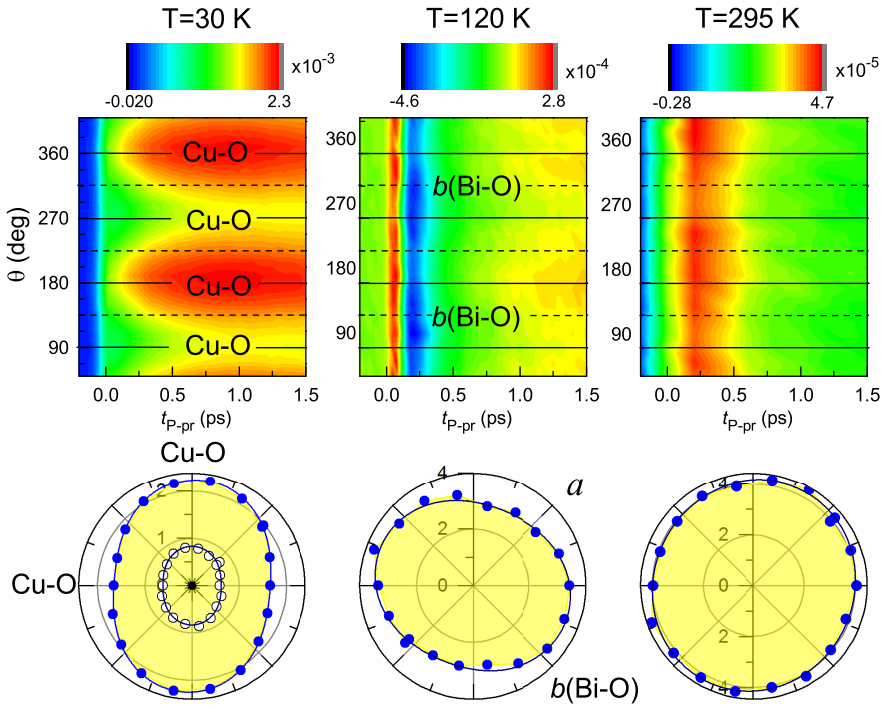


Figure 3.7: The probe-polarization dependence under excitation with 800 nm pump. The measurements are conducted in the superconducting state ($T = 30$ K), in the pseudogap state ($T = 120$ K) and in the normal state. $T_c = 81$ K. Polar plots show the magnitude of the $\Delta R/R(\times 10^{-4})$ (at 30 K open circles correspond to the $\Delta R/R$ readout at 20 ps scaled for visibility). Note that in the polar plot at 120 K the magnitude of the negative pump-probe response is shown, which results in apparent difference as if compared to Fig. 3.6 where the negative PG component appears on the wing of the positive hot electron energy relaxation component.

In Fig 3.6 we present the results of a set of probe polarization studies for different temperature regions conducted with $\lambda_{pump} = 400$ nm on the UD sample ($T_c = 69$ K) by Prof. Toda in Hokkaido. At temperatures above T^* the response is nearly isotropic but it shows clear anisotropy in the pseudogap and superconducting states. We remind here that no dependence on the pump beam polarization has been observed. Remarkably the major axis of the anisotropy in the superconducting state

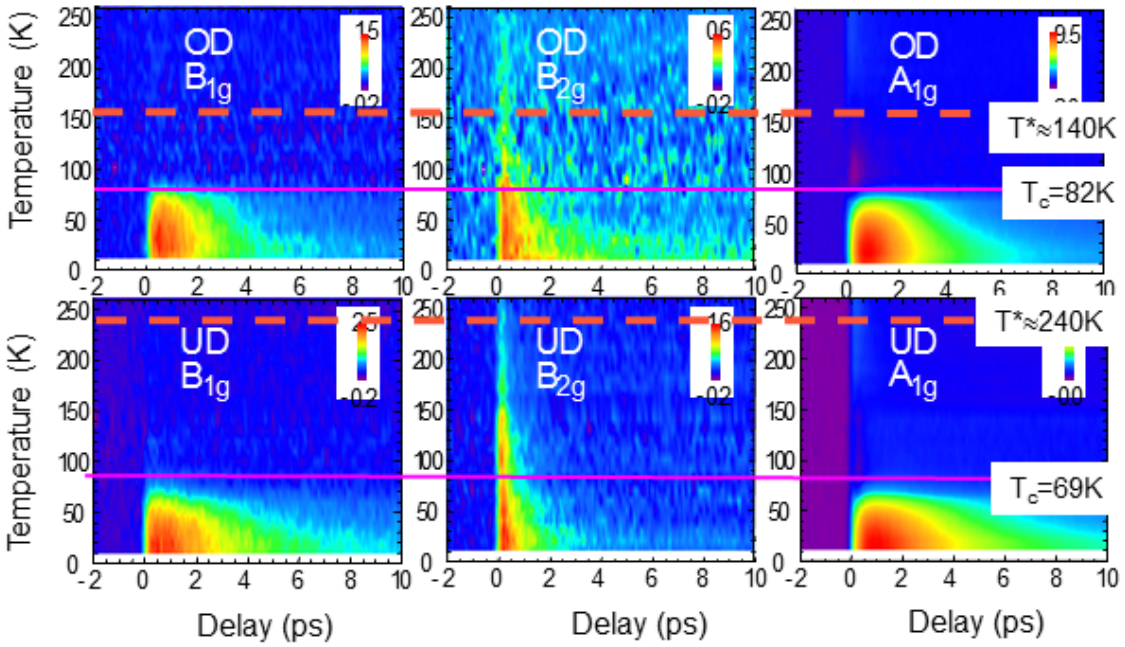


Figure 3.8: Temperature dependencies of the B_{1g}, B_{2g} and A_{1g} components obtained from fits by equation (3.3) for overdoped and underdoped samples. SC and PG responses appear in B_{1g} and B_{2g} symmetries respectively. Both components and the hot-electron energy relaxation component are present in A_{1g} response.

is $\sim$ 45 deg. rotated with respect to that observed in the pseudogap state, and coincides with the Cu-O direction in contrast to crystal axis (Bi-O) alignment of the pseudogap response. By fitting the response $\Delta R(\theta)/R$ at each delay to the equation (3.3) one can discriminate time and temperature evolutions of each component. The results of the fits are presented in Fig. (3.8). The B_{1g} component has the temperature dependence and the relaxation time (>2 ps) characteristic of the superconducting response. In contrast, the B_{2g} component corresponds to the previously singled-out in wavelength dependent experiments[79] PG response: it shows a gradual appearance upon cooling and a fast (<1 ps) relaxation time. Both, the superconducting and the pseudogap, as well as hot electrons energy relaxation are present in the symmetric A_{1g} component of the response, which is the strongest and thus data appear less noisy. Note that the pseudogap response has a negative sign.

In Fig. 3.7 we provide the results of the transient reflectivity probe angular dependence measurements with λ_{pump} =800 nm excitation conducted in Ljubljana on the UD sample (T_c=81 K) . While the result is qualitatively similar there are certain differences. Specifically the anisotropy of the pseudogap response appears to be much weaker, but still detectable even at room temperature.[2] Here we must note that for these measurements we did not orient the crystal with the X-ray diffraction, the crystal axis are estimated directly from the long-lived component anisotropy at low temperatures (the anisotropy axes are assumed to be parallel to the Cu-O direction according to the data presented above). Remarkably this direction coincides with the preferential orientation of the macroscopic cracks observed under

[2]Unfortunately measurements were not conducted on the same sample so we cannot exclude that the phenomenon is sample specific.

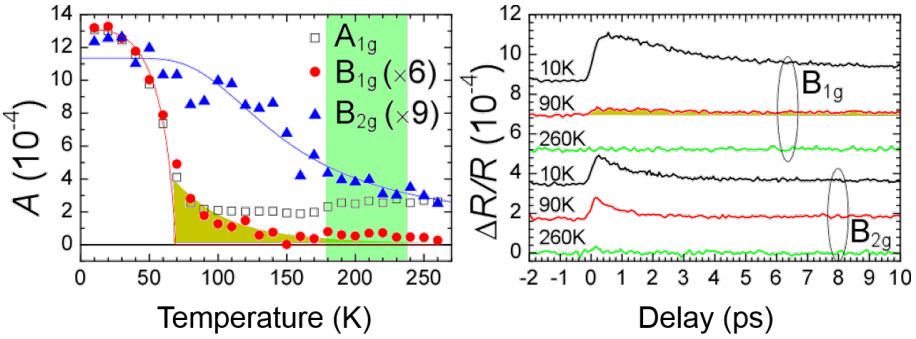


Figure 3.9: Temperature dependence of the amplitudes of the non-symmetric components. Left panel: Temperature dependencies of the B_{1g}, B_{2g} and A_{1g} component amplitudes for the underdoped sample. Solid lines are fits by Eq. (1.7) and (1.5) for the B_{1g} and B_{2g} components respectively. Right panel: Representative transient reflectivity traces at characteristic temperatures for the B_{1g} and B_{2g} components.

the optical microscope. Note that for the 120 K polar plot we present the magnitude of the negative response so it appears rotated 90 degrees when compared to the case of with λ_{pump} =400 nm shown in Fig. 3.6, where negative component appeared on the wing of the stronger isotropic positive component.

Fig. 3.9 shows the temperature dependence of the amplitudes of different components for λ_{pump} = 400 nm excitation. Below T_c the amplitude of the B_{1g} component is well fitted by Eq. (1.7) assuming the BCS temperature dependence of the gap. Note that the pump fluence was just above the photodestruction fluence $\mathcal{F}_{\rm th}^{400nm} = 1\,\mu{\rm J/cm}^2$ in these experiments. Above $T_{\rm c}$ the signal is still significant (filled region) and can be ascribed to the superconducting fluctuations described in Chapter 5. The B_{2g} component is fitted by the temperature independent gap model given by Eq. (1.5). Obtained gap value is 41 meV for the UD sample in reasonable agreement with other estimates of the pseudogap on the similar samples[58].

The only explanation of the observed probe polarization dependence in the absence of the coherent ISRS process is a reduction of the parent D_{4h} symmetry due to the presence of a dynamic, local or hidden order. First we must note that for Bi2212 the D_{4h} lattice symmetry is strictly speaking broken already above the room temperature by the incommensurate Bi-O super modulation[128]–[130]. In resulting D_{2h} point group the B_{2g} excitations of the parent group become fully symmetric and can thus be excited via the DE mechanism. The coherent excitation of the B_{1g} modes requires however a further reduction of symmetry down to C_{2h}, which by taking into account presence of a significant response due to superconducting fluctuations occurs already above T_c. This symmetry reduction cannot be explained by the presence of the Bi-O supermodulation.

Importantly the B_{2g} modulation is present only in the pseudogap response and not in the room-temperature component indicating that its presence is not a simple consequence of underlying orthorombicity. With this regard it is remarkable also that the superconducting component does not appear in the B_{2g} channel.

Despite the fact that the superconducting gap has the d-wave symmetry correspondent to the B_{1g} transformation the observed polarization dependence cannot be linked directly to the gap symmetry. Because the SC order parameter is a complex number it can enter optical constants only as integer powers of $|\Delta|^2$ and consequently

contribute only to the A_{1g} channel. This is consistent with the strong A_{1g} response observed in our experiments.

The appearance of the B_{1g} response can be explained by the underlying lattice modulation oriented along the Cu-O bonds. This unidirectional bond-centered modulation has been previously observed on the surface in the electron-hole asymmetry map measured by STS[33]. Noting that in our experiment the probe penetration depth is above 100 nm and the B_{1g} anisotropy $(\Delta R/R)_{B_{2g}}/(\Delta R/R)_{A_{1g}}$ exceeds 10 % we conclude that this stripe order persists in the bulk of the sample.

The absence of the superconducting response in the B_{2g} channel can be explained by the sensitivity of the Raman vertex to the $(\pm\pi/2, \pm\pi/2)$ direction, where the superconducting gap has the nodes. On the other hand the appearance of the pseudogap component in the B_{2g} response suggests the presence of the pseudogap even in the nodal direction as suggested also by the recent Raman and cellular dynamical mean-field studies[80]. The absence of the pseudogap in the PG response in the B_{1g} channel suggests a weak coupling of the PG excitations to the underlying in-plane order in contrast to the apparently strong coupling of the superconducting order.

As our experiment is stroboscopic and we average over 125 000 pulses the observed symmetry breaking should be persistent at least on the time-scale of the distance between the pulses ($\sim 4\,\mu s$). While the Bi-O supermodulation is known to be static and have a long range character meaning that experiments are most likely conducted on a single domain, modulation in the Cu-O_2 planes appears to be short range and the orthogonal contributions are expected to average out. The observed anisotropy can thus be explained by extrinsic defect structure or strain, orienting the Cu-O_2 planes modulation.

3.3 Photodestruction of the Pseudogap State

First we present photodestruction of the pseudogap state results measured in the conventional two-pulse experiments. Let us first summarize the phenomenology of the pump-probe response before we proceed to the fluence dependence. The photoinduced reflectivity ($\Delta R/R$) below T^* ubiquitously shows two relaxation components [Fig.3.10a)]. One is the PG response (which appears as a photoinduced decrease in the reflectance, and whose amplitude we define as A_{PG}) and the other arising from the hot electrons energy relaxation (and appears as an increase in the reflectance)[63], [79]. The hot electron energy relaxation component does not change with temperature[79], whereas A_{PG} gradually appears upon cooling [Fig.3.10a)].

In Fig.3.10 c) we show the normalized fluence dependence of $\Delta R/R$. At low fluence both components increase linearly with $\mathcal{F}$, so the initial few traces overlap when normalized. However, starting from some threshold value $\mathcal{F}_{\mathrm{th}}$ the negative PG component begins to saturate while the hot electron energy relaxation component remains linear with $\mathcal{F}$ up to the highest measured fluence of $500\mu\mathrm{J}\ /cm^2$.

In Fig. 3.10 f) and g) we plot the fluence dependence of the amplitude A_{PG} of the pseudogap response at different temperatures and dopings, respectively, normalized to the saturation value (here and further on we plot the absolute value of the peak amplitude of the pseudogap component). We assume that the linearity of A_{PG} and correspondingly the density of the photoexcited quasiparticles is preserved until all the carriers forming the state are excited, i.e. the pseudogap is destroyed, in accordance to the model described in Section 1.2.4. Inhomogeneous excitation arising

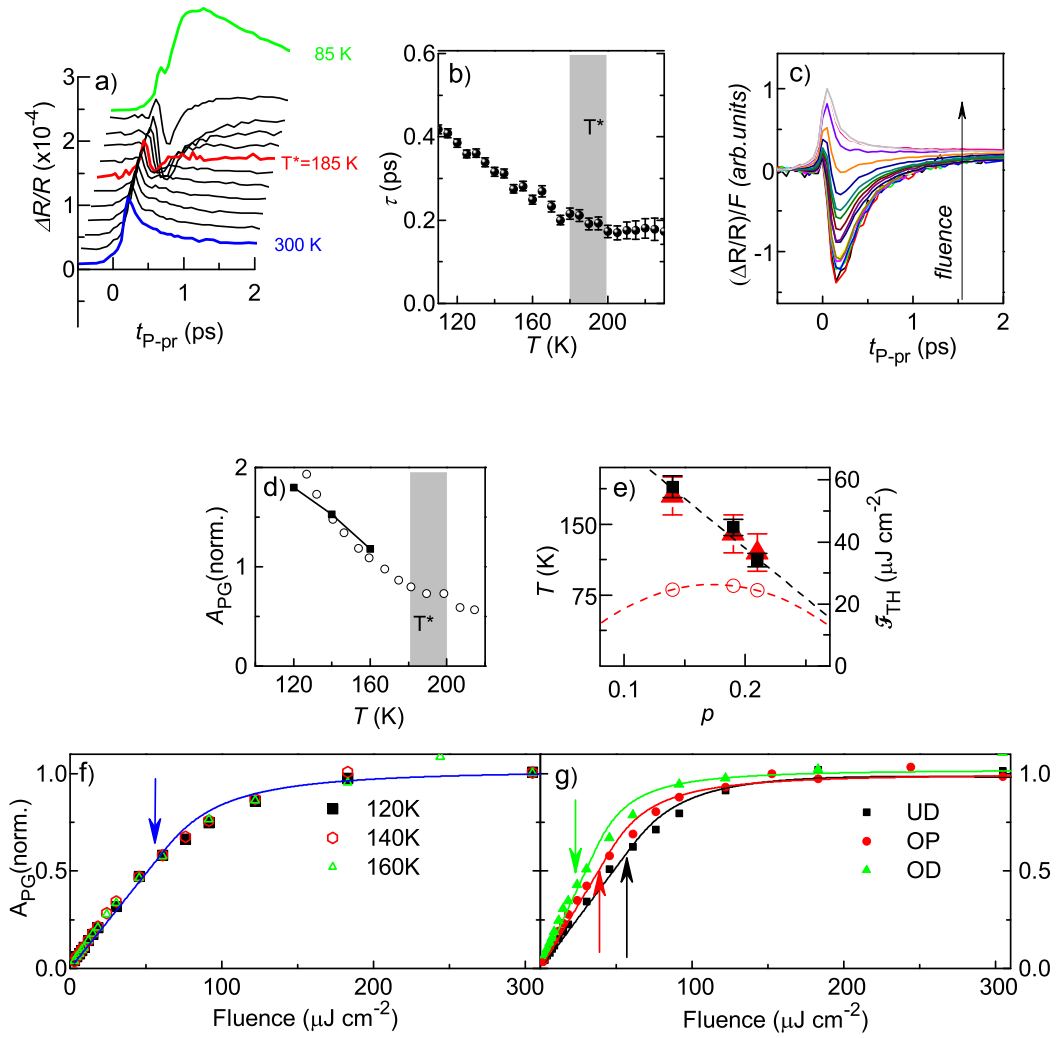


Figure 3.10: Pseudogap response as a function of fluence. a) A waterfall plot of $\Delta R/R$ as a function of pump-probe delay in the temperature region from 85 K to 300 K. b) The relaxation time of the negative pseudogap component as a function of temperature c) The transient reflectivity normalized by the incident fluence $(\Delta R/R)/\mathcal{F}$ for the underdoped sample at 120K. At low excitation the response is linear and the curves overlap. At low excitations the negative pseudogap component is dominant, whereas at high excitations it is saturated and the hot-electron energy relaxation component is prevailing. d) The amplitude of the saturated pseudogap signal ($\Delta R_{\mathrm{SAT}}/R$) as a function of temperature (black squares). For comparison the normalized low fluence temperature dependence of the amplitude from [79] is plotted (open circles) e) The value of the photodestruction threshold fluence (black squares, right axis) as a function of doping. For comparison the doping dependencies of T^* (red triangles) and T_c(red circles) are shown in the same plot. f) Normalized fluence dependence of the amplitude of the pseudogap component at different temperatures for the underdoped sample. The threshold fluences are marked by arrows. g) Normalized fluence dependence of the pseudogap component amplitude for different doping levels: underdoped (UD) at 120 K, optimally doped (OP) at 120 K and overdoped (OD) at 110 K, the threshold fluences are marked by arrows.

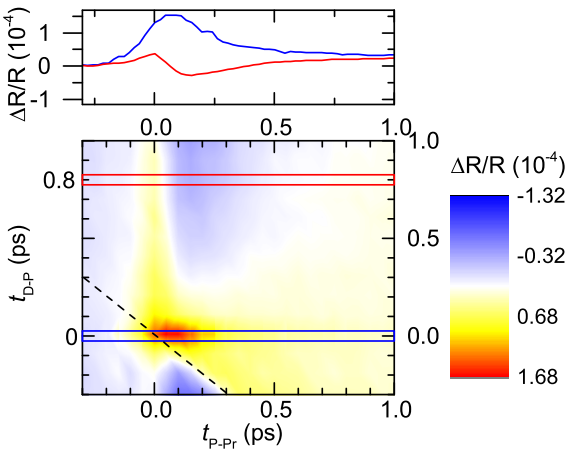


Figure 3.11: Typical result of the three pulse experiment. Underdoped sample at 120 K, the D pulse fluence is 204 μJ cm^{-2}. The time of the D pulse arrival is shown by the dashed line. The D pulse suppresses the negative pseudogap component, whereas the hot electron energy relaxation response remains intact (Readout at $t_{\mathrm{D-P}} = 0$ ps is shown on the top panel in blue). Note that at later $t_{\mathrm{D-P}}$ the positive component is masked by the stronger negative PG component with a slower rise time. The readout at $t_{\mathrm{D-P}} = 0.8$ ps is shown on the top panel in red.

from a finite light penetration depth rounds the kink in the fluence dependence. Fits with equations (1.15), (1.16) to the data are shown by solid lines in Fig. 3.10 f) and g).

As shown in Fig. 3.10 f), $\mathcal{F}_{\mathrm{th}}$ is not very temperature dependent. The value of $\Delta R/R$ at the saturation decreases with increasing temperature [shown in black squares in Fig. 3.10 d)] and follows the T-dependence of A_{PG} in the weak excitation regime [open circles in Fig. 3.10d)]. In Fig. 3.10g) we plot the fluence dependence of A_{PG} for three different doping levels. The fluence dependence is very similar for all doping levels, but differs in the threshold value. $\mathcal{F}_{\mathrm{th}}$ increases monotonically with T^*, and accordingly decreases with doping [Fig. 3.10e)]. Estimated heating corresponding to the largest value of $\mathcal{F}_{\mathrm{th}} = 58\,\mu\mathrm{J}/cm^2$ for the underdoped sample is ~6 K, so the effects we observe are clearly of a non-thermal origin.

3.4 Recovery of the Pseudogap State

To investigate the recovery of the pseudogap state, we measure the time-evolution of A_{PG} through the transition with the three pulse technique schematically described in Section 2.3. In this experiment we use an additional strong "destruction" (D) pulse ($\mathcal{F}_{\mathrm{D}} = 14 - 204\,\mu$J cm^{-2}) to destroy the state and probe the evolution of the quasiparticle response by performing the pump-probe (P-pr) experiment at variable delays between the D and P pulses.

Typical results of these experiments are shown in Fig. 3.11 for the UD sample. First, we note that the *hot electron energy relaxation response* remains unaffected by the D pulse. This is additionally confirmed by the 3 pulse experiment at room temperature, i.e. above T^*, where the response has not been suppressed at all. This allows us to subtract the hot electron energy relaxation component in all further

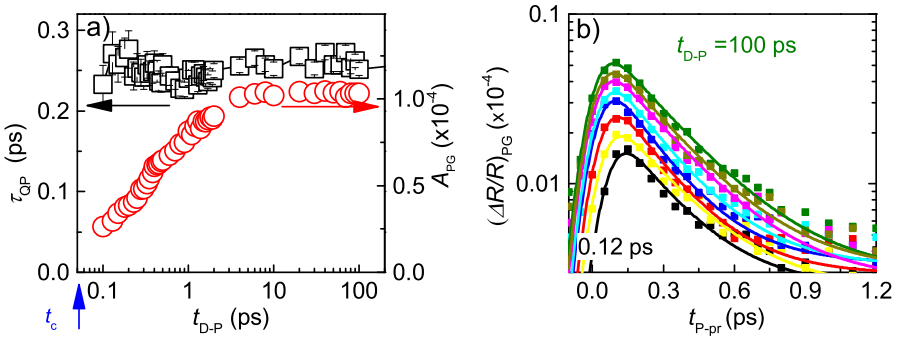


Figure 3.12: Evolution of the pseudogap resonse amplitude and the QP relaxation time. Left: The quasiparticle relaxation time (black dots, left axis) and the amplitude (red open circles, right axis) of the pseudogap component (data shown in inset) as a function of $t_{\mathrm{D-P}}$. The quasiparticle relaxation time remains constant for all values of t_{D-P} . Right: The pseudogap component for different values of $t_{\mathrm{D-P}}$ ($\mathcal{F} = 204\mu\mathrm{J}\ cm^{-2}, T = 120$ K).

data analysis. The pump induced *pseudogap response* is suppressed at the moment when the D pulse arrives (shown by the dashed line in Fig. 3.11). At later delays $t_{\mathrm{D-P}}$ we observe recovery of A_{PG}.

In Fig. 3.12 b) we plot A_{PG} after the subtraction of the positive component, measured at room temperature. The relaxation is best described as a bi-exponential. In the following we discuss only the strongest fast component, as the errors in the estimate of the weak component are comparable to its amplitude. The relaxation times obtained from the exponential function fit to the data are shown in Fig. 3.12. Within experimental error, the PG relaxation time is constant throughout the PG recovery, at $\tau_{\mathrm{PG}} = 0.26 \pm 0.05$ ps. Remarkably, and in contrast to the established behavior in CDW[131] and superconducting[132] systems investigated so far, no critical behavior of the quasiparticle (QP) response is observed anywhere near zero delay between D, P and p.

To compare the dynamics of the pseudogap recovery at different destruction fluences we plot in Fig. 3.13 the normalized A_{PG} as a function of $t_{\mathrm{D-P}}$ at different temperatures. Remarkably, for all temperatures and fluences, the PG recovery shown in Fig. 3.13 has an exponential form. Within the accuracy of the measurement the PG recovery time τ_{rec} is virtually independent of $\mathcal{F}$. In general this is not the case for the recovery of the SC and CDW orders,[131], [132] where the dynamical recovery behavior associated with the formation of a collective state can be more complicated. However, such a simple exponential recovery is consistent with uncorrelated dynamics of independent particles.[3]

The distinct absence of the critical behavior as $t \to t_{\mathrm{c}}$ in the PG state gives

[3]At 100 K fluence dependence of the recovery time is apparent. For the lowest fluences suppression is very weak and appears noisy when normalized and is not presented in Fig. 3.12. For higher fluences the recovery is slightly faster than exponential, and fit by an exponential function gives short recovery times.This specific behavior can be explained by the presence of the superconducting fluctuations described in Chapter 5, which still give significant contribution of the opposite sign to the signal. The recovery time of these superconducting fluctuations is comparable to the pseudogap recovery time, while the saturation amplitude is significantly lower. This gives rise to an apparent fluence dependence of the relaxation time: for the lowest fluence the superconducting and pseudogap contribution are comparable, whereas for the highest fluence the superconducting component is negligibly small.

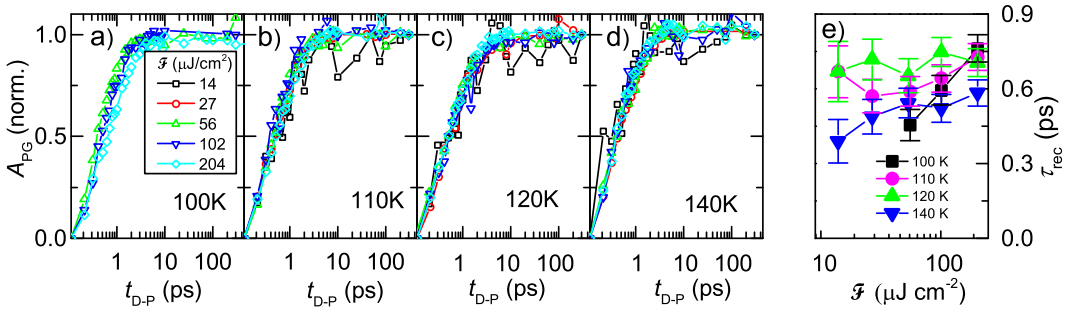


Figure 3.13: Recovery of the PG state after destruction by a laser pulse as a function of fluence at different temperatures. The normalized amplitude of the pseudogap component as a function of $t_{\mathrm{D-P}}$ for different fluences at a number of temperatures is plotted. Right panel: the recovery time τ_{rec} as a function of fluence $\mathcal{F}$ at different temperatures.

us new insight into the mechanisms for its formation. One possibility is that the normal to pseudogap transition is of first order. However, in this case we expect to observe an obvious step-like change of the relaxation time at T^* [133]. Such effect has not been observed (see Fig 3.10 b), so a first order transition can be ruled out. Rather, the absence of a divergence in the QP excitation dynamics is a signature of finite size of the system either limited externally or just indicating a local nature of the states involved. The < 50 fs resolution-limited uncertainty of the measured value of τ_{QP} allows us to put an upper limit on the correlation size of the pseudogap state. It has been shown that the speed of propagation of exchange bosons reaches the fermi velocity[134] which is equal to $v_F \sim 150\,\mathrm{nm\ ps^{-1}}$[135], so that within 50 fs the correlations can reach $\xi_{\mathrm{cor}}^{\mathrm{max}} \sim 75$ Å. A more precise estimate is based on a formula that links the correlation length and the relaxation time in the critical regime via the corresponding diffusion constant $\xi \simeq \sqrt{D\tau}$[136], so that the divergence of corresponding quantities is given by the uncertainty of the experimental estimate $\xi_{\mathrm{cor}}^{\mathrm{max}} = \sqrt{D}\frac{\Delta\tau}{2\sqrt{\tau}}$. D in turn can be estimated from measurable experimental parameters v_{F}[135] and normal state conductivity σ[137]: $D = \frac{1}{3}lv_{\mathrm{F}} = \frac{1}{3}\frac{m^*\sigma v_{\mathrm{F}}}{ne^2}v_{\mathrm{F}}$. This estimate gives $\xi_{\mathrm{cor}}^{\mathrm{max}} \sim 25$ Å , which is nearly coincident to the correlation length observed in diffraction experiments[26].

A number of experiments suggest that the pseudogap is associated with bound (or localized) states [80], [138]–[142]. A simple but plausible picture [64] is that photoexcitation leads to excitation of carriers from these states into itinerant states. Delocalization likely occurs in the process of avalanche carrier excitation rather than during the initial photon absorption. This is seen from the slight delay of the negative pseudogap response with respect to the hot-electron energy relaxation (see Fig. 3.11). Thereafter trapping takes place on a timescale given by τ_{rec} which is nearly independent of fluence and temperature, again indicating non-collective behavior. This picture is supported by the fact that the pseudogap is filled rather than destroyed (i.e. closed) after photoexcitation [143], i.e. a number of delocalized "in-gap states appear" without strongly altering the binding energy. This is tantamount to saying that the states do not act cooperatively, and there is *no change of the energy scale*, as the system evolves through t_{c} in time.

In systems where photoexcitation of the gap-forming carriers is indirect, only a part of the energy is used for the excitation of QPs and the destruction of the gapped

state[90]. The total photodestruction energy is the sum of the lost energy $U_{\rm lost}$ which arises from excitation of sub-gap phonons and is a monotonic function of the gap, and a much smaller binding energy for excitation across the gap $U_{\rm bind} = \triangle \cdot n$ [90], here n is a number of localized carriers. For a temperature independent pseudogap[13] only $U_{\rm bind}$ would depend on temperature via the temperature dependence of $n(T)$, while the lost energy $U_{\rm lost}$ is independent of temperature thus explaining the apparent temperature independence of the photodestruction energy. By increasing the doping level the gap linearly decreases leading to the decrease of both $U_{\rm lost}$ and $U_{\rm bind}$ contributing to the photodestruction energy as shown in Fig. 3.10 e).

Regarding the mechanism for localisation, CDW formation is conventionally attributed to a Fermi surface instability arising from the wavevector nesting [127]. However, recent ARPES studies in $Bi_2Sr_{2-x}La_xCuO_{6+\delta}$ have revealed that the wavevector of the observed modulation does not correspond to the nesting between the parallel sheets of the FS at the antinodes but rather to the vector connecting the "endpoints" of the "Fermi arcs", so apparently no "true" nesting takes place.[26] In contrast, very different physics is responsible for "stripe" textures (which may occur on a similar scale), which are usually considered to be a result of the competing interactions, such as microscopic strain caused by localised holes and the Coulomb repulsion between them [49], [50], [144]–[146], or the hole kinetic energy competing with the Coulomb interaction within Hubbard or $t - J$ models[31], [147]–[149]. We speculate that within such stripe models, a weak FS instability may act to additionally stabilize hole pairs, enhancing spatial charge modulations through the Friedel oscillations. The degree of nesting for the states at the Fermi surface[10] would add an additional material-specific component which has a direct effect on $T_{\rm c}$.

To conclude, the data presented here, particularly the behaviour of the PG relaxation time through the coherently excited dynamical transition in Fig. 4 and exponential PG recovery dynamics in Fig. 5 imply a pseudogap state characterized by a short-range correlated localized carriers, pairs or very small clusters, locally breaking the rotational symmetry[150], rather than proper charge density wave segments.[127] The observations in Bi2212 are thus more consistent with a polaronic picture than a dynamically fluctuating charge density wave with long range order. Our experiments also clearly show that the character of the PG state does not change with doping. Only the energy associated for its destruction diminishes, reflecting the change of the localization energy (and T^*) with increasing screening.

3.4.1 Comments and remarks

Here we would like to add two comments which slightly fall out of the presented discussion.

Firstly we would like to highlight the inconsistency of the bottleneck model developed for the low excitation experiment with current results. In this model electrons and hot bosons with energy $\hbar\Omega$ form a quasi-equilibrium with no change in the density of states. This can be approximately described in the framework of the two-level system (if $\hbar\Omega \simeq \Delta$), for which it is known that it is impossible to excite all the carriers from the ground state. However in this case the density of photoexcited quasiparticles is expected to have a dependence on fluence of the form $n \sim \mathcal{F}/(1 + const \cdot \mathcal{F})$. After inhomogeneity of excitation is taken into account, this becomes $\Delta R/R(\mathcal{F}) \sim \int \mathcal{F}\, e^{-z/\lambda}/(1 + const \cdot \mathcal{F}\, e^{-z/\lambda})\, dz = ln(1 + const{\cdot}\mathcal{F})/const$ which predicts a much weaker dependence on $\mathcal{F}$ than observed experimentally (see

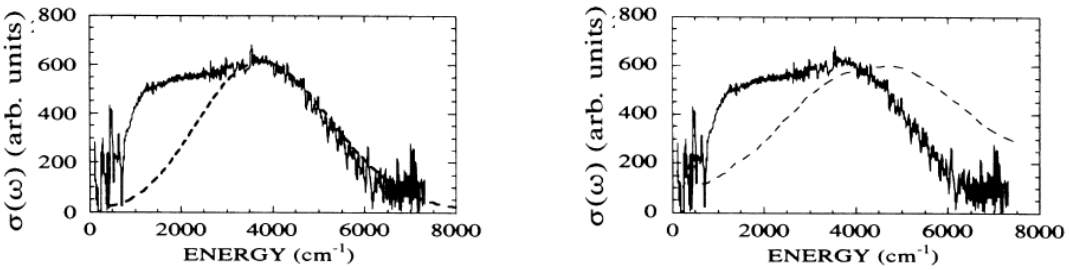


Figure 3.14: Mid-IR polaronic feature in photoinduced conductivity. Left: The photoinduced infrared conductivity $\sigma_{\rm p}(\omega)$ (solid line) in the insulator precursor for $La_{2-x}Sr_xCuO_4$ and fit produced by polaron-transport theory (dashed line)[151]. Right: $\sigma_{\rm p}(\omega)$ (the same as on the left) compared with chemically doped superconducting $La_{2-x}Sr_xCuO_4$. Figure is adopted from [151].

Fig 3.10 f). In reality we observe that the change in reflectivity and consequently n are linear with fluence in a wide range of fluences and are in good agreement with the model described in Section 1.2.4.

Secondly we would like to highlight the difference between the quasiparticle relaxation time and recovery time. Apparently the quasiparticle relaxation time, which in the range of studies varies from 0.2 to 0.4 ps [See Fig. 3.10 b)], is smaller than the recovery time, which varies from 0.35 to 0.75 ps [Fig. 3.13 b)]. Even though the obtained value of the recovery time has significant standard error [4] the trend seems to be universal. This might serve as an indication that the formation of the pseudogap state is more complicated than the formation of a (bi-)polaron. We intend to clarify this issue in future experiments, which would single out the pseudogap response experimentally without using the extrapolations from high temperatures of the hot-electron energy relaxation component.

3.5 Polaronic Interpretation of the Long-Lived Response

Here we briefly report the temperature dependence of the long-lived response and discuss its relation to the long-lived mid-infrared (IR) polaronic features observed in pump-probe and photo-induced absorption measurements.

A characteristic peak related to the hole polarons appears in the optical conductivity of the photo- as well as chemically doped Mott insulators (Fig. 3.14). While in the former state the polarons eventually decay, in the latter case they are basically static. The characteristic energy of the peak corresponds to the average phonon energy weighted by the electron phonon coupling constant $\alpha_j(\mathbf{q})$: $\omega_0 = \frac{\sum_{j,\mathbf{q}} \alpha_j(\mathbf{q}) \sin^2(\frac{1}{2}q)\omega_j^2(\mathbf{q})}{\sum_{j,\mathbf{q}} \sin^2(\frac{1}{2}q)\omega_j(\mathbf{q})}$.[151] Importantly, for the spectral feature to be observable in the photoconductivity measurements its lifetime has to be at least of the order of a microsecond (that is why the experiments are typically conducted at low temperatures).

Surprisingly the very similar spectral feature with much shorter life-time has been observed in the pump-probe experiments at room temperature on La_2CuO_4

[4] We should note that most of the non-linear fitting programs use approximate algorithms for the standard error calculation which can lead to its underestimation.

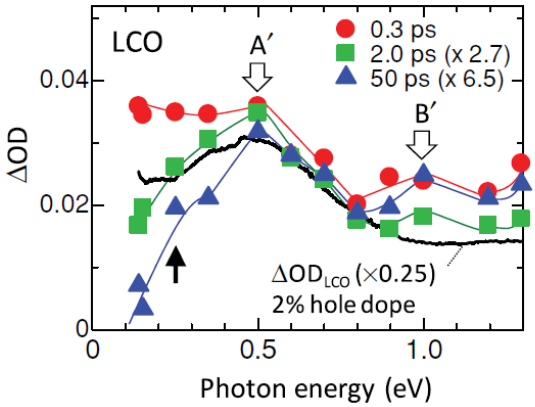


Figure 3.15: Polaronic Mid-IR features in transient reflectivity response. Normalized change in the optical density (ΔOD) in La_2CuO_4(2.25 eV pump) at different delays after the pump pulse. A′ and B′are the hole and electron polarons. For comparison the change of the optical density due to the chemical doping is shown with solid line. Figure is adopted from [112].

(LCO)[112], peak A′ in Fig. 3.15. The polaronic response in this case has been directly measured to decay within 400 ps, which is much shorter than the timescale of the photoinduced conductivity. Another mid-IR peak at 1 eV observed *only* in the ultrafast response has been attributed by authors to the electron-polaron which recombines with hole-polaron. It has also been shown that mid-IR peaks appear in the result of the spectral weight transfer from the charge-transfer band($\sim$ 1.8 eV for LSCO). This indicates that the optical experiments presented in this chapter are representative of the polarons dynamics.

Appearance of the polaronic peak on multiple time-scales is poorly understood. Possible explanations are related to trapping on defects or collective ordering. While in the underdoped regime polarons might be considered as independent in the superconducting samples their interactions might become important.[151] It is however hard to track the mid-IR feature close to the optimal doping as it merges with the Drude peak.

3.5.1 Evidence for multi-scale behavior from near-IR pump-probe experiments

Here we provide an evidence of similar multiple time-scale behavior observed in the near-IR pump-probe experiments close to the optimally doping. Namely we show that the pseudogap response, which is mostly decayed within the first picosecond, is revealed in the long lived response under an intense photoexcitation. In Fig. 3.16 we show the temperature dependence of the pump-probe response in UD BSCCO under 108 μJ/cm^2 photoexcitation (at twice the threshold). In the top panel of Fig. 3.16 we compare the signal averaged over the first 2 picoseconds with the average of the signal between 150 and 200 ps. In the short-lived component one can clearly see the negative pseudogap response discussed above which gains the intensity with cooling. The T-dependence of the long-lived component resembles that of the short-lived with important difference that it is significantly offset above zero. The upturn at low temperatures is related to the appearance of the superconducting response

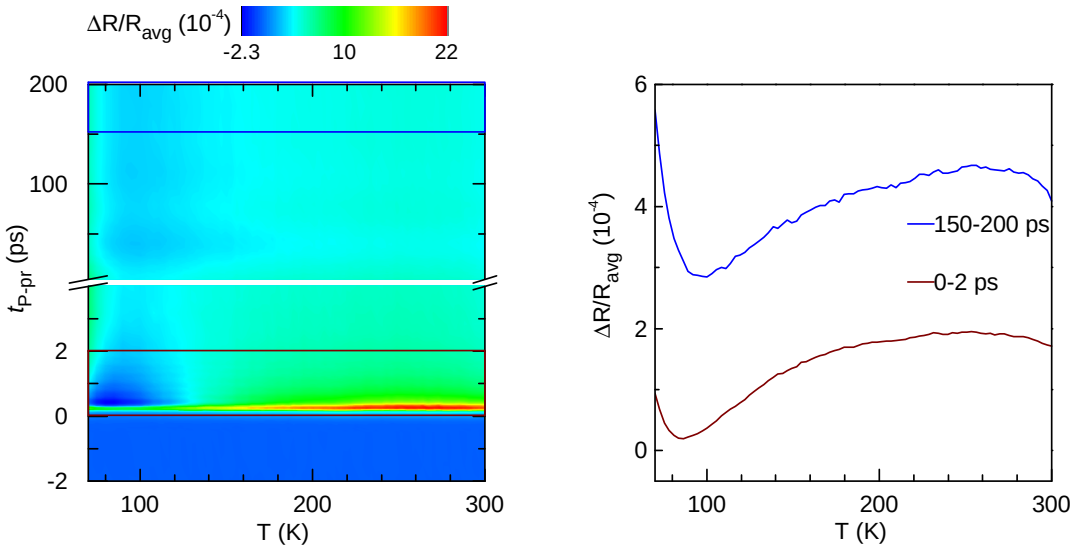


Figure 3.16: Comparison of the sub-ps and nanosecond transient responses. Left panel: Temperature dependence of the pump-probe response in UD BSCCO. $\mathcal{F}_{\mathrm{D}}$ =108 μJ/cm^2. Right panel: average of the signal from 150 to 200 ps (blue line) compared to scaled average of the signal from 0 to 2 ps (red line).

which is subjected to the critical slowing down.

While the two shapes appear similar further analysis and more systematic studies are required to make solid conclusions.

Summary

In this chapter we present the high excitation experiments in the pseudogap state as well as the polarization analysis of the ultrafast response for metallic and superconducting component. In Section 3.2 we show the ultrafast signature of the broken rotational symmetries in the pseudogap and superconducting states. By considering possible excitation mechanisms and excluding the ISRS we conclude that the dependence of the transient reflectivity on probe polarization has its origin in the reduction of the D_{4h} point group symmetry to the D_{2h} below $T^*$and further down to C_{2h} with the onset of superconducting fluctuations.

In Section 3.3 we presented temperature and doping studies of the pseudogap photodestruction. The fluence dependence fits well with the saturation model previously used for SC and CDW responses. The photodestruction fluence has no clear temperature dependence and scales with the T^* and accordingly Δ_{PG}, which is explained by the energy loss to the subgap phonons in agreement to the previous observation for large gap superconductors.

The study of the recovery of the pseudogap component by means of the 3 pulse technique revealed that the quasiparticle relaxation time is nearly constant along the transition which we interpreted as a signature of the short range order in the pseudogap state. The recovery of the pseudogap optical signature is nearly independent on temperature and excitation fluence in the temperature region $T_{\mathrm{c}} < T < T^*$.

Finally we've indicated similarity in the temperature of the fast pseudogap re-

sponse and nanosecond response, which suggests relation of both to the polaronic states.

Chapter 4

Normal-to-Superconducting Phase Transition

In this chapter we present results of the measurements of the characteristic time of photodestruction of the superconducting condensate as well as measurements of the condensate recovery with the three pulse technique. We compare the results on LSCO, BSCCO samples with varying temperature and fluence of the destruction pulse. We also numerically simulate the phase transitions within the TDGL theory and compare the results with the experiment. As single layer LSCO compound has a relatively small fluctuations signal and exhibits relatively low anisotropy[152] it is expected to be better described by the TDGL theory than other samples, so we concentrate on this sample.

4.1 Response Function

Before one attempts to compare experiments with simulations it is important to establish the *response function*, i.e. the correspondence between measured and calculated quantities, namely between $\Delta R/R$ and the order parameter $\psi(t)$. The problem of the response function in pump-probe experiments is not an easy one. Here we will discuss a phenomenological approach that we will use, whereas at the end of the chapter we will also discuss its limitations.

One strict assumption on the response function which we make within the phenomenological approach is that the response is a function of a single collective variable - the superconducting order parameter ψ which is the quantity we simulate:

$$\Delta R/R = A_s(\psi). \tag{4.1}$$

As we aim to simulate the dynamics of the order parameter with the TDGL theory we also expect the theory to be applicable under equilibrium conditions. This implies that we assume that the Ginzburg-Landau temperature dependence of the gap $\Delta = |\psi| \sim \sqrt{1 - T/T_c}$ stays valid in the whole experimental range of temperatures. We proceed by establishing the correspondence between the reflectivity change and the gap from the measured temperature dependence of $\Delta R/R$ (left panel of Fig. 4.1). The resulting dependence is shown in the right panel of Fig. 4.1. The desired response function $A_s(|\psi|)$ used for the simulation is the linear interpolation to the data points.

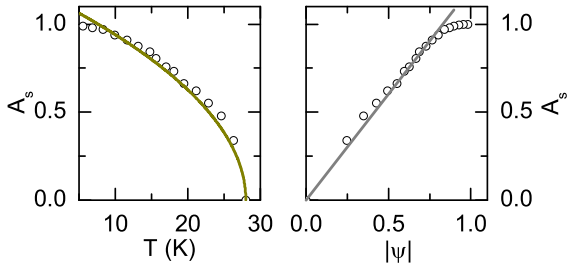


Figure 4.1: The response function. Left panel: Normalized amplitude of the superconducting component in the low excitation regime ($0.14\ \mu\mathrm{J/cm^2} \approx 0.03\,\mathcal{F}_{th}$) and fit by the GL gap function $\Delta = |\psi| \sim \sqrt{1 - T/T_c}$. Right panel: The same data as on the left plotted as a function of the GL $|\psi|$.

In the case of BSCCO and HBCCO it is much harder to provide such a relation as both classes have a significant fluctuation region above T_c (see Chapters 5 and 6), which is not taken into account by the TDGL theory.

4.2 Destruction of the Superconducting Condensate in LSCO and BSCCO

When a high intensity laser pulse is absorbed by a superconductor two photoinduced phase transitions occur: the first one is from the superconducting to the normal state (destruction of superconductivity) followed by the subsequent normal to superconducting state phase transition (recovery). The first one occurs in a highly non-equilibrium conditions, where the concept of the temperature is not applicable as long as the electron and phonon distribution functions are very far from their equilibrium shapes. The experiments suggest that the superconducting state is not excited directly in the process of photon absorption but rather Cooper pairs are destroyed by the above-gap phonons generated in the process of the initial hot electrons relaxation: one observation which supports this point is relatively long rise time of superconducting signal observed in LSCO (while the rise time in the normal state is only $\sim$ 70 fs[62] in the superconducting state it can reach 800 fs; additionally, the comparison of the energy density required to destroy the superconducting state U_D with the condensation energy U_c in a number of superconductors[90] has shown that for the large gap superconductors the ratio of U_D/U_c is typically above 5. This is due to the fact that most of the energy is spent on the excitation of the sub-gap phonons (U_lost) and only a small number of high-energy phonons contribute to photodestruction $U_{\Omega>2\Delta} = U_c$. Thus $U_\mathrm{D} = U_c + U_\mathrm{lost}$.

While the rise-time in two pulse experiments under the strong excitation condition $\mathcal{F}_\mathrm{Pump} > \mathcal{F}_\mathrm{th}$ reflects the destruction time of the superconducting condensate it is often contaminated with the normal state response which can overcome the superconducting signal (the normal state response does not saturate with the fluence) and has a faster rise time. It is thus instructive to use the three pulse technique in a configuration when the D pulse comes after the P pulse to study the process of superconducting gap destruction. The results of this experiments for LSCO are presented in Fig. 4.2. As usually $\mathcal{F}_\mathrm{Pump} \ll \mathcal{F}_\mathrm{th}$ in the three pulse experiments so

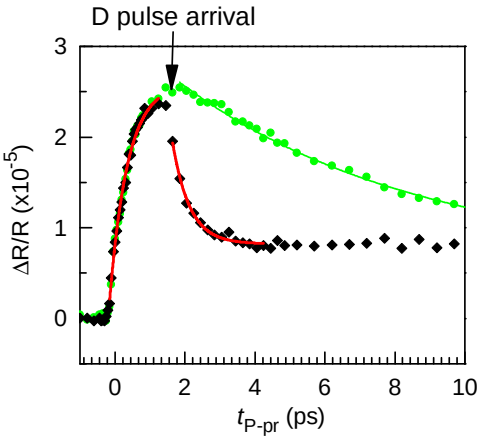


Figure 4.2: The superconducting condensate photodestruction in LSCO. Black dots - the three pulse experiment with the D pulse coming after the P pulse (D pulse fluence $\mathcal{F}_{\rm D}= \mathcal{F}_{\rm th} = 4.5$ μJ/cm^2). Green dots are the quasiparticle response in the absence of the D pulse. Red curves are the fits by a single exponential (see text). The moment of the D pulse arrival is shown by the arrow. Red lines are exponential fits of the rise and destruction of the superconducting response.

the superconducting component dominates in the response. The quasiparticle relaxation is subjected to a strong bottleneck $\tau_{\rm SC} = 6.8 \pm 0.25$ ps (green dots), which is a relatively slow process. When the D pulse arrives the system is driven into the metallic state and the gap is closed, the bottleneck is suppressed and $\Delta R/R \to 0$ (in Fig. 4.2 the gap is destroyed only on the surface, so that in the depth the gap remains finite and pump-induced quasiparticles still have to relax through the gap. This is why the signal remains finite even after arrival of the D pulse). It is clearly seen that the condensate destruction time $\tau_{\rm D} = 0.49 \pm 0.04$ ps coincides with the rise-time of the QP response $\tau_{\rm r} = 0.52 \pm 0.04$ ps in the low-excitation experiment.

To generalize the observation we repeat the experiment systematically varying the delay between P and D pulses, the fluence of the D pulse, and the temperature. For this we have chosen UD BSCCO system which has a higher T_c, but also relatively high (compared to optimally and overdoped samples) $\mathcal{F}_{\rm th}^{PG}$ (see Chapter 3). In Fig. 4.3 a) we present dependence of the superconducting response photodestruction on the fluence of the D pulse. At the lowest fluence, which is just below the threshold $\mathcal{F} = 9.6$ μJ/cm^2, the gap is not closed completely but the quasiparticle temperature rises enough to reduce the relaxation time significantly (see Fig. (1.6)). With increasing the fluence up to $\mathcal{F} \sim 30$ μJ/cm^2 the condensate is destroyed on the surface but the part of the sample with undestroyed condensate produces a detectable signal. With further increase of the fluence the signal becomes non-monotonous and at even higher fluence clearly changes sign, eventually above 384 μJ/cm^2 both the positive and negative contributions disappear and $\Delta R/R = 0$.

To better understand the observed transient reflectivity we must take the presence of the pseudogap into account. As we completely suppress the superconducting condensate and, for the highest fluence value, also the pseudogap state, it is illustrative to consider the evolution of the *absolute value* of reflectivity upon arrival of the P and D pulses [Fig. 4.3 d)]. The transient reflectivity in our experiment

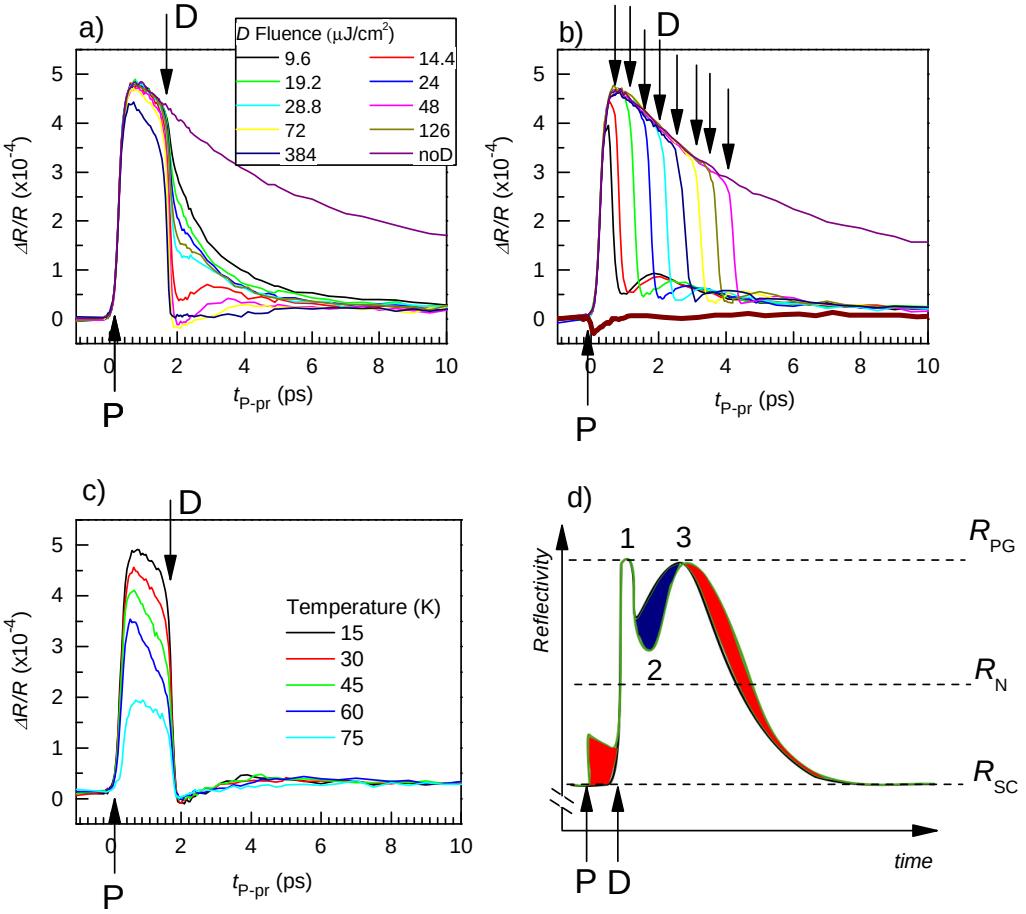


Figure 4.3: Superconducting condensate photodestruction in BSCCO. a) Fluence dependence. Note that $\mathcal{F}_{\rm th}^{\rm SC} = 13.9 \pm 0.5$ μJ/cm^2 and $\mathcal{F}_{\rm th}^{PG} = 58 \pm 3.5$ μJ/cm^2. b) Destruction of the superconducting condensate at different delays between P and D pulses, thick line is a transient reflectivity in the pseudogap state at 120 K (shown for comparison). c) Temperature dependence of the condensate photodestruction ($T_{\rm c}$=81 K). d) Schematic representation of the changes in absolute reflectivity caused by P and D pulses (arrows). Green line represents the case when both pulses are present, black line - only the D pulse. Filled areas represent differential reflectivity measured in the experiment.

corresponds to the difference in the reflectivity in the presence and in the absence of the P pulse. The actual change of the absolute value of the reflectivity caused by the D pulse is much larger than that produced by the pump. In Fig. 4.3 the reflectivity change for the D pulse fluences above $\mathcal{F}_{\rm th}^{PG}$is shown by the black curve in the absence of the P pulse and by the green curve in the presence of the P and D pulses. Prior to the D pulse arrival the P pulse slightly increases the reflectivity (red filled area in Fig. 4.3, we exaggerate pump induced changes for the sake of illustration). When the D pulse arrives the system is driven into the normal state. Because the superconducting and the pseudogap contribution have opposite signs the normal state reflectivity $R_{\rm N}$ falls between the reflectivity in the pseudogap phase $R_{\rm PG}$ and reflectivity in the superconducting state $R_{\rm SC}$. We schematically show that the reflectivity first reaches $R_{\rm PG}$ at point 1, which corresponds to the complete destruction of the superconducting state, and then decreases to the point 2 which corresponds

to the partial suppression of the pseudogap state. In reality two processes occurs approximately simultaneously, and we separate them just to stress that in the case of the low D pulse fluences only the superconducting condensate is destroyed while at higher $\mathcal{F}_{\mathrm{D}}$ also the pseudogap is. For the moderately strong fluences ($28 - 128$ $\mu\mathrm{J/cm}^2$) the pseudogap response is not suppressed completely and, as in the presence of both the P and D pulses the total excitation is slightly higher compared to just the D pulse, the suppression of the pseudogap is slightly stronger and overall reflectivity is smaller, which results in the negative response (between points 2 and 3 on the graph). In other words, the pump excited quasiparticles subject to bottleneck relaxation across the superconducting gap are re-exited across the pseudogap by the D pulse. Further appearance of the positive component (beyond the point 3 on the graph) is caused by the similar effect - in the presence of the P pulse the recovery of the condensate is slightly delayed which leads to the positive differential reflectivity. For the highest value of the D pulse fluence $\mathcal{F} = 386$ $\mu\mathrm{J/cm}^2$ the negative component does not appear any more [Fig. 4.3 a)]. This can be explained by a complete destruction of the pseudogap state. As we have seen in the previous chapters the pseudogap recovery time is independent of the D pulse fluence. Thus when it is completely destroyed it recovers independently of the initial excitation, giving zero contribution to the differential reflectivity. The delayed recovery of the positive signal is still observed even in this case.

The suggestion that the small negative and positive responses, which appear after the D pulse arrival, originate from reexcitation of the pump excited quasiparticles is reaffirmed by the following fact: with an increasing delay between the P and D pulses the amplitudes of these components decay at the timescale of the quasiparticle relaxation in the absence of the D pulse. The destruction time and the amplitude of the signal suppression by the D pulse are apparently delay independent [Fig. 4.3 b)].

The fact that the destruction time is apparently temperature and fluence independent suggests inapplicability of the TDGL for the description of the superconducting-to-normal phase transition. Indeed in this case the optical pulse can be considered as an instantaneous excitation and destruction time would be a direct measure of the $\tau_{\mathrm{GL}}(T) \sim 1/(T - T_{\mathrm{c}})$, here T is the final temperature after the pulse arrival and is roughly proportional to $\sqrt{\mathcal{F}}$.

4.3 Recovery of the Superconducting Condensate in LSCO

4.3.1 Experimental

The main interest of our experiment is the normal-to-superconducting transition or, in other words, the recovery of the superconducting condensate which we will discuss in this section. We present studies by means of the three pulse technique and modeling of the response within the TDGL framework.

In contrast to the previous section, the pump-probe measurements were conducted at the set of delays *after* the D pulse. In Fig. 4.4 we present a characteristic result of the three pulse experiment. As already mentioned in the absence of the D pulse the response consists of the normal state short-lived PG response and the strong superconducting response. In the presence of the D pulse at short $t_{\mathrm{D-P}}$ delays the superconducting component is strongly suppressed. The response gradually recovers as $t_{\mathrm{D-P}}$ increases on the timescale of tens of picoseconds. In contrast the

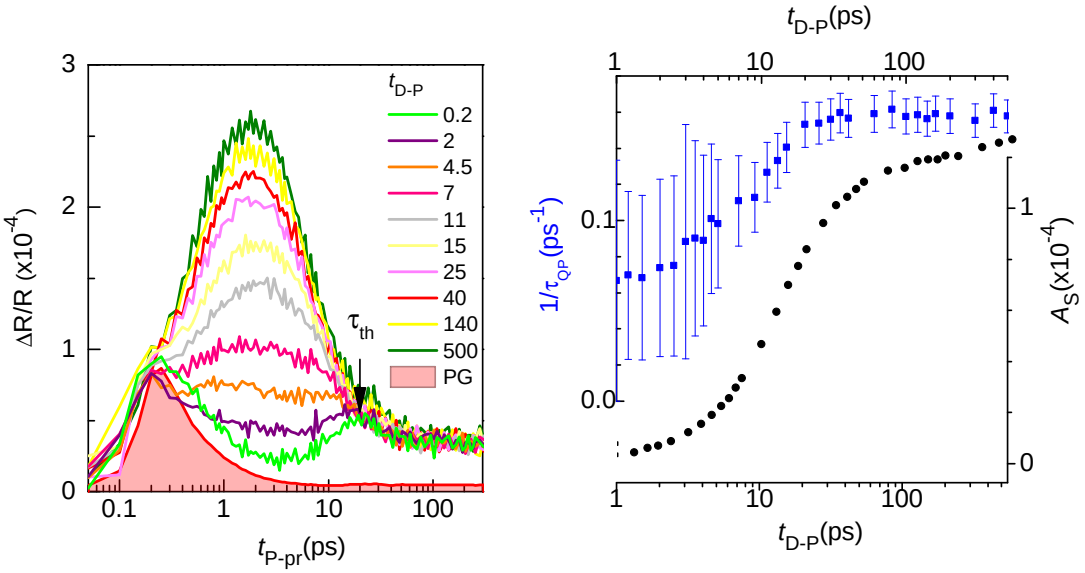


Figure 4.4: Recovery of the superconducting response in LSCO Left panel: transient reflectivity $\Delta R/R$ for LSCO at 4 K as a function of $t_{\mathrm{P-pr}}$ for different $t_{\mathrm{D-P}}$ (1, 10 and 100 ps are designated). The D pulse fluence is $\mathcal{F}_{\mathrm{D}} = 12\,\mu\mathrm{J/cm}^2$. The red line indicates the pseudogap signal (three exponential fit to the measured data at 36 K). Right panel: Right axis: the same data as in the left panel but shown as a function of $t_{\mathrm{D-pr}}$ in the logarithmic scale, black dots indicate the peak of the quasiparticle response (see text for details). Left axis: blue squares are $1/\tau_{\mathrm{QP}}$ obtained from exponential fits to the data shown on the left after the subtraction of the $t_{\mathrm{D-P}}$=0 ps curve.

pseudogap response seems to be unaffected at all by the D pulse, which is explained by a very high photodestruction fluence ($\mathcal{F}_{\mathrm{th}}^{\mathrm{PG}}$=750 $\mu\mathrm{J/cm}^2$) of the pseudogap state in LSCO [153], while the highest fluence used in current study was $\mathcal{F} = 34\ \mu\mathrm{J/cm}^2$. As the pseudogap response is temperature independent below 100 K[62] it should also not be affected by transient heating so we subtract it from the data in further analysis.

A gradual recovery of the SC gap can also be seen in the pump-probe transients at short $t_{\mathrm{D-P}}$ delays as a *characteristic hump* that is present at τ_{th} ∼30 ps. These effects can have two possible origins. Firstly, in bulk of the sample where the gap is not closed completely the signal recovers with recovery of the gap. This explanation is not sufficient as the signal at τ_{th} in this case is expected to be proportional to the volume of the incomplete gap suppression region weighted with the depth as $e^{-z/\lambda}$. In reality the signal at τ_{th} is comparable to the signal in the absence of the D pulse, and does not depend on the delay between D and P pulses. This leads us to the second possible explanation: most likely the signal originates from transient heating and the relaxation after τ_{th} corresponds to the heat diffusion out of the surface. The convergence of all curves at τ_{th} is an indication that all degrees of freedom are thermalized and the evolution of the response can be described by a single temperature, i.e. the quasiparticle and lattice temperatures coincide, which is an indication of the gap recovery.

It is rather hard to define what should be measured as the amplitude and the relaxation time of the pump-probe response at early $t_{\mathrm{D-P}}$ delays. We will define it ignoring the aforementioned *gap recovery hump*, i.e. by subtracting the $t_{\mathrm{D-P}}$=0.2 ps curve.[1] We compare the amplitude of the response with the quasiparticle relaxation rate obtained from exponential decay fits (Fig. 4.4). The relaxation rate recovers on the same time scale as the amplitude in agreement with Eq. (1.8) $1/\tau_{\mathrm{QP}} \sim \Delta(t_{\mathrm{D-P}})$.

The recovery of the condensate occurs in two steps. Firstly, fast exponential growth within first 30 ps occurs where the system freely evolves through the transition, the dynamics of the condensate in this part is defined by the TDGL theory, then the system reaches a quasi-equilibrium and after 100 ps the dynamics is driven by the thermal diffusion out of the excited volume (see also Fig. 4.14).

The presented 3 pulse measurements were repeated systematically with the D fluence varying it from $\mathcal{F}_{\mathrm{th}}^{SC} = 4.5$ μJ/cm^2 to 34 μJ/cm^2, the fluence at which the transient lattice heating exceeds T_{c}.

4.3.2 TDGL modeling

We aim to simulate the phase transition within the TDGL model. TDGL is a model describing evolution of the order parameter which in principle can take into account the evolution of the potential in which the system relaxes. For the basics of the TDGL theory we refer the reader to Section 1.3. As the simplest approximation we ignore phase inhomogeneity and dynamics of vortices related to it, concentrating on the dynamics of the amplitude of the order parameter. Within the TDGL model an external perturbation can be described as the free energy potential change caused by temperature evolution so that the time dependent equation now reads

$$-\gamma\hbar\frac{\partial\psi}{\partial t} = \alpha_0(1 - T(t)/T_{\mathrm{c}})\psi + \beta\psi|\psi|^2 + \frac{1}{4m}\left(i\hbar\nabla\right)^2\psi. \tag{4.2}$$

For simplicity of the calculation we rewrite the equation in natural units of length $\xi(T=0)$ and time $\tau_{\mathrm{GL}}(T=0) = \gamma_0\hbar/\alpha_0$, normalizing the order parameter to 1. We also limit ourselves to the 1D problem as the optical penetration depth $\lambda_{@800nm} = 150$ nm is much smaller than the lateral spot size ~ 60 μm, and the lateral dynamics is thus irrelevant. The equation (4.2) reduces to

$$\frac{\partial\psi}{\partial t} - (1 - T(t)/T_{\mathrm{c}})\psi + \psi^3 - \frac{\partial^2\psi}{\partial z^2} = 0, \tag{4.3}$$

which is to be solved with the boundary conditions $\left(\frac{\partial\psi}{\partial z}\right)_{z=0} = 0$ and $\psi_{z\to\infty} = \sqrt{1 - T_{\mathrm{bath}}/T_{\mathrm{c}}}$ and the initial conditions (IC)

$$\psi_{t=0} = \sqrt{1 - T_{\mathrm{bath}}/T_{\mathrm{c}}}. \tag{4.4}$$

As mentioned before the temperature is the driving term of the equation. We simulate the temperature evolution with time by numerically solving the two-temperature model Eq. (1.1)-(1.2), where the P term corresponds to the absorbed energy density ($P = \mathcal{F}/\lambda$).[2] In the Fig. 4.5 we show the dependence of lattice and electronic

[1] It would be more precise to subtract $t_{\mathrm{D-P}}$=0 ps curve. However at the highest fluences the non-linear effects are present if D and P pulses arrive simultaneously, which obscure the response.

[2] In the introduction we have highlighted general inapplicability of the TTM. In [71] authors show that in the low temperature limit the exact relaxation rate is of the same order as given by TTM, indicating

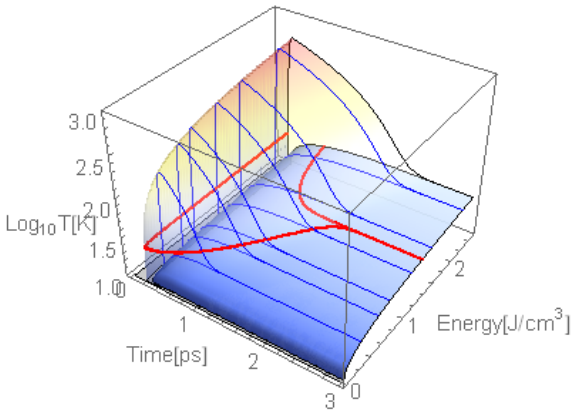


Figure 4.5: The results of the simulation by the two-temperature model. Electronic and lattice temperatures at the surface of the sample are represented as semi-transparent and opaque surfaces, respectively. The red-line designates T_c, the blue lines mark experimentally used values of the D-pulse absorbed energy density.

temperature at the surface of the sample as a function of the delay after the D pulse and the absorbed energy density. The blue lines correspond to experimentally used values of the D pulse fluence and one can see that for the two highest fluences the lattice temperature exceeds T_c (the red line). The complete thermalization occurs rapidly and is not strongly fluence dependent - the thermalization time varies from 0.6 to 1.6 ps, which is much faster than the recovery time of superconducting response. As it is necessary to include thermal diffusion to properly describe the data we solve the two-temperature model (TTM) as a function of time and depth for each fluence. To properly describe the diffusion part one needs to know the thermal diffusivity $\alpha_T = \frac{k}{\rho C_p}$, here k is the thermal conductivity, ρ - the density, and C_p is the specific heat capacity. Both k and C_p diminish as $T \to 0$ leading to a large error in the thermal diffusivity estimate. As there is no available literature on measurements of both k and C_p in the same sample we rather preserve α_T as a fit parameter and allow it to slowly vary with the fluence.

In Fig. 4.7 a) we present the results of the simulation as formulated together with experimental data. Apart from the diffusion constant the only fit parameter is $\tau_{GL}(T = 0)$ (in further we will just use τ_{GL}) shared for all the curves. While by varying τ_{GL} it is possible to fit one of the curves, the observed dependence on fluence is never reproduced. Moreover, for the moderate excitations, the following trend is observed: if τ_{GL} is set to a value large enough to provide an observable recovery time ($\tau_{GL} \gtrsim 1$ ps) the superconductivity is never sufficiently suppressed, and conversely, if we set τ_{GL} to the value that gives an observable suppression of the superconducting response the condensate recovers faster than observed experimentally (see Fig. 4.6). The most probable reason for such behavior is the comparability of the temperature burst duration and τ_{GL} both being of the order of 1 ps. This means that during

that TTM can still serve as an approximation. We use the TTM as a starting point for our study because the formulation of the TDGL in terms of the temperature is much easier and less numerically demanding than in terms of the distribution function. As we shall show the TTM fails to produce reliable fits, and is not relevant for our final consideration.

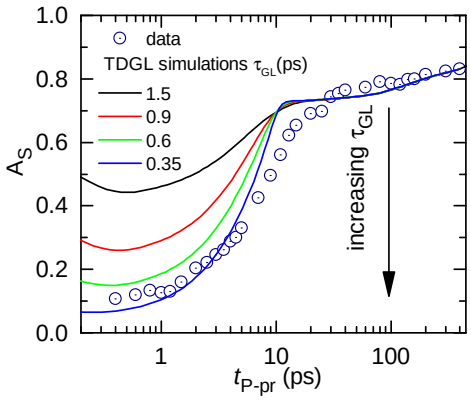


Figure 4.6: Solution of the TDGL equations with initial condition given by Eq. (4.4) for different values of τ_{GL}. Note that stronger destruction results in steeper recovery. Data for the destruction beam fluence $\mu\mathrm{J/cm}^2$.

the temperature pulse the condensate is suppressed only e times, which clearly contradicts the experimental observation. This adds to the argument from the previous section that the superconducting to normal phase transition descriptions should go beyond the TDGL theory.

Many authors argued that the two-temperature model is not accurate and it is more appropriate to introduce an additional temperature which describes the bosonic degrees of freedom strongly coupled to electrons[11], [154], so that there is a direct energy exchange between the electrons and the strongly coupled bosons, and the strongly coupled bosons and the remaining lattice. We simulate this situation separately the deducing electron boson coupling from room-temperature pump-probe measurements[56]. There is however no significant change in the simulated $A_{\mathrm{S}}(t_{\mathrm{D-P}})$ as the transition time (time at which T_{e} crosses T_{c}) is delayed by less than 100 fs.

We proceed by ignoring the destruction part of the trajectories trying to provide adequate initial conditions for the recovery of the condensate. To avoid the suppression of the initial condition during the temperature burst we replace $T_{\mathrm{e}}(t)$ by $T_{\mathrm{L}}(t)$ in TDGL equations. As a starting point we use the model which we apply for the description of the fluence dependence in the two-pulse experiment, namely

$$\psi(0,z)=\begin{cases}0 & ,\mathcal{F}(z)>\mathcal{F}_{\mathrm{th}};\\ (1-\frac{\mathcal{F}_0}{\mathcal{F}_{\mathrm{th}}}e^{-z/\lambda})\sqrt{1-T_{\mathrm{L}}(0,z)/T_c} & ,\mathcal{F}(z)<\mathcal{F}_{\mathrm{th}}.\end{cases} \tag{4.5}$$

With sufficiently low numerical noise the observed solution is a N/S boundary propagating towards the surface in a form of soliton without changing the shape. Increasing fluence in this case shifts the initial N/S boundary depth by $ln(\mathcal{F}/\mathcal{F}_{\mathrm{th}})$, and delays the soliton arrival to the surface as $T\rightarrow T_{\mathrm{c}}$. Varying τ_{GL} we can change the time when the soliton will reach the surface but hardly affect the shape of the simulated $A_{\mathrm{S}}(t_{\mathrm{D-P}})$. The closest average result is achieved when $\tau_{\mathrm{GL}}=50$ fs which is slightly shorter than the microscopic theory value $\tau_{\mathrm{GL}}=\frac{\pi\hbar}{8kT_{\mathrm{c}}}\approx 100\,fs$. The calculated solitonic solution is shown in Fig. 4.7 b). The obtained trajectory

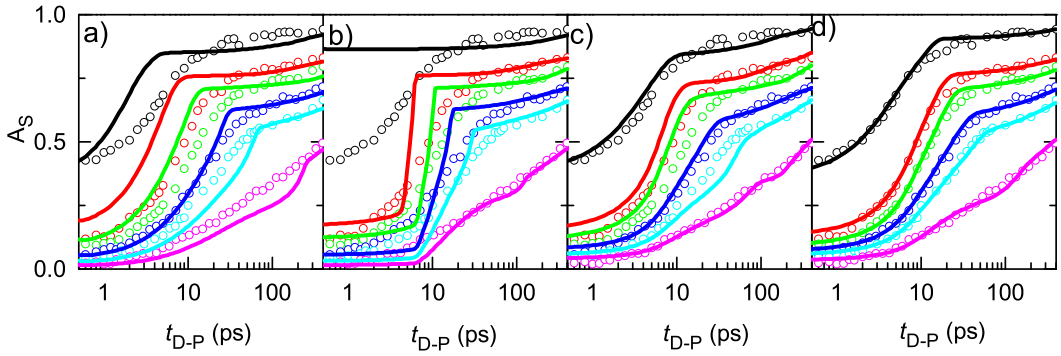


Figure 4.7: Results of the numerical simulation of the TDGL equations: comparison of the calculated A_{SC} obtained within different formulations of the problem (solid lines) and experimentally measured data (circles, values of the fluence are 4 (black), 9 (red), 12 (green), 18 (blue), 24 (cyan), and 34 (magenta) μJ/cm^2). The TDGL solution with the initial conditions described by a) Eq. (4.4), b) Eq. (4.5), c) Eq. (1.33) (represented in Fig. 4.8), d) Eq. (4.6) (represented in Fig. 4.8). The theories from panel a) and b) have the single free parameter $\tau_{\rm GL}$ equal to 1 and 0.05 ps respectively. The theory from panel c) has only two variable parameters (for all datasets) $\tau_{\rm GL} = 0.6$ ps and the proportionality factor for the amplitude of the fluctuations (1.33) set to 2.5. The theory from panel d), which shows the best agreement, is based on phenomenological initial conditions with overall 13 independent variable parameters used to fit all curves simultaneously (two for each curve and one shared $\tau_{\rm GL}$). The best fit of the theory from the panel d) is obtained if parameter a) (4.6) is set to zero for all curves, parameter b has the values 0.25, 0.23, 0.162, 0.13, 0.1, 0.06 in the order of the increasing fluence, and $\tau_{\rm GL} = 1.1$ ps.

is much steeper than observed experimentally. For the smallest excitation when $\mathcal{F}(z=0) = \mathcal{F}_T = 4.2\mu$J/cm^2 and the condensate is destroyed only at the surface the recovery occurs in 50 fs. In the case of the strongest excitation the lattice temperature at the surface remains above $T_{\rm c}$ for significant time so that the S/N boundary follows the temperature front.

The soliton reaches the surface on the timescale of the order of the recovery time $\tau_{rec} \sim 30$ ps which is much larger than the transition time $\tau_{\rm c} \sim 1$ ps. As a result between the N/S boundary and the surface there is a supercooled region unstable to the formation of the ordered phase. Thus we expect that growth of the order parameter here will be defined by fluctuations. In the introduction we presented the theory developed by Volovik final result of which is given by Eq. (1.33). The amplitude of the fluctuations within the theory is defined by the quench rate $(1/\tau_{\rm Q})$ which in principle can be calculated from the TTM. The obtained shape of the initial conditions is shown in the left panel of Fig. 4.8. These IC result in a trajectory that resembles experimental data better than the previous two approaches but the discrepancy is still notable (4.7 c).

Finally we introduce a phenomenological initial condition in the simplest form of a linear depth dependence of the fluctuations magnitude allowing the fitting parameters to vary with fluence (in contrast to the previous case where only two parameters, shared between all curves, were varied: proportionality factor for the

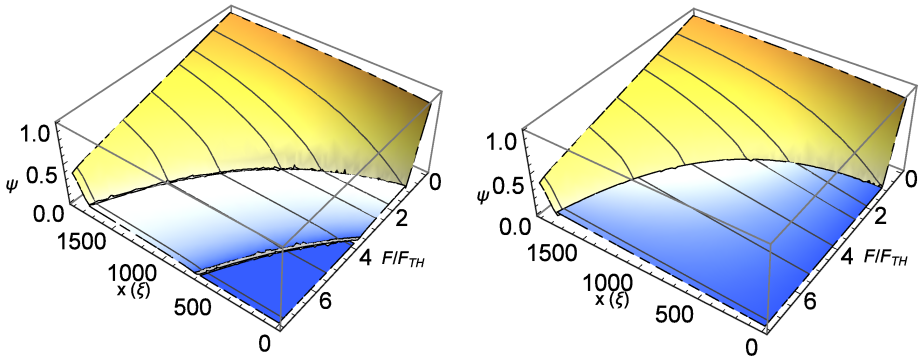


Figure 4.8: Initial conditions used with TDGL equation. Fluctuations are shown in blue (region $\mathcal{F}(z) > \mathcal{F}_{\rm th}$), in yellow is shown suppressed ordered parameter (for $\mathcal{F}(z) < \mathcal{F}_{\rm th}$) which is given by $(1 - \frac{\mathcal{F}_0}{\mathcal{F}_{\rm th}} e^{-z/\lambda})\sqrt{1 - T_{\rm L}(0,z)/T_c}$. Left: fluctuations described by Eq. (1.33) which result in the trajectory 4.7 c). Right: phenomenological initial conditions given by Eq. (4.6) which result in trajectory 4.7 d).

magnitude of the fluctuations and $\tau_{\rm GL}$)[3]:

$$\psi(0,z) = \begin{cases} a + b\,z & ,\mathcal{F}(z) > \mathcal{F}_{\rm th}; \\ (1 - \frac{\mathcal{F}}{\mathcal{F}_{\rm th}} e^{-z/\lambda})\sqrt{1 - T_{\rm L}(0,z)/T_c} & ,\mathcal{F}(z) < \mathcal{F}_{\rm th}. \end{cases} \tag{4.6}$$

The shape of these initial conditions is shown in the right panel of Fig. 4.8. A remarkable feature of these initial conditions is that there is nearly no fluctuations at the surface of the sample (coefficient a is always negligibly small and can be set to 0) while the coefficient b falls almost linearly with fluence. These initial conditions can hardly be considered as physical within set forth theory: the amplitude of fluctuations is defined solely by the temperature evolution $\psi(0,z) \approx \psi(t_c,z) = f(T(t,z)_{t\to t_c})$, which, neglecting the ballistic and diffusive transport and long-range interactions (which are suppressed in the case of the fast quench), is a unique function of the absorbed energy which has an exponential with the depth shape $T(t,z) = f(P_0 e^{-z/\lambda}) = T_0(ln(P_0) - z/\lambda)$, parentheses indicate a functional dependence, P_0 is the absorbed energy density at the surface. In other words increasing fluence should logarithmically shift $\psi(0,z)$ deeper, which is clearly not the case for Eq. (4.6). Nevertheless it is instructive that the two-parameters fit can produce reliable trajectories.

In conclusion, the TDGL model in the presented formulation fails to produce a reliable description of the superconducting-to-normal and normal-to-superconducting phase transitions simultaneously. Considering only the normal-to-superconducting transition with realistic initial conditions gives good results. Though the soliton propagation occurs on the realistic time scale calculated shape of $A_{\rm S}(t_{\rm D-P})$ recovery is too steep. Accounting for fluctuations results in trajectories close to those observed experimentally and it is enough to provide a two-parameter phenomenological initial conditions describing the fluctuations to simulate the observed trajectories.

[3]Note that in this case for the lowest fluence curve we artificially set the fluence to 0.8 of experimentally measured value in order to fit the diffusion part. As the heat capacity diminishes with $T \to 0$ inaccuracies in the fluence measurements lead to larger errors in $T_{\rm L}$ and consequently $A_{\rm S}(t_{\rm D-P})$ errors in the quasi-equilibrium regime.

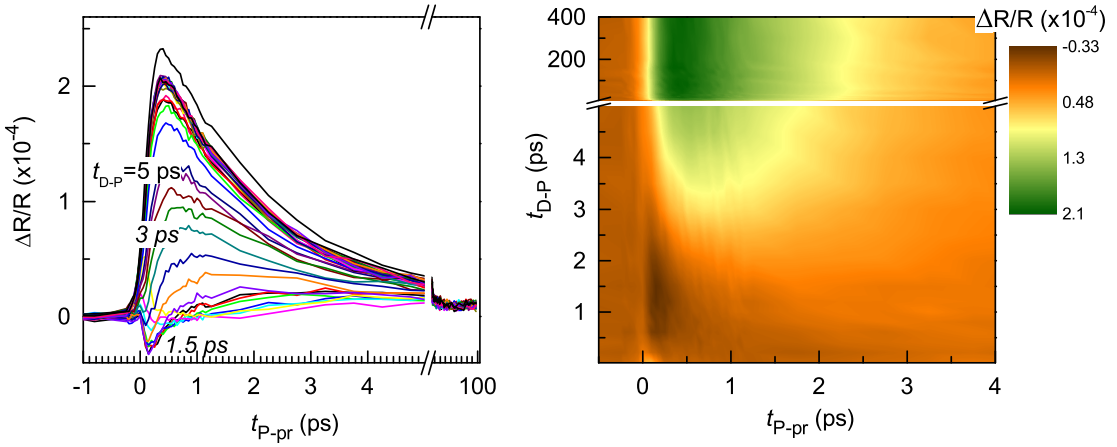


Figure 4.9: Recovery of the superconducting response in BSCCO. Left panel: transient reflectivity $\Delta R/R$ for UD BSCCO at 15 K as a function of $t_{\mathrm{P-pr}}$ for different $t_{\mathrm{D-P}}$ (0.4, 3 and 9 ps are designated). The D pulse fluence is $\mathcal{F}_{\mathrm{D}} = 132\,\mu\mathrm{J/cm}^2$. Right panel: The same data as in the left panel but shown as a colormap in $t_{\mathrm{D-P}}$ - $t_{\mathrm{P-Pr}}$ plane.

4.4 Recovery of the Superconducting Condensate in BSCCO

In this section we present the results of the three-pulse experiments in the superconducting state in UD BSCCO with $T_{\mathrm{c}} = 81$ K. First we conducted the standard (as in the previous sections) three pulse experiments systematically varying the D fluence (from $\mathcal{F}_{\mathrm{th}}^{\mathrm{SC}}$ to $10\,\mathcal{F}_{\mathrm{th}}^{\mathrm{SC}}$) and temperature (at 15 K, 40 K, 65 K, 83 K), all three beams were at the same wavelength of 800 nm.

With respect to the data analysis and applicability of TDGL theory BSCCO has several disadvantages compared to LSCO but also a major advantage, a higher T_{c}. The main issue which affects purity of the experiment is the presence of the pseudogap response with a relatively low photodestruction threshold $\mathcal{F}_{\mathrm{th}}^{\mathrm{PG}} \approx 4\mathcal{F}_{\mathrm{th}}^{\mathrm{SC}}$. As a result already for a moderate D pulse fluence the pseudogap response is suppressed and cannot be separated from the superconducting by subtraction.

A typical result of the experiment is presented in Fig. 4.9 measured at 15 K with $\mathcal{F}_{\mathrm{D}} \approx 10\,\mathcal{F}_{\mathrm{th}}^{SC}$(the left panel shows the raw data, the right panel - the same data as in the left panel shown as a color-plot in the $t_{\mathrm{D-P}} - t_{\mathrm{P-pr}}$ plane). We remind that in BSCCO three components are distinguished in the pump-probe data: the positive metallic, the negative pseudogap and the positive superconducting. In the presented dataset at early times both the pseudogap and the superconducting signals are suppressed. The pseudogap component rapidly recovers on the 0.5 ps timescale. The superconducting response recovers much slower with a characteristic recovery time $\tau_{\mathrm{rec}}^{SC} \sim 3$ ps. While in Chapter 3 we have shown that at high temperatures experiments reveal that τ_{rec}^{PG} is nearly independent on the fluence and temperature we cannot confidently claim the same for the temperatures below T_{c}. Nevertheless we analyze the data using this assumption to further compare the results with more direct measurements of the superconducting component based on the polarization selection rules described further in text.

For the purpose of comparison of $\Delta R/R(t_{\mathrm{P-pr}})$ evolution with the evolution of the order parameter it is more reliable to read-out the value of the $\Delta R/R(t_{\mathrm{P-pr}})$ at a fixed early delay $t_{\mathrm{P-pr}}$(when the signal is already large) than to follow the

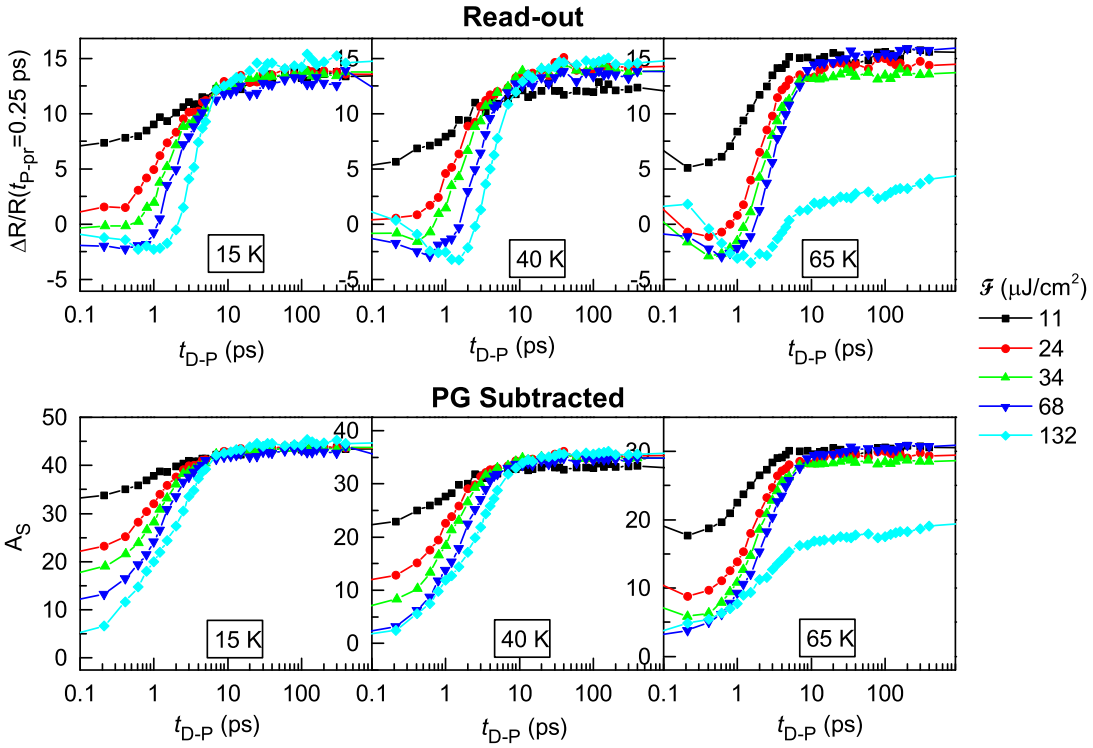


Figure 4.10: Evolution of the superconducting component in BSCCO. Top panel: read-out values of $\Delta R/R(t_{\mathrm{P-pr}} = 0.25)$ ps as a function of $t_{\mathrm{D-P}}$ for different $\mathcal{F}_{\mathrm{D}}$ at different temperatures. Bottom panel: data from the top panel with the PG component subtracted (see text).

maximum of the response which can occur at a very different $t_{\mathrm{P-pr}}$ due to the changes in the relaxation time as well as the recovery of the gap (see Section 2.3). The position of the maximum $\Delta R/R(t_{\mathrm{P-pr}})$ varies from 0.6 up to 5 ps (Fig. 4.9). In Fig. 4.10 we present the data obtained in this way. As we are aiming to subtract the pseudogap component we select to read-out the amplitude at the delay $t_{\mathrm{P-pr}} =$ 0.25 ps, i.e. of the maximum negative $\Delta R/R(t_{\mathrm{P-pr}})$ where the PG contributes the most. We notice that for the highest fluence at 15 K and starting already from $\mathcal{F}_{\mathrm{D}} \approx 34$ μJ/cm^2 at 65 K, first recovery of the negative PG component is observed which is thereupon overtaken by the positive SC component. For each temperature we fit the pseudogap component $A_{\mathrm{PG}}(t_{\mathrm{D-P}})$ of the largest D fluence dataset with an exponential function. We simultaneously fit all the temperatures and share the recovery time $\tau_{\mathrm{rec}}^{\mathrm{PG}}$ parameter assuming that it is temperature and fluence independent (assuming the observation made in Chapter 3 to remain valid at low T). The best agreement is achieved for $\tau_{\mathrm{rec}}^{\mathrm{PG}} = 0.75$ ps. Subsequently we scale the pseudogap component $A_{\mathrm{PG}}(t_{\mathrm{D-P}})$ with the fluence to the lower D fluence curve, where the pseudogap component is not explicit. The scaling is done in accordance with the fluence dependence measured at $T > T_{\mathrm{c}}$ and subtract it from the read-out $\Delta R/R(t_{\mathrm{D-P}})$. The result of the subtraction is presented in Fig. 4.10. We fit the recovery by an exponential function with an additional term describing the heat

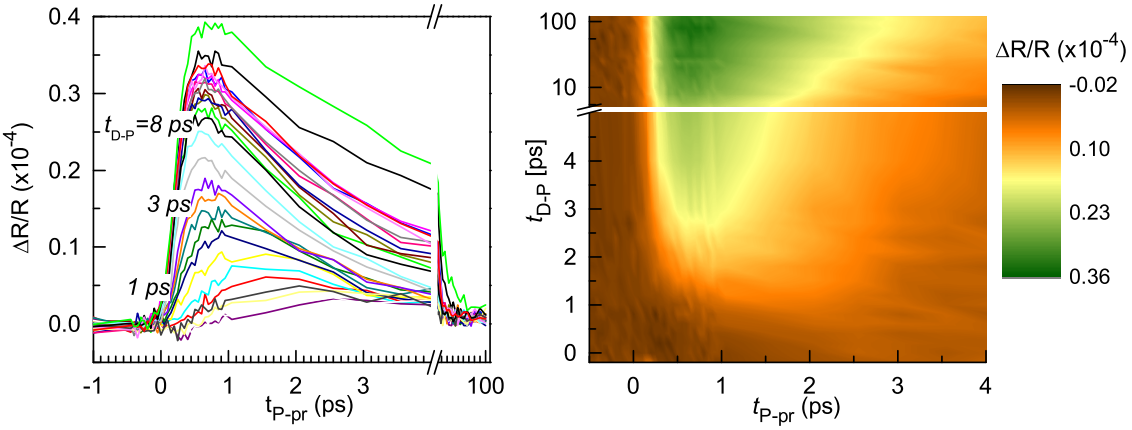


Figure 4.11: A typical result of the balanced 3 pulse experiment. Left panel: transient reflectivity $\Delta R/R$ for UD BSCCO at 15 K as a function of $t_{\mathrm{P-pr}}$ for different $t_{\mathrm{D-P}}$ (0.4, 3 and 9 ps are designated). The D pulse fluence is $\mathcal{F}_{\mathrm{D}} = 102\,\mu\mathrm{J/cm^2}$. Right panel: the same data as on the left panel but shown as a colormap in $t_{\mathrm{D-P}}$ - $t_{\mathrm{P-Pr}}$ plane.

diffusion (see for instance Supplementary to[155])

$$A_{\mathrm{S}} = 1 - A_{\mathrm{ne}} e^{-t/\tau_{\mathrm{rec}}} - A_{\mathrm{th}}/\sqrt{t/\tau_{\mathrm{D}} + 1}. \tag{4.7}$$

The resulting parameter values are present in Fig. 4.13.

The presented analysis is based on a number of assumptions which are hard to validate. Alternatively one can modify the experiments to extract the superconducting component experimentally by taking into account dependence of the signal on the probe polarization discussed in the Section 3.2. Namely we are using the balanced scheme presented in Section 2.4. By balancing the detector and subtracting the orthogonal polarizations which are aligned in this case in agreement with the perpendicular Cu-O directions we detect only a doubled B_{1g} component of the pump-probe response rejecting A_{1g} and B_{2g}. Consequently the pseudogap and the hot-electron energy relaxation components are rejected. The signal to noise ratio is significantly lower than in the case when the whole signal is recorded - the ratio of B_{1g}/A_{1g} is only 0.1. While most of the contribution from the $A_{1\mathrm{g}}$ channel is rejected it can still leak to the signal due to imperfect balance of the orthogonal polarizations, this does not affect the shape of $A_{\mathrm{S}}(t_{\mathrm{D-P}})$ significantly as the symmetric component is dominated by the superconducting component, but can give an observable variation in the absolute value. In this experiment we used a frequency doubled pump beam.

In Fig. 4.11 we present the raw data for the balanced detection 3 pulse experiment measured at 15 K with $\mathcal{F}_{\mathrm{D}} \approx 8\,\mathcal{F}_{\mathrm{th}}^{\mathrm{SC}}$ which can be compared with the result of the conventional 3 pulse measurements presented in Fig. 4.9. In the balanced detection case no signatures of the pseudogap response is observed while the recovery of the superconducting component occurs in a similar way to the standard experiment. We analyze the data in a way similar as presented before: to reduce the noise we average $\Delta R/R$ in the 0.2 ps vicinity of the fixed delay $t_{\mathrm{P-pr}}$=0.8 ps which corresponds to the maximum of the recovered signal. The result of such analysis is presented in Fig. 4.12.

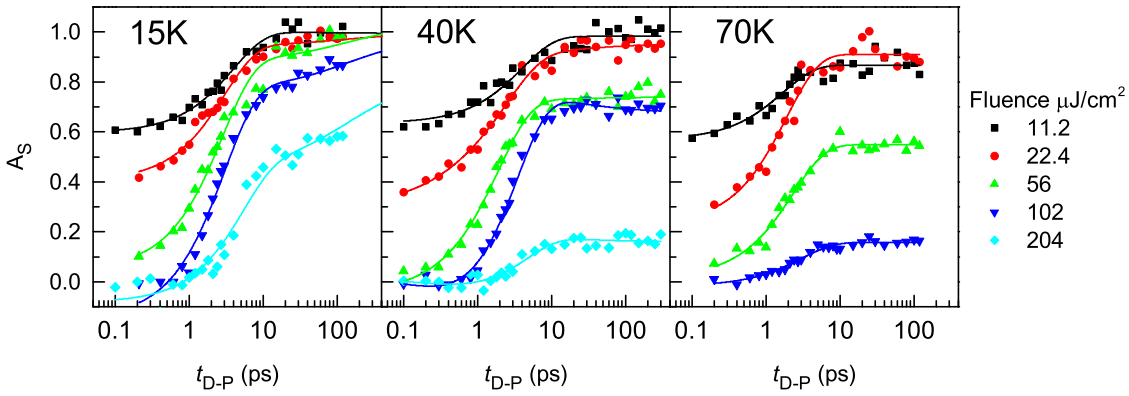


Figure 4.12: Amplitude of the superconducting component as a function of $t_{\mathrm{D-P}}$ for different $\mathcal{F}_{\mathrm{D}}$ at different temperatures measured in the balanced 3 pulse experiment. Lines are fits with a sum of the exponential recovery and heat diffusion term (see text).

The recovery is fitted with the same phenomenological function Eq. (4.7) as in the case of the standard experiment. While for the intermediate fluences the fit is reliable for the highest two values of fluence there is a significant discrepancy at early delays. This is due to the fact that recovery of the superconducting condensate is delayed and there is nearly no signal for up to 1 ps. This effect has been previously observed in a high power two-pulse experiment.[79] The recovery times τ_{rec} obtained from the aforementioned fits are presented in the Fig. 4.13. Variation of the recovery time with fluence is weak and only slightly exceeds the standard deviation of the fit. Qualitatively at low temperatures a minimum around 50 μJ/cm^2 is observed, while at temperatures close to T_{c} recovery time monotonically increases with fluence. It is instructive to compare the recovery time obtained in the 3 pulse experiment with the quasiparticle relaxation time measured in 2 pulse experiment shown in open squares. The QP relaxation time shows similar fluence dependence - it also has a minimum which appears to be shifted towards lower fluences.

The absolute values of the relaxation time measured above appear to be higher than from the estimates obtained via the PG subtraction in the conventional 3-pulse experiment. This is presumably due to inaccuracy in the assumptions used in the PG subtraction.

In the low excitation limit the reduction of the relaxation time with increasing fluence can be explained within the bottleneck RT model[4] (Eq. (1.12)). However at $\mathcal{F}_{\mathrm{D}} \approx \mathcal{F}_{\mathrm{th}}^{SC}$ it is not applicable anymore. Increase of the relaxation time with fluence can be explained by the transient lattice heating which leads to the slowing down of the recovery in the vicinity of T_{c}. The errors in τ_{rec} determination are however too large to confirm or disprove this hypothesis.

The similarity between $\tau_{\mathrm{rec}}(\mathcal{F})$ and $\tau_{\mathrm{QP}}(\mathcal{F})$ indicates firstly that changes in the reflectivity observed in the two-pulse response at delays $t_{\mathrm{P-pr}} > 1$ ps are caused by the recovery of the superconducting state and secondly the quasiparticle recombination leads directly to the formation of the Cooper pairs without any intermediate steps (such as pseudogap formation).

In the Fig. 4.14 we plot the dependence of the quasiparticle relaxation rate $1/\tau_{\mathrm{QP}}$

[4] Note that it is valid only for low temperatures.

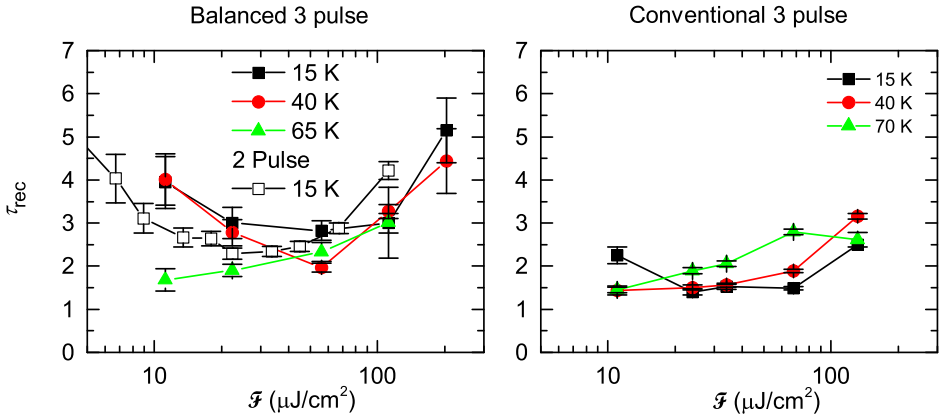


Figure 4.13: Recovery time of the superconducting component as a function of D pulse fluence for different temperatures. Left panel presents data measured by balanced 3 pulse technique, right panel - conventional 3 pulse measurements with subsequent PG subtraction. Quasiparticle relaxation time measured in 2 pulse experiment is shown for comparison.

on $t_{\mathrm{D-P}}$ measured at 40 K, $\mathcal{F}_{\mathrm{D}} \approx 50\,\mu\mathrm{J/cm}^2$.[5] For comparison on the same graph amplitude of the superconducting component is shown. In the non-equilibrium part of the trajectory two data sets nearly coincide in a similar way as it has been seen in LSCO. In the thermal part $1/\tau_{\mathrm{QP}}$ decreases exhibiting a weak increase with cooling in accordance to Eq. (1.12) and Fig. (1.6).

Application of the TDGL theory to BSCCO system is less reliable than to LSCO due to several reasons. Firstly BSCCO has a significant response due to the fluctuations above T_{c}, described in Chapter 5, which are not included in the TDGL theory. Secondly the recovery of the SC signal is one order of magnitude faster and becomes comparable with the timescales of the two-temperature model. This makes the solution much more sensitive to the exact time- and depth- dependence of the electronic temperature, which as we already mentioned, is poorly defined on this timescale. Finally the signal is very weakly dependent on temperature in the low T region (see Fig. 1.5) which makes it hard to establish a well-defined response function. From the experimental point of view the aforementioned leakage of the $A_{1\mathrm{g}}$ component can introduce an error in the magnitude of the amplitude, which is crucial for the modeling.

4.5 Criticism

Let us now discuss the applicability of the assumptions that we have made, and discuss possible issues with the presented model.

Firstly let us cover possible issues with the presented response function $g(\psi)$. The assumption that our response is defined solely by the order parameter, contradicts to the theory presented in the Section 1.2.3, in which the number of the photoinduced quasiparticles is a complicated function of temperature and order parameter. Within

[5] We intentionally presented the data at 40 K to avoid significant contribution from the low-T divergence described by Eq. (1.12)

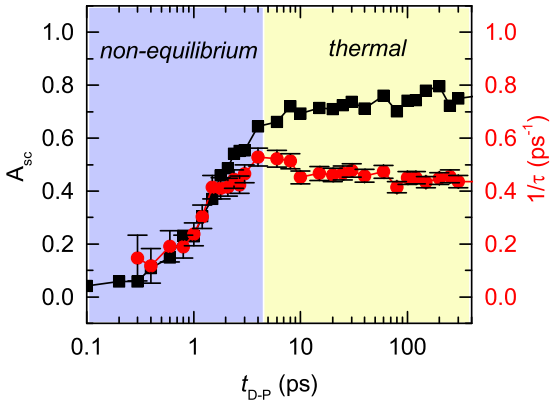


Figure 4.14: Evolution of the quasiparticle relaxation rate and amplitude of the superconducting component measured in balanced 3 pulse experiment at $T = 40$ K and $\mathcal{F}_D \approx 50\,\mu J/cm^2$. By background color we divide the trajectory in non-equilibrium stage where $1/\tau_{QP} \sim \Delta$ is valid and quasiequilibrium thermal part where $1/\tau_{QP}$ can be described by Eq. (1.12).

this theory the gap term dominates $\Delta R/R(T)$ closer to T_c, while at intermediate temperatures changes in $\Delta R/R(T)$ are mostly due to temperature dependence of the energy balance conditions between electrons and phonons, which is defined by their heat capacities. This can be clearly seen from the $T-$dependence of the pseudogap response, which corresponds to the $T-$independent gap [compare Fig. 1.5 a) and b)]. In the presented experiment on LSCO the surface lattice temperature exceeds 0.5 T_c even for the lowest fluence and on the surface the response is mostly defined by the gap behaviour. However further in the depth the temperature is lower and the number of photoexcited quasiparticles changes with $T(z)$ even if the gap was uniform.

Another issue of the presented response function is the linearity of the response with the order parameter presented in Fig. 4.1. As the order parameter is a complex number it must enter the measurable quantities as a square to preserve the gauge invariance. However if we use instead of the GL expression $|\psi| = \Delta = \Delta_0\sqrt{1 - T/T_c}$ the standard approximation for the BCS gap function $|\psi| = \Delta = \Delta_0 \tanh(1.74\sqrt{T_c/T - 1})$ and fit the $T-$dependence with the Mattis-Bardeen expression Eq. (1.7) which is approximately equal to Δ^2,[6] the agreement with the data will be of the same quality (Fig. 4.15). Though the BCS expression should be described by the GL formula at $T \to T_c$, it is its square which coincides with the GL order parameter nearly in the whole temperature region.

Of course physically the most correct is the description of the gap by the BCS formula, but then there is no such simple and elegant theory as the TDGL theory to describe order parameters dynamics. We should admit that the observed inconsistency is due to the application of the GL theory outside of its natural applicability domain.

[6] The logarithmic term $ln(\frac{\hbar\omega}{\Delta})$ in Eq. (1.7) for $\hbar\omega \gg \Delta$ varies much slower than Δ^2 and can be dropped.

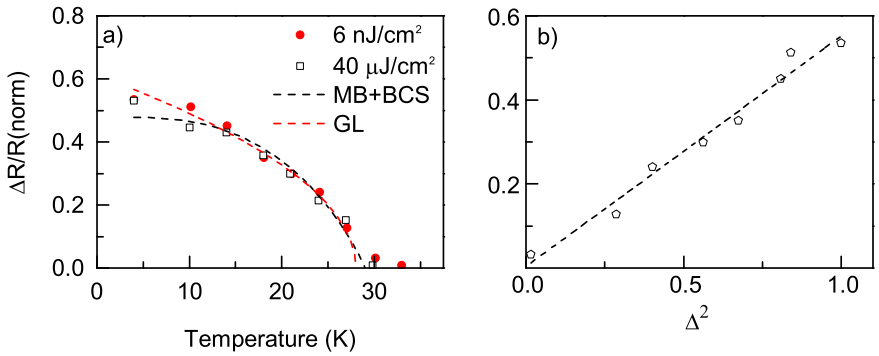


Figure 4.15: The response function with GL versus BCS gap dependence. a) Temperature dependence of the normalized transient reflectivity in high (40 μJ/cm^2) and low (6 nJ/cm^2) excitation regimes in LSCO (data from [103]). Dashed lines correspond to the fit by Mattis Bardeen formula Eq. (1.7) and BCS order parameter dependence (black) and GL order parameter dependence $|\psi| = \Delta = \Delta_0\sqrt{1 - T/T_c}$ (red). b) Dependence of the low excitation transient reflectivity on Δ^2 (approximation of the Mattis-Bardeen expression for high fluence data Eq. (1.7)) extracted from a). The line is a power law fit to the data, the fitted value of the power is 1.1.

Summary and Conclusions

In this chapter the physical concepts dealing with the normal-to-superconducting phase transition are presented. In the first Section we presented the phenomenological response function which relates the order parameter to the the transient reflectivity in the low perturbation limit.

In Section 4.2 the 3 pulse studies of the destruction of the superconducting condensate are presented, systematically with fluence and temperature. We show that the photodestruction time is independent on experimental conditions, interpreting this fact as a signature of highly non-equilibrium, i.e. not describable by the TDGL theory, superconducting-to-normal phase transition.

The recovery of the superconducting condensate is presented in Sections 4.3 and 4.4. The superconducting component recovers in the range of 30 ps in LSCO and 5 ps in BSCCO. The comparison of the observed trajectory to the numerical simulation of the TDGL equations reveals the importance of fluctuations for the growth of the ordered phase in the non-homogeneous experiment. Previously reported model for the amplitude of the fluctuating order parameter in combination with the TTM gives approximate correspondence of the simulated trajectories to the experimentally observed. We show that the phenomenological two parameter function describing order parameter fluctuations density can give good agreement to the observed data.

In Section 4.4 we devise the method to extract the superconducting component of the transient reflectivity based on the polarization selection rules reported in previ-

ous chapter and compare it to more indirect data analysis based on the extrapolation of high-temperature pseudogap behavior into the superconducting region. We report temperature and fluence dependence of the superconducting recovery time and find reliable agreement.

Chapter 5

Superconducting Fluctuations

In this chapter we consider fluctuations of the superconducting order which cannot be considered separately from some unconventional but strongly advocated concepts of phase transition in the cuprates, which we describe in the first section. Further we show how the three-pulse technique provides an unique way to separate the superconducting response from the pseudogap response and present the dynamics of the superconducting condensate. Comparison of the optical data with the published THz data is provided. It allows us to establish a correspondence between the pump-probe response and the "bare" superfluid density and discriminate between the dynamics of the amplitude and phase of the superconducting order parameter.

5.1 Superconducting Fluctuations: General Overview

The Ginzburg-Landau theory deals with the order parameter averaged over fluctuations, assuming that fluctuations are uncorrelated (Gaussian fluctuations). Its applicability is limited by the applicability of the Taylor expansion at low temperatures and by the applicability of the description of fluctuations as uncorrelated in the vicinity of the transition. The temperature at which fluctuations become significant and consequently correlated is called the Ginzburg temperature T_{Gi} (we will also use the Ginzburg parameter $\mathrm{Gi} = \frac{\Delta T_{\mathrm{fluc}}}{T_{\mathrm{c}}} = \frac{T_{\mathrm{c}} - T_{\mathrm{Gi}}}{T_{\mathrm{c}}}$). The estimate of this parameter can be obtained by equating the energy cost of the fluctuation formation in the ξ^3 volume [1] to the temperature. For three dimensional isotropic superconductors one can estimate[91] $\mathrm{Gi} \sim (k_{\mathrm{F}}\xi_0)^{-4}$. In conventional superconductors where the coherence length is much larger than the interatomic distance $k_{\mathrm{F}}\xi_0 \sim 100$ and $\mathrm{Gi} \ll 1$ so the fluctuating region is always negligibly narrow. For the cuprates as well as pnictides and other layered anisotropic or amorphous superconductors with a short coherence length the estimate given above is generally not applicable. In the case of dirty superconductors the coherence length is significantly smaller, $\xi_{\mathrm{d}} = \sqrt{\xi l}$, here l is the mean free path, leading to a significantly broader fluctuation region. In the case of anisotropic cuprate superconductors (especially BSCCO) a two-dimensional consideration is more appropriate: now we should consider the energy cost of the fluctuation creation in the volume $\xi_0^2 d$, where d corresponds to the out-of-plane coherence length (for thin films d marks the film thickness). The Ginzburg parameter is much larger[91] in this case $\mathrm{Gi}_{2D} \sim \frac{1}{k_{\mathrm{F}}^2 \xi_0 d}$ which is of the order of 10^{-2}. Thus the temperature region where fluctuations are large is accessible for experimental

[1] If the spatial extent of the fluctuations reaches ξ they are considered as correlated.

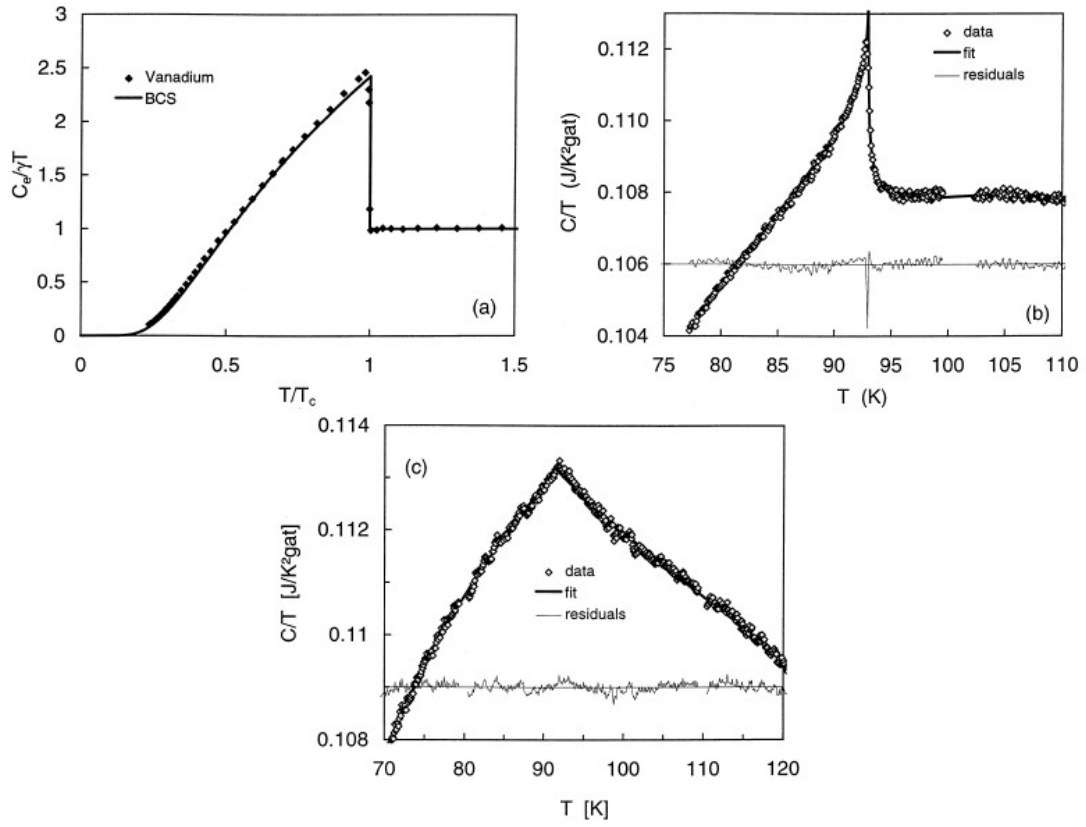


Figure 5.1: The specific heat of the representatives for different classes of superconductors which are best described by different models. (a) Data for vanadium and a BCS fit. (b) 3D XY specific heat of ^{4}He (line) scaled to that of $YBa_2Cu_3O_{6.92}$(dots) (c) The specific heat of the Bose condensation and corresponding fit to the optimally doped $Bi_2Sr_2CaCu_2O_x$ data. The figure is adopted from [156].

observation.

In the fluctuating region the long-wavelength fluctuations dominate thermodynamic properties and behavior of the system is no longer defined by material specific quantities, but solely by the space dimensionality, the dimensionality of the order parameter and the Hamiltonian symmetry which altogether define its membership in a particular universality class. Each universality class is characterized by unique $T-$dependence of thermodynamic quantities, typically represented by a power law of reduced temperature ϵ with the power called the critical exponent. This temperature behavior differs significantly from predictions of Ginzburg-Landau theory and thus experimental observations can establish directly the extent of the fluctuation region. One pedagogical example is heat capacity measurements. The three-dimensional complex order parameter belongs to the 3D XY universality class (Heisenberg ferromagnet model with an easy plane). The critical exponents are not only known from the theory but measured precisely for superfluid helium. In Fig. 5.1 b) comparison of optimally doped $YBa_2Cu_3O_{6.92}$ and ^{4}He shows a perfect agreement indicating the fluctuation region extending to several K. For illustration of the narrowness of the fluctuation region in the conventional superconductor specific heat data for vanadium are shown in Fig. 5.1 a).

The situation is however significantly more complicated in more anisotropic com-

pounds. Here the 3D XY behavior is expected only within the narrow region $\epsilon_{cross} \sim \left(\sqrt{m_c/m_a m_b}\right)^{-3/2}$, where m_a, m_b, m_c are the carrier effective masses along corresponding directions. ϵ_{cross} varies from 0.08 in YBCO to 0.00025 in BSCCO. Outside this region but still within the fluctuation region the behavior is expected to be described by 2D XY critical exponents. However, as with the increase of the anisotropy the coherence length is typically reduced and becomes comparable to the wavelength of holes[157], the Bose-Einstein Condensation description of the phase transition appears to be more appropriate. For instance in the most anisotropic cuprate BSCCO ($\sqrt{m_c/m_a m_b} \sim 250$) the specific heat anomaly [Fig. 5.1 c)] becomes symmetric and approaches triangular shape of BEC which belongs to the universality class of the spherical model of ferromagnetism. The principle physical difference between BEC and GL approaches is that the specific heat anomaly in the case of BEC is produced by short range fluctuations rather than that of long range. More detailed description of different universality classes in the cuprates can be found in [156], [158].

The peculiar behavior of the superconducting fluctuations response in BSCCO has also been observed by other techniques (listed below) in a temperature range significantly wider than $\epsilon <$ Gi, which provided arguments for an alternative to aforementioned BCS and BEC scenarios. The most prominent argument is the interpretation of the transition as being of the Berezinski-Kosterlitz-Thouless [159]–[161] (BKT) type. In the BKT theory phase transition in a 2D superconductor is considered. At finite temperatures thermally activated vortex-antivortex pairs exist in the superconductor and their density is defined by the Boltzmann distribution with the pair creation energy over $k_{\mathrm{B}}T$ in the exponent. As long as vortices and antivortices remain paired (due to the attractive interaction) they do not contribute to the transport properties. However with the increasing temperature the pair density increases. This leads to screening of the vortex-antivortex interaction. At the transition temperature T_{BKT} the pairs break and vortices start to move freely forming a vortex plasma. Due to large condensate phase fluctuations resulting from the vortex movement macroscopic order parameter averages to zero, even though $T_{\mathrm{BKT}} < T_{\mathrm{MF}}$ given by the Ginzburg-Landau theory.

Somehow close to the BKT scenario is the description of the transition as the one driven by phase fluctuations given by Emery and Kivelson [162], [163]. They have introduced the characteristic energy scale for phase fluctuations - the zero temperature "phase stiffness" $V_0 = \frac{\hbar^2 n_s(0) a}{4m^*}$, which defines the temperature T_Θ of the transition if all the other degrees of freedom are considered as ordered: $V_0 \approx AT_\Theta$, here $a \sim \sqrt{\pi}\xi_0$, and A varies from 0.9 in the 2D case to 2.2 in the isotropic 3D superconductor. While for conventional superconductors the ratio T_Θ/T_{MF} is above 10^3, for the cuprates the two temperatures are of the same order. This is because of small zero-temperature superfluid density $n_s(0)$, which owing to the generally low carrier density in the cuprates produces a low phase stiffness. Basically authors argue that phase fluctuations are responsible for T_{c} in the underdoped region of the phase diagram and become less significant with doping. On the overdoped side of the SC dome T_{c} approaches the pseudogap T^* line which is attributed to the mean-field transition temperature.

In their later work[164] authors discriminate between the pairing onset and the pseudogap. They summarize early experimental observations and on their basis define the onset temperature of the superconducting correlations without the long-

range phase coherence responsible for the spin gap observed in NMR and narrowing of the in-plane Drude peak and, at higher temperatures, the onset of the short-range stripe correlations which gives rise to the Knight shift and c-axis ac conductivity pseudogap (spectral weight transfer to higher frequencies). The presence of two crossovers in the normal state is nowadays widely accepted though the origin of the superconducting response above T_c is still not settled.

5.2 Observation of Superconducting Response above T_c by Three Pulse Technique

The superconducting response has been previously observed above T_c by a number of experiments: transport[165]–[169], magnetic susceptibility[170], [171], specific heat[158], [172] and ARPES[173]. In all of them however there is a problem with separating the response due to superconducting fluctuations from the PG. One inevitably has to make extrapolations, or assumptions about the response functions and underlying temperature dependencies. This may at best introduce inaccuracies in the temperature scales, and at worst lead to erroneous conclusions. Alternatively one can separate out superconducting component by suppressing it by high magnetic fields of the order of 60 T [174]. In such experiments there exists a risk of inducing new states by such a high field [175].

Here we propose a new way to discriminate between the two responses and moreover separate fluctuations of the amplitude $\delta\psi$ (related to the pairing gap) and phase $\delta\theta$ of the complex order parameter $\Psi = \psi e^{i\theta}$. We rely on the fact that, at least for the underdoped BSCCO the energy required to suppress superconductivity via photoexcitation ($F_{\rm th}^{\rm SC} = 13\ \mu J/cm^2$) is much smaller than that for the pseudogap photodestruction ($F_{\rm th}^{\rm PG} = 58\ \mu J/cm^2$). Consequently the range of fluences, where the superconducting response is completely suppressed while the pseudogap response is still nearly linear with the excitation fluence, is available.

To take the advantage of the aforementioned property and separate the SC component from the PG component we use the 3 pulse technique. First a relatively strong "destruction" (D) pulse, with fluence just above the superconducting state photodestruction threshold $F_{th}^{\rm SC} = 13\ \mu J/cm^2$[79], destroys the superconducting condensate[90] and suppresses the SC response. As the pseudogap response remains in the linear regime there is no effect of the D pulse on it within the noise level confirmed by measurements at 120 K presented in Fig. 5.2 e)[2] Note that here and further in the text the noise level at different data sets vary due to different signal accumulation times, the noise level at 120 K $\sigma_{\Delta R/R} \lesssim 0.4 \times 10^{-5}$ is smaller than that for the superconducting signal discussed further.

[2]Strictly speaking this is not true. From the previous chapter one can see that it is already possible to measure the pseudogap suppression even at fluence four times smaller than the threshold. The suppression of the pseudogap response in this case is below 10% which with currently used fluences of the pump beam will give the signal change of the order of 0.5×10^{-5} at 100K. This is still two times smaller than the smallest measured value of the superconducting response. The suppression of the pseudogap response in the three-pulse experiments appears due to the imperfect linearity of the response with fluence, which from the physical point can be considered as a weak dependence of the efficiency of the quasiparticle excitation on the number of the excited carriers in the pseudogap state.

5.2.1 Results

A typical result of the 3 pulse experiment is presented in Fig. 5.2g). In the absence of the D pulse the signal consists of the positive SC and the negative PG component. After the arrival of the D pulse we see a disappearance of the SC part and only the PG component is present [the dark-red line in Fig. 5.2c)]. With increasing $t_{\mathrm{D-P}}$ the superconducting response gradually re-emerges [the blue line in Fig. 5.2c)]. As most of the condensate in the probe volume is "destroyed" by the D pulse we can extract the superconducting component by subtracting the signal remanent after the destruction (measured 200 fs after the D pulse) from the signal obtained in the absence of the D pulse. Such an extracted superconducting component is plotted in Fig. 5.2b). The signal is detectable up to $T_{onset} = 104$ K, which is 0.28 T_c above T_c but much lower than $T^* \approx 2.5\ T_c$. In Fig. 5.2h) we show the recovery of the amplitude of the superconducting component A_{sc} as a function of the time delay $t_{\mathrm{D-P}}$ after the D pulse for 90 K. The temperature dependence of the amplitude of the SC component measured by 3-pulse technique $A_{\mathrm{sc}}^{\mathrm{3pulse}}$ is shown in Fig. 5.3b).

For comparison, standard pump-probe measurements need to separate the SC relaxation from the PG relaxation by subtraction of the high temperature response extrapolated into the superconducting region. This approach suffers from the same uncertainties as other techniques such as conductivity, heat capacity, diamagnetism and ARPES. The actual T-dependence of the PG response can vary with doping and probe wavelength [45], [79]. However, the subtraction procedure with the use of a temperature independent pseudogap model [64], [79] gives results in agreement with the direct 3 pulse measurements (Fig. 5.3). The remaining discrepancies in the amplitude can be explained by an incomplete destruction of the fluctuating superconducting state in the 3 pulse experiment and errors in the PG subtraction.

In Fig. 5.3a) we see that the QP relaxation time τ_{QP}^{3Pulse} obtained by fitting an exponential function to the data Fig. 5.2b) decreases rather gradually with increasing T above T_c and nearly coincides with the QP relaxation time obtained by the pseudogap subtraction procedure $\tau_{QP}^{Subtraction}$. The recovery time τ_{rec} obtained from exponential fits to the recovery of the SC response amplitude above T_c (Fig. 5.2 h) shows a similar T-dependence. The experiments thus show that the recovery of the SC gap and the QP relaxation show very similar dynamics above T_c.

We now compare these data to THz measurements in a sample with a very similar doping level and $T_c = 85$ K [176], [177]. Measurements of the ac susceptibility temperature dependence at different frequencies can reveal important information on the dynamics of the phase of the order parameter. In the low frequency limit vortices[3] move in response to the current and the conductivity is an inverse of the flux-flow resistivity. In the high frequency limit ($\omega \gg 1/\tau_\theta$) the vortices are immovable and the conductivity is defined by the fluctuating condensate density very similarly to the conductivity behaviour below T_c: $\sigma(\omega) \rightarrow \frac{e^2\hbar}{d}\frac{\rho_0}{(-i\omega)}$, here d - is the bilayer thickness and the constant ρ_0 is called the bare superfluid density in direct analogy to the superfluid density below T_c. In general within the BKT picture[178] the conductivity satisfies the scaling relation $\sigma(\omega) \rightarrow \frac{e^2\hbar}{d}\rho_0\tau_\theta S(\omega\tau_\theta)$ which allows experimental estimate of the $\tau_\theta(T)$ done in [176], [177]. Dependence of the $\tau_\theta(T)$ on the vortex density defined by the Boltzmann distribution gives a theoretical expression[176] for the phase relaxation time in the vortex plasma regime,

[3]While we preserve here the original consideration, which treats SC transition as BKT transition, the very similar arguments can be used to discuss the THz response from fluctuating superconducting patches.

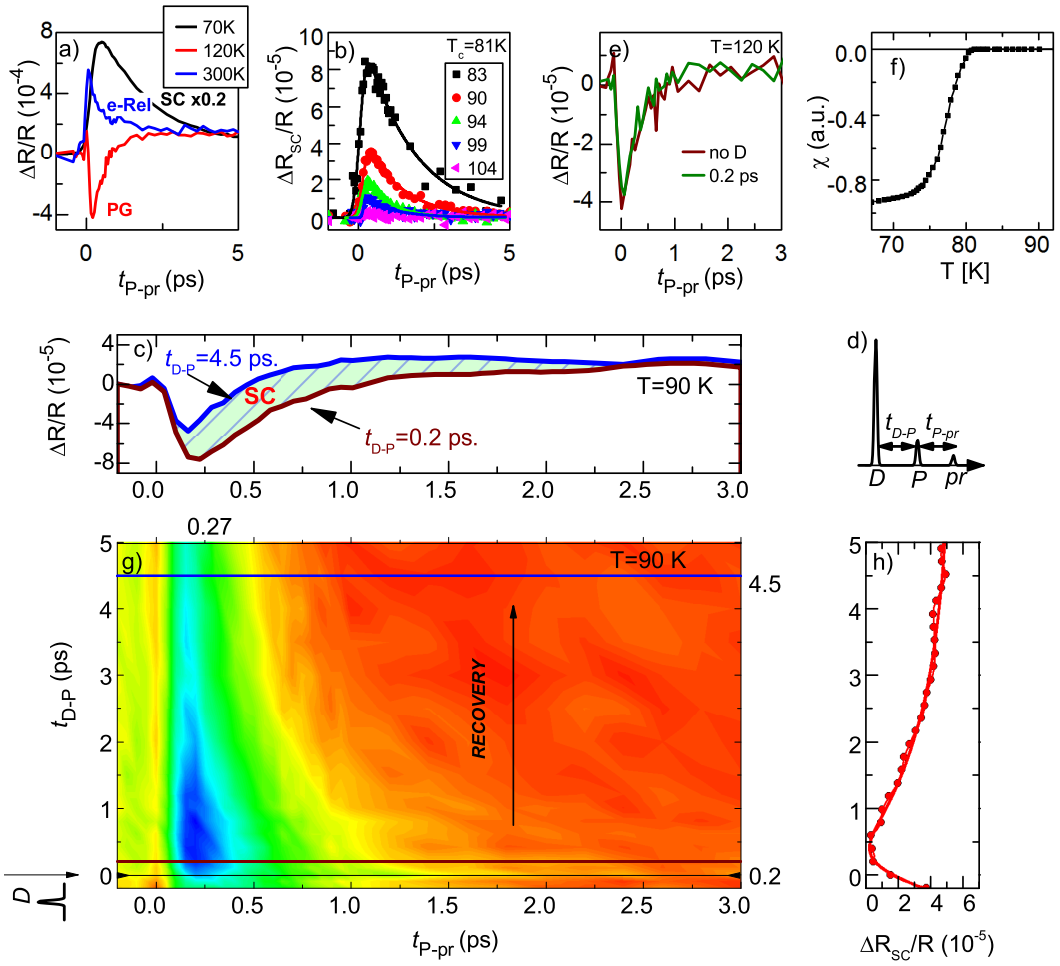


Figure 5.2: Description of the 3 pulse method and pump-probe signals. Underdoped sample data: a) Transient reflectivity signals observed at different temperatures in Bi-2212 - the SC signal, the PG signal and energy relaxation of hot carriers. b) The QP recombination at different T above T_c. c) Two typical 3-pulse pump-probe traces at t_{D-P} 0.2 and 4.5 ps show the signal with a suppressed and recovered superconducting component, respectively. d) The pulse sequence and delays notation in 3-pulse experiment. e) The pump-probe response at 120 K in the absence of the D-pulse and 0.2 ps after the D pulse arrival. f) The susceptibility curve shows $T_c = 81$ K for the underdoped sample. g) A typical result of three pulse experiments at 90 K shows the suppression of the SC component after the D pulse arrival and a gradual recovery with t_{D-P}. Readings along the blue and dark-red line are shown in Fig. 5.2c). The color represents the amplitude of the reflectivity change. The values of the color bars indicate $\Delta R/R \times 10^{-5}$. h) Recovery of the superconducting component amplitude with t_{D-P}.

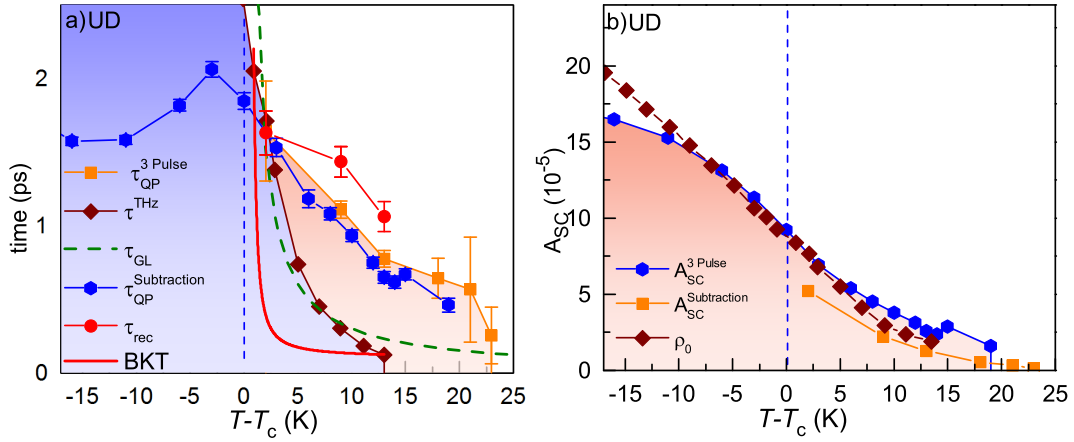


Figure 5.3: Comparison of pairing amplitude and phase coherence dynamics. a) The recovery time of the optical superconducting signal ($\tau_{\rm rec}$), the QP recombination time $\tau_{\rm QP}^{3Pulse}$ measured by the three pulse technique and the QP recombination time $\tau_{\rm QP}^{Subtraction}$ from the two pulse Pump-probe pulse measurements obtained by subtraction of the PG signal. A fit to the data using the BKT model (Eq. (5.1)) is shown by the solid red line. The dashed line shows the fluctuation lifetime $\tau_{\rm GL}$ given by the TDGL theory. The phase correlation time τ_θ^{THz} obtained from the THz conductivity measurements [177] is also shown for comparison. b) The amplitude of the SC signal measured by the three pulse technique ($A_{\rm SC}^{3Pulse}$) and the two pulse measurements with the PG signal subtracted ($A_{\rm SC}^{Subtraction}$). The bare phase stiffness ρ_0 [177] (normalized at T_c) shows remarkable agreement with the optical response.

$$\tau_\theta^{BKT}(T)^{-1} \sim [\exp(-\frac{E_c}{T})]^{\frac{T}{T-\pi\rho_s/8}}. \tag{5.1}$$

In Fig. 5.3 b) we compare the amplitude of the superconducting ultrafast response $A_{\rm SC}$ with the bare superfluid density ρ_0. The agreement between ρ_0 and $A_{\rm SC}$ is remarkably good over the entire range of measurements $0.8\,T_c < T < 1.3\,T_c$. This agreement is important because, taking into account $n_s \sim |\Psi|^2$, it validates the approximation that the pump-induced changes in the reflectivity or dielectric constant ϵ for small $n_{\rm s}$ are related to the order parameter Ψ as $\delta R \sim \delta\varepsilon \sim |\Psi|^2$.

In contrast to $A_{\rm SC}$ and ρ_0, remarkable differences are seen in the temperature dependencies of the *characteristic lifetimes* obtained by the optical techniques and the THz conductivity measurements [Fig. 5.3a)]. The phase correlation time τ_θ^{THz} determined from the THz conductivity [176] dies out very rapidly above $T_{\rm c}$ with increasing temperature, while the T-dependence of the amplitude relaxation ($\tau_{\rm QP}^{3Pulse}$, $\tau_{\rm QP}^{Subtraction}$ or τ_{rec}) is much more gradual.

Measurements on an optimally doped sample [Fig. 5.4c), d)] show qualitatively the same results with $T_{\rm onset}$ ~102 K, which is 17 K above $T_{\rm c}$, and slightly faster decrease of both the amplitude and the QP relaxation time with the temperature. For the overdoped sample, $\mathcal{F}_{\rm th}^{PG}$ becomes comparable to $\mathcal{F}_{\rm th}^{SC}$, so the superconducting component cannot be significantly suppressed without affecting the pseudogap. Nevertheless the superconducting component is clearly observable in the 2-pulse response up to $T_{\rm onset} \sim 93$ K, i.e. 13 K above $T_{\rm c}$. Comparison of 2-pulse data for different doping levels is shown in Fig. 5.4 e)-g), showing qualitatively similar

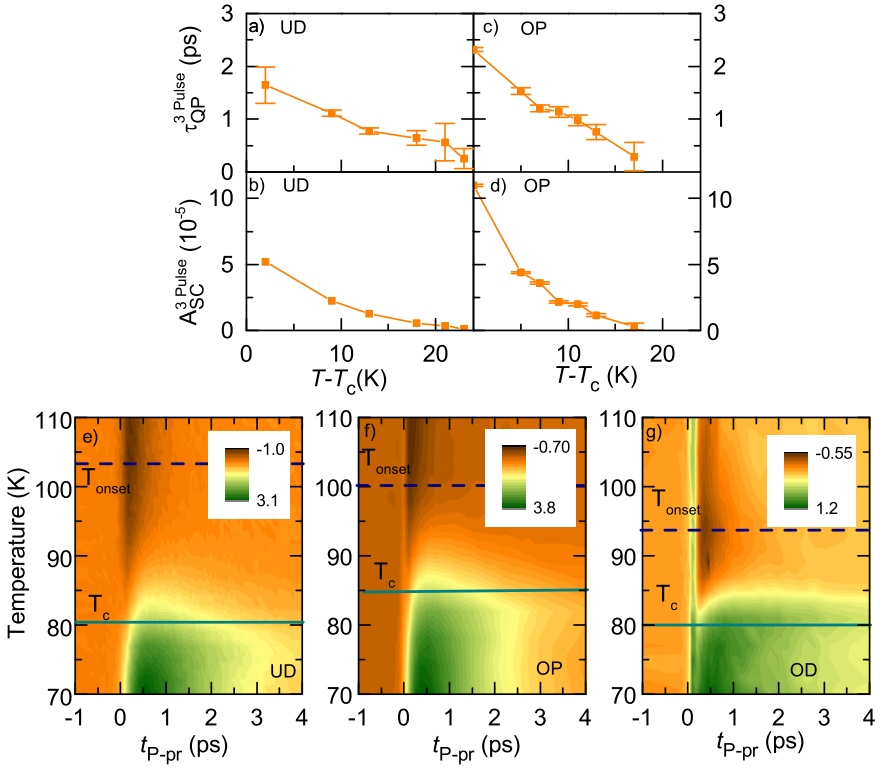


Figure 5.4: Dynamical critical behavior for different doping levels. Comparison of the QP recombination time $\tau_{\mathrm{QP}}^{3Pulse}$ a) and c) and the amplitude of the SC signal b) and d) measured by the three pulse technique for under-(UD) and optimally(OP) doped samples, respectively. e) - g) T-dependence of 2-pulse response for under-(UD), optimally(OP) and overdoped(OD) samples. Blue dashed and cyan solid lines mark T_{onset} and T_{c} respectively. T_{onset} shows gradual decrease with doping. The values of the color bars indicate $\Delta R/R \times 10^{-4}$.

behavior of the SC amplitude above T_{c}.

5.2.2 Discussion

The co-existence and distinct dynamics of the PG and SC excitations above T_c underlines the highly unconventional nature of these states. A possible explanation for the coexistence of the SC and PG excitations is that the SC and PG quasiparticles which are giving rise to the observed processes are associated with relaxation at different regions on the Fermi surface. Recent Raman and cellular dynamical mean-field studies [80] have suggested that the PG may originate from the states inside the Mott gap, which are characterized by s-wave symmetry and very weak dispersion. Such a localized nature of the PG state excitations is consistent with the arguments put forward in Chapter 3. In contrast, the superconducting gap fluctuations have predominantly *d*-wave symmetry and are more delocalized. This would explain the simultaneous presence of the SC fluctuations and PG components in the pump-probe experiments.

The BSCCO family is the most two-dimensional of the cuprate materials, so here the BKT mechanism for describing the signal above T_c is expected to be most

applicable [177]. However, the data in Fig. 5.3a) show that the drop in τ_θ is not nearly as abrupt as the BKT model predicts. One possibility is that this broadening arises from chemical inhomogeneity of the sample, but the absence of a peak in the heat capacity at T_{onset} [158] also appears to exclude the possibility of a pure BKT transition, and implies amplitude fluctuations might be present between T_c and T_{onset} as well [172]. Thus additional mechanisms beyond BKT may also be present which would broaden the phase coherence transition, such as inter-layer phase fluctuations. In this case the observed T-dependence would reflect the interlayer de-coherence [176], [177].

In more traditional approaches using the TDGL theory[15], thermal fluctuations are small for temperatures higher than $\sim$ 2 K above T_c [179], but can give an observable contribution to the conductivity in this temperature range [165]–[169]. Relaxation within TDGL theory has a "longitudinal" relaxation time τ_Δ, which corresponds to the relaxation of the magnitude of the SC order parameter, and a transverse relaxation time τ_θ which corresponds to the relaxation of its phase. They are related to each other in magnitude and have the same temperature dependence near T_c, namely $\tau_{GL} \sim 1/(T - T_c)$ [180]. Perhaps unexpectedly, the temperature dependence of τ_θ^{THz} nearly coincides with the behavior predicted for τ_θ by time-dependent Ginzburg Landau theory for Gaussian fluctuations. Fig. 5.3a) suggests that the phase coherence within this system is established in a narrow, $\sim$ 5 K temperature interval. However, the distinctly different critical behavior of the pair amplitude dynamics speaks in favor of unconventional models of superconductivity in which pairing and phase coherence occur independently, by different mechanisms. The implication is that the observed pairing amplitude which extends to more than 25 K above T_c reflects the response of an inhomogeneous ensemble of gapped patches which are not mutually phase coherent. The weak temperature dependence of the amplitude cannot be described either by TDGL or BKT models.

Beyond the BKT vortex and TDGL scenario, other aforementioned phase-locking scenarios, such as the Bose-Einstein condensation of bipolarons [47], [181], [182] and phase-coherence percolation [140], [183] may also be consistent with the observed behaviour. In both of these cases pairing and phase coherence are also distinct processes. The former comes from the condensation of pairs at T_c as pre-formed pair kinetic energy is reduced, while the latter is associated with the time dynamics of Josephson tunneling between fluctuating pairs or superconducting patches. The percolation timescale τ_J is given by the Josephson energy $E_J = I_c\phi_0/2\pi$, where I_c is the critical current and ϕ_0 is the flux quantum. In cuprates, $\tau_J = \hbar/E_J \simeq 300$ fs, which is compatible with the dynamics of the phase shown in Fig. 5.3a).

A picture exemplified by Fig. 5.3 thus emerges in these materials where the relaxation of the phase θ is faster than relaxation of the amplitude ψ of the complex order parameter $\Psi = \psi e^{i\theta}$, the dynamics of ψ and θ being governed by microscopically different processes. It is worth remarking here that the opposite situation is found in charge density wave dynamics, where the phase relaxation is slow compared to the amplitude relaxation[184].

Summary

In this chapter we devised a method to single out from the total transient reflectivity the response due to the superconducting fluctuations above the critical temperature. The approach is based on selective destruction of the superconducting condensate

and is conceptually close to the suppression of the superconducting state in high magnetic fields. The comparison of the transient reflectivity data to the previously reported THz conductivity measurements revealed the proportionality of the superconducting response to the bare superfluid density and difference in the critical behavior of the amplitude and the phase of the superconducting order parameter, contrary to the behavior expected in TDGL theory. The BKT theory predictions do not agree with the observed behavior but other phase locking scenarios are still to be compared to the experimental data.

Chapter 6

Pump-probe Characterization of $HgBa_2CuO_{4+\delta}$

In this chapter we present pump-probe experiments on the cuprate superconductors $HgBa_2CuO_{4+\delta}$ not reported previously in literature. We investigate three samples from the strongly underdoped to the optimally doped, concentrating on the limiting two. In general the pump-probe response of HBCO qualitatively and quantitatively resembles the main features of BSCCO, even though it is a single layer unlike the two-layer BSCCO. HBCO at the optimal doping has $T_c^{max} = 97$ K [17] - the highest of the single layer compounds. For the samples available to us the susceptibility data were available only for the most underdoped sample, which has $T_c = 68$ K, the T_c of the other two samples can be estimated from the divergence of the relaxation time in the 2 pulse pump-probe experiment (Fig. 6.1). The corresponding values of T_c are 79 and 90 K.[1]

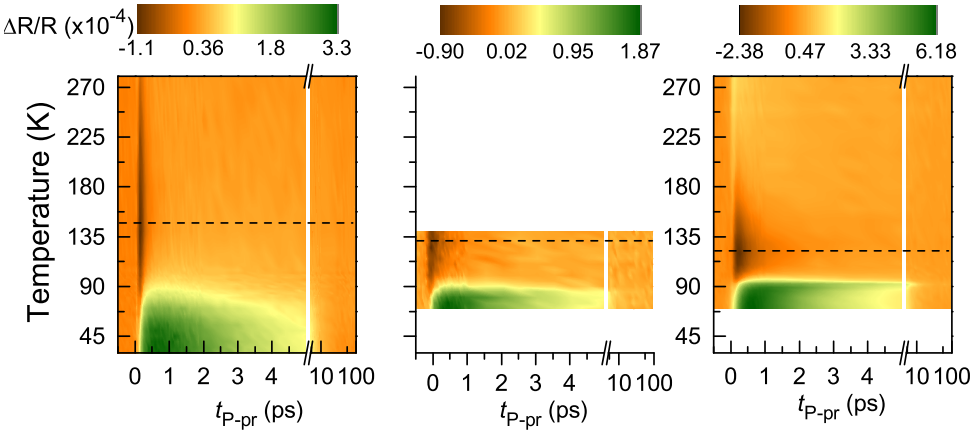


Figure 6.1: Temperature dependence of the pump probe response in HBCO. Data are presented for the samples from the underdoped to the optimally doped (from left to right), measured with $\mathcal{F}_P$= 61 μJ/cm^2, 1.83 μJ/cm^2, and 1.83 μJ/cm^2, respectively. The dashed lines mark the onset temperature of the superconducting fluctuations.

[1]These values are approximate, in BSCCO T_c determined from the relaxation time divergence can differ from that estimated from magnetization by up to 5 K (see Fig. 5.4). The main source of discrepancy lies in the definition of T_c: in the magnetization it is the temperature of the onset of the diamagnetic response, which might lie higher than the actual average T_c due to either inhomogeneities or fluctuations.

In Fig. 6.1 we present the temperature dependencies of the pump-probe response for all three samples. Remarkably the transient reflectivity both in the superconducting and the pseudogap state increase with doping. Because of this the most underdoped sample was measured with significantly higher fluence in order to achieve reliable signal to noise ratio. Another remarkable feature directly visible from the colormaps data is an increase of the relaxation times of the pseudogap component (from 0.15 to 0.68 ps) with doping. The relaxation time of the superconducting as well as the metallic components does not vary significantly with doping. The onset temperature of the superconducting fluctuations can be determined qualitatively as the onset of the positive response on top of the negative pseudogap response monotonously increasing with cooling. T_{onset} monotonously decreases with doping (Fig. 6.1, dashed line) in agreement with observation done in BSCCO (see Fig. 5.4).

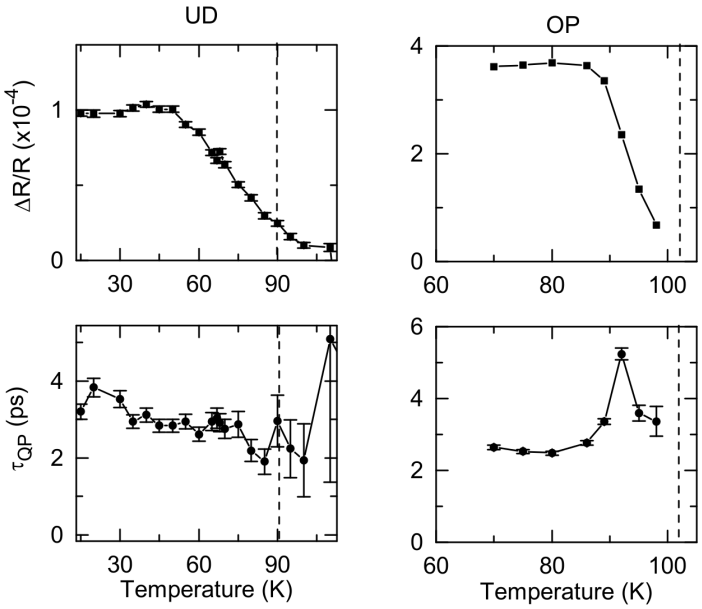


Figure 6.2: The amplitude and relaxation time of the superconducting component for the UD and OP samples. The pump fluences are 6 and 1.83 μJ/cm^2 correspondingly. Divergence of the relaxation time as $T \to T_c$ is observed only for the OP sample.

In Fig. 6.2 the temperature dependence of the amplitudes and relaxation times of the superconducting response is displayed. For the underdoped sample to stay in the linear regime we reduced the fluence of the pump beam just below the threshold $\mathcal{F}_P = 6\ \mu J/cm^2$. Remarkably at T_c (dashed line) the signal in both cases is equal to approximately half of the maximum value - indicating a large contribution from the superconducting fluctuations. The temperature span of the fluctuating region is remarkably wide and is comparable to that observed in BSCCO. While in the optimally doped sample the relaxation time shows a clear divergence it is nearly absent in the underdoped sample. This might be explained by a high level of disorder in the underdoped samples which, apart from the trivial smearing effect, in certain cases leads to the "granular" superconductivity[185]. The presence of disorder is also a typical explanation for the absence of divergence of the relaxation time as $T \to T_c$ expected in the bottleneck model. The impurities act as a scattering center enhancing the anharmonic decay of the high-frequency phonons.

The dependence of the superconducting and pseudogap amplitudes on the probe polarization is presented in Fig. 6.3. Qualitative difference is observed between the underdoped and optimally doped samples - while both the SC and the PG components are isotropic in the OP, at least the PG response shows strong ellipticity for the UD sample. The superconducting response also has a weak ellipticity with the major axis rotated $\lesssim 45$ deg with respect to that of the pseudogap response. The X-ray data are not available for this sample so the correspondence between anisotropy and the crystal orientation is currently not established. The striking similarity of these data with measurements on BSCCO allows one to assume a generality of the effect for all cuprates. Moreover HBCO has no supermodulation in the charge buffer layer and remains always tetragonal. Whether the anisotropy should be attributed to the short-range CDW, which has been recently reported to be the reason of the Fermi-surface reconstruction recently deduced from the Shubnikov-de Haas oscillations[24], is a subject of further investigation. The absence of anisotropy for the optimally doped sample hints that there is no straightforward relation between the pseudogap and broken rotational symmetry. This observation favours scenario in which CDW state appears within the pseudogap but at $T_{\mathrm{CDW}} < T^*$. To test this hypothesis the crystal orientation should be defined so that the symmetry of the pseudogap state can be identified. Another possible explanation for the absence of anisotropy in the optimally doped samples is the presence of multiple domains within the probe volume, which have the broken symmetry but are orthogonally

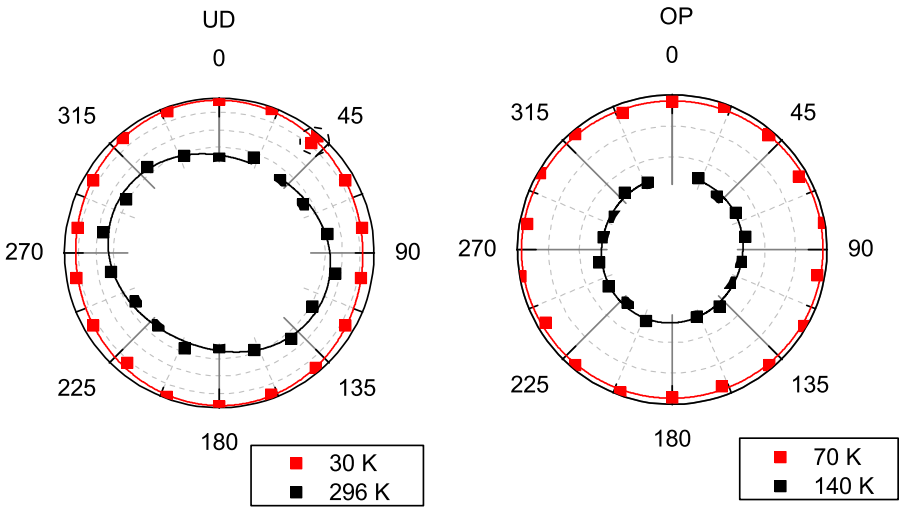


Figure 6.3: Dependence of the amplitude of the pseudogap (black) and superconducting (red) responses on the probe pulse polarization for the underdoped (left) and optimally doped sample. Data are measured only for half a circle and copied in the second half for convenience. The pump fluence is equal to 36 and 120 μJ/cm^2 at 30 and 296 K, respectively for the UD sample and 0.8 and 2.75 μJ/cm^2 at 70 and 140 K for the OP sample, respectively. Data are scaled for convenience and do not represent real ratio between SC and PG amplitudes.

oriented with respect to each other.

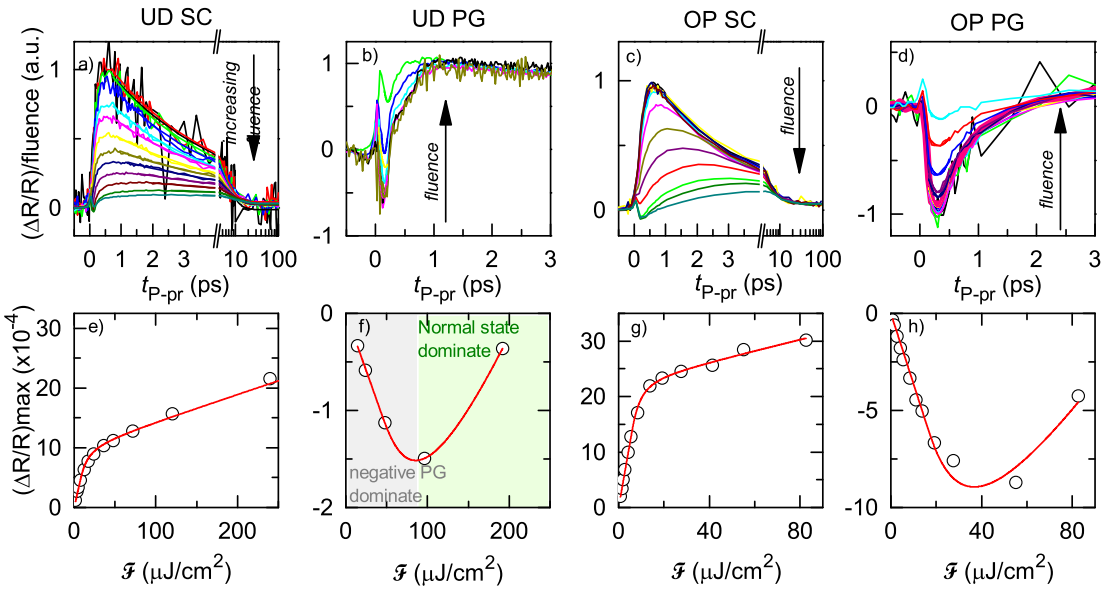


Figure 6.4: Fluence dependence of the pseudogap and superconducting responses. a)-d) Normalized to the fluence transient reflectivity data at a) 30 K and b) 295 K for the UD sample and c) 70 K and d) 120 K for the OP sample for a number of fluences (the direction of fluence increase is shown with the arrows). e)-h) Amplitude of the $\Delta R/R$ is shown in a)-d) as a function of fluence. Solid lines are fits by the saturation model described in Section 1.2.4.

The fluence dependence of the superconducting and pseudogap responses is presented in Fig. 6.4. In the top row we present the raw data normalized to the fluence and in the bottom row the corresponding dependence of the amplitude and fits by the model described in Section 1.2.4. The behavior of both components agrees with the previously observed: at low excitation the response is linear and the traces overlap when normalized to fluence, above the $\mathcal{F}_{\rm th}$the signal saturates. While for the superconducting component determination of the threshold is straightforward, in the case of the pseudogap response, which appears on the wing of the strong normal relaxation component, the determination of the amplitude at high fluences is dependent on the analysis and thus subjected to large errors. In the data presented we fitted the dip in the $\Delta R/R(t_{\rm P-pr})$ traces by a parabolic function and plotted the vertex value as the amplitude of the response. The obtained values of the thresholds of the superconducting component are 7.2±0.6 and 5.6±0.2 μJ/cm^2 for the UD and OP samples and 42±1 and 15±1.7 μJ/cm^2 of the pseudogap component for the UD and OP samples, respectively. The presented errors note the standard deviation of the fit.

Finally we conduct the three pulse experiment on the HBCO sample. Due to the $\Delta R/R$ growth with doping it was possible to obtain a reasonable signal-to noise ratio for the pump fluence before the destruction threshold (i.e. in the linear regime) only for the optimally doped sample. While the thresholds for the superconducting and pseudogap components are comparable and both responses are isotropic we

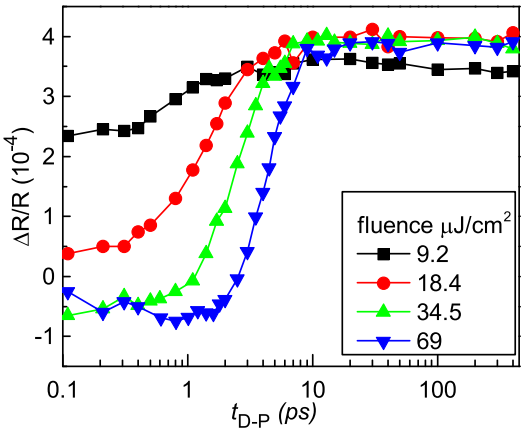


Figure 6.5: Evolution of the transient reflectivity response. Transient reflectivity $\Delta R/R$ at $t_{\mathrm{P-pr}} = 0.25$ ps as a function of the delay between the D and P pulses at different values of the D pulse fluence. Measurements are conducted at 70 K. The pump fluence $\mathcal{F}_{\mathrm{P}}$ =0.8 μJ/cm^2.

were not able to reliably separate them. Thus in Fig.6.5 we plot the read-out value of the $\Delta R/R$ at $t_{\mathrm{P-pr}} = 0.25$ ps which corresponds to the maximum of the pseudogap response, in a similar way as we did for BSCCO in Fig.4.10. As in BSCCO the superconducting state is progressively suppressed with fluence. The pseudogap response becomes dominant at early $t_{\mathrm{D-P}}$ at $\mathcal{F}_{\mathrm{D}} = 34.5$ μJ/cm^2. At the highest measured fluence both the pseudogap and the superconducting responses are strongly suppressed. Initially, the recovery of the pseudogap component dominates the signal with an ensuing take-over by the superconducting response. The magnitude of the recovery time is also very close to that observed in BSCCO. At the highest fluence the response is completely recovered in 5 ps.

Summary

In this chapter we presented the pump-probe characterization of the single layer HBCO compound. The observed relaxation times for the metallic, the pseudogap and the superconducting components are very close to that of BSCCO compound. The similarity is also observed in the temperature dependencies of the corresponding components as well as in the presence of the large superconducting fluctuations region.

The similarity of the measured properties in BSCCO and HBCO systems indicates universality of the observed phenomena. Despite the simpler crystal structure of HBCO the polarization dependent studies indicate a broken 4-fold rotational symmetry in the pseudogap state. This remarkable observation should stimulate the search for a direct evidence of unidirectional charge ordered states. The similarity of the superconductivity recovery time in BSCCO and HBCO and difference from LSCO allows to propose a simple relation $\tau_{\mathrm{rec}} \propto 1/T_{\mathrm{c}}$ expected from the microscopic theory [98], despite the fact that large fluctuations in BSCCO and HBCO compounds do not allow direct application of the TDGL approach.

Chapter 7

Conclusions and Outlook

The present thesis investigated the non-equilibrium phase transitions and related problems in the cuprate superconductors. The main technique implemented in the study was the all-optical ultrafast 3 pulse technique for the first time applied to the superconducting systems.

By studying the dependence of the ultrafast response on the polarization of both the pump and probe pulses we deduce the dissipative character of the quasiparticle excitations. Moreover we observed the spectroscopic signature of the reduction of the parent D_{4h} point group symmetry to the D_{2h} at least below T^* and further down to C_{2h} at least with the onset of superconducting fluctuations. This confirms the presence in-bulk of the unidirectional charge order previously reported by STM. Within the consideration we presented how the pump-probe response can be described in terms of the Raman-like tensor for the first time in the field of correlated electronic systems.

The symmetry breaking in the pseudogap state is however hard to relate to a real phase transition with the establishment of the long range order. The independence of the quasiparticle relaxation time on the amplitude of the pseudogap response as it recovers after the photodestruction we interpret as the signature of the absence of long range correlations. This, together with a nearly temperature and fluence independent pseudogap recovery time, as well as the similarity of the sub-picosecond and nanosecond responses temperature dependencies, agree with the polaronic interpretation of the pseudogap state.

The normal-to-superconducting phase transition has been studied in details in LSCO system. Here the clear divergence of the quasiparticle relaxation time on the appearance of the ordered phase has been confirmed. The comparison of the experimental trajectories with the numerical simulations of the TDGL model allowed to highlight the dominant role of the superconducting fluctuations in the recovery of the superconducting order.

For the BSCCO system we devised the novel method to extract the superconducting component of the transient reflectivity based on the polarization selection rules. We have shown that the strong photoexcitation leads to the restoration of the rotational symmetry, which subsequently breaks again as the superconducting order reappears.

The 3 pulse technique allowed us to experimentally single-out the response due to the superconducting fluctuations above the critical temperature. The detailed study of this response allowed to establish direct proportionality of the superconducting response to the bare superfluid density and to reveal the difference in the critical

behavior of the phase and the amplitude of the superconducting order parameter.

Finally we presented the ultrafast characterization of the HBCO compound and found a number of similarities with BSCCO cuprate.

To summarize: we have shown that it is possible to apply the conventional TDGL theory to describe the normal-to-superconducting transition in the least anisotropic compounds, whereas in the highly anisotropic compounds there is a significant response due to the superconducting fluctuations not taken in consideration by the TDGL theory. Both superconducting and pseudogap orders are associated with the broken rotational symmetry states at least in the underdoped region of HBCO and BSCCO systems.

Appendix A

Material Constants

In the following table we collect the material constants used in the thesis.

Material		$La_{1.9}Sr_{0.1}CuO_4$(LSCO)	$Bi_2Sr_2CaCu_2O_{8+\delta}$(BSCCO)	$HgBa_2CuO_{4+\delta}$(HBCO)
Critical temperature	T_c^{opt}(K)	38.5	86	98
Molar mass	M(g/mol)	400.22	888.4	556.05
Unit cell dimensions	$a \times b \times c$ (Å×Å×Å)	$5.34 \times 5.4 \times 13.5$[152]	$5.4 \times 5.4 \times 30.89$[152]	$3.88 \times 3.88 \times 9.5$[186]
Hole effective mass	$m*/m$	1.5[187]	2.14[125]	2.45[188]
Reflectivity	$R_{@1.5eV}$	0.11	0.07	0.07[189]
Optical penetration depth	$\lambda_{op@1.5eV}$(nm)	150[89]	124[79]	121[a]
Superconducting gap	$\Delta_{\mathrm{opt}}(0)$(meV)	10[103]	25[190]	31[190]
Sommerfeld coefficient	γ_{n}(mJ/K^{2}mole)	7.5 [187]	15 [125]	-
Second moment of the Eliashberg function[b]	$\lambda\langle\omega^2\rangle$ (meV^2)	800 ± 200 [56]	~ 800 [55]	~ 600 [55]

Table A.1: Material specific constants of the samples under investigation.

[a] Calculated from static data given in [189]

[b] Values for BSCCO and HBCO were calculated from the initial relaxation rates using the Eq.(1.4)

References

[1] J. G. Bednorz and K. A. Müller, "Possible highT c superconductivity in the Ba-La-Cu-O system," *Zeitschrift für Physik B Condensed Matter*, vol. 64, no. 2, pp. 189–193, Jun. 1986, ISSN: 0722-3277. DOI: 10.1007/BF01303701. [Online]. Available: http://link.springer.com/10.1007/BF01303701.

[2] A. Mann, "High-temperature superconductivity at 25: Still in suspense.," *Nature*, vol. 475, no. 7356, pp. 280–2, Jul. 2011, ISSN: 1476-4687. DOI: 10.1038/475280a. [Online]. Available: http://www.ncbi.nlm.nih.gov/pubmed/21776057.

[3] T. W. B. Kibble, "Topology of cosmic domains and strings," *J. Phys. A: Math. Gen.*, vol. 9, no. 8, pp. 1387–1398, 1976.

[4] W. H. Zurek, *Cosmological experiments in superfluid helium?* 1985. DOI: 10.1038/317505a0.

[5] ——, "Cosmological experiments in condensed matter systems," *Physics Reports*, pp. 177–221, 1996.

[6] B. Keimer, S. A. Kivelson, M. R. Norman, S. Uchida, and J. Zaanen, "From quantum matter to high-temperature superconductivity in copper oxides," *Nature*, vol. 518, no. 7538, pp. 179–186, 2015, ISSN: 0028-0836. DOI: 10.1038/nature14165. [Online]. Available: http://www.nature.com/doifinder/10.1038/nature14165.

[7] M. Hashimoto, I. M. Vishik, R.-H. He, T. P. Devereaux, and Z.-X. Shen, "Energy gaps in high-transition-temperature cuprate superconductors," *Nature Physics*, vol. 10, no. 7, pp. 483–495, Jun. 2014, ISSN: 1745-2473. DOI: 10.1038/nphys3009. [Online]. Available: http://www.nature.com/doifinder/10.1038/nphys3009.

[8] M. Vojta, "Quantum phase transitions," *Rep. Prog. Phys.*, vol. 66, no. 12, pp. 2069–2110, Dec. 2003, ISSN: 0034-4885. DOI: 10.1088/0034-4885/66/12/R01. [Online]. Available: http://stacks.iop.org/0034-4885/66/i=12/a=R01?key=crossref.c536678c9f7b611291c4445db9c68861.

[9] ——, "Lattice symmetry breaking in cuprate superconductors: stripes, nematics, and superconductivity," *Advances in Physics*, vol. 58, no. 6, pp. 699–820, Nov. 2009, ISSN: 0001-8732. DOI: 10.1080/00018730903122242. [Online]. Available: http://www.tandfonline.com/doi/abs/10.1080/00018730903122242.

[10] A. Damascelli and Z.-X. Shen, "Angle-resolved photoemission studies of the cuprate superconductors," *Reviews of Modern Physics*, vol. 75, no. 2, pp. 473–541, Apr. 2003, ISSN: 0034-6861. DOI: 10.1103/RevModPhys.75.473. [Online]. Available: http://link.aps.org/doi/10.1103/RevModPhys.75.473.

[11] R. D. Averitt and A. J. Taylor, "Ultrafast optical and far-infrared quasiparticle dynamics in correlated electron materials," *Journal of Physics: Condensed Matter*, vol. 14, no. 50, R1357–R1390, Dec. 2002, ISSN: 0953-8984. DOI: 10.1088/0953-8984/14/50/203. [Online]. Available: http://stacks.iop.org/0953-8984/14/i=50/a=203?key=crossref.e17bb4e599e6ef65b215f1aa22ee2fc0.

[12] D. N. Basov, *Electrodynamics of high- T_c superconductors*, 2005. DOI: 10.1103/RevModPhys.77.721.

[13] M. R. Norman, D. Pines, and C. Kallin, "The pseudogap: friend or foe of high T_c ?" *Advances in Physics*, vol. 54, no. 8, pp. 715–733, Dec. 2005, ISSN: 0001-8732. DOI: 10.1080/00018730500459906. [Online]. Available: http://www.tandfonline.com/doi/abs/10.1080/00018730500459906.

[14] T. Timusk and B. Statt, "The pseudogap in high-temperature superconductors: an experimental survey," *Reports on Progress in Physics*, vol. 62, no. 1, pp. 61–122, Jan. 1999, ISSN: 0034-4885. DOI: 10.1088/0034-4885/62/1/002. [Online]. Available: http://stacks.iop.org/0034-4885/62/i=1/a=002?key=crossref.275453a29918de617da6c6f3c8e930f2.

[15] A. Larkin and A. Varlamov, *Theory of Fluctuations in Superconductors*. Oxford University Press, Jan. 2005, ISBN: 9780198528159. DOI: 10.1093/acprof:oso/9780198528159.001.0001. [Online]. Available: http://www.oxfordscholarship.com/view/10.1093/acprof:oso/9780198528159.001.0001/acprof-9780198528159.

[16] T. Schneider and J. M. Singer, *Phase Transition Approach to High Temperature Superconductivity*. Imperial College Press, 2000.

[17] N. Plakida, *High-Temperature Cuprate Superconductors*, ser. Springer Series in Solid-State Sciences. Berlin, Heidelberg: Springer Berlin Heidelberg, 2010, vol. 166, ISBN: 978-3-642-12632-1. DOI: 10.1007/978-3-642-12633-8. [Online]. Available: http://link.springer.com/10.1007/978-3-642-12633-8.

[18] V. M. Loktev, "Mehanism of high temperature superconductivity of copper oxides. (in Russian)," *FNT(Ukrainian)*, vol. 22, no. 1, pp. 3–45, 1996.

[19] K. M. Shen and J. C. . Davis, *Cuprate high-T_c superconductors*, Sep. 2008. DOI: 10.1016/S1369-7021(08)70175-5. [Online]. Available: http://linkinghub.elsevier.com/retrieve/pii/S1369702108701755.

[20] A. L. Solov′ev and V. M. Dmitriev, "Fluctuation conductivity and pseudogap in YBCO high-temperature superconductors (Review)," *Low Temperature Physics*, vol. 35, no. 3, p. 169, 2009, ISSN: 1063777X. DOI: 10.1063/1.3081150. [Online]. Available: http://link.aip.org/link/LTPHEG/v35/i3/p169/s1&Agg=doi.

[21] J. M. Tranquada, B. J. Sternlieb, J. D. Axe, Y. Nakamura, and S. Uchida, "Evidence for stripe correlations of spins and holes in copper oxide superconductors," *Nature*, vol. 375, no. 6532, pp. 561–563, Jun. 1995, ISSN: 0028-0836. DOI: 10.1038/375561a0. [Online]. Available: http://www.nature.com/doifinder/10.1038/375561a0.

[22] S. A. Kivelson, I. P. Bindloss, V. Oganesyan, J. M. Tranquada, A. Kapitulnik, and C. Howald, "How to detect fluctuating stripes in the high-temperature superconductors," *Reviews of Modern Physics*, vol. 75, no. 4, pp. 1201–1241, Oct. 2003, ISSN: 0034-6861. DOI: 10.1103/RevModPhys.75.1201. [Online]. Available: http://link.aps.org/doi/10.1103/RevModPhys.75.1201.

[23] D. LeBoeuf, N. Doiron-Leyraud, J. Levallois, R. Daou, J.-B. Bonnemaison, N. E. Hussey, L. Balicas, B. J. Ramshaw, R. Liang, D. a. Bonn, W. N. Hardy, S. Adachi, C. Proust, and L. Taillefer, "Electron pockets in the Fermi surface of hole-doped high-T_c superconductors.," *Nature*, vol. 450, no. 7169, pp. 533–536, 2007, ISSN: 0028-0836. DOI: 10.1038/nature06332. arXiv: 0806.4621.

[24] N. Doiron-Leyraud, S. Lepault, O. Cyr-Choinière, B. Vignolle, G. Grissonnanche, F. Laliberté, J. Chang, N. Barišić, M. K. Chan, L. Ji, X. Zhao, Y. Li, M. Greven, C. Proust, and L. Taillefer, "Hall, Seebeck, and Nernst Coefficients of Underdoped $HgBa_2CuO_{4+\delta}$: Fermi-Surface Reconstruction in an Archetypal Cuprate Superconductor," *Physical Review X*, vol. 3, no. 2, p. 021 019, Jun. 2013, ISSN: 2160-3308. DOI: 10.1103/PhysRevX.3.021019. [Online]. Available: http://link.aps.org/doi/10.1103/PhysRevX.3.021019.

[25] E. H. da Silva Neto, P. Aynajian, A. Frano, R. Comin, E. Schierle, E. Weschke, A. Gyenis, J. Wen, J. Schneeloch, Z. Xu, S. Ono, G. Gu, M. Le Tacon, and A. Yazdani, "Ubiquitous interplay between charge ordering and high-temperature superconductivity in cuprates.," *Science*, vol. 343, no. 6169, pp. 393–6, Jan. 2014, ISSN: 1095-9203. DOI: 10.1126/science.1243479. [Online]. Available: http://www.ncbi.nlm.nih.gov/pubmed/24356110.

[26] R. Comin, A. Frano, M. M. Yee, Y. Yoshida, H. Eisaki, E. Schierle, E. Weschke, R. Sutarto, F. He, A. Soumyanarayanan, Y. He, M. Le Tacon, I. S. Elfimov, J. E. Hoffman, G. A. Sawatzky, B. Keimer, and A. Damascelli, "Charge order driven by Fermi-arc instability in $Bi_2Sr_{(2-x)}La_(x)CuO_(6+\delta)$.," *Science (New York, N.Y.)*, vol. 343, no. 6169, pp. 390–2, Jan. 2014, ISSN: 1095-9203. DOI: 10.1126/science.1242996. [Online]. Available: http://www.ncbi.nlm.nih.gov/pubmed/24356115.

[27] J. E. Hoffman, E. W. Hudson, K. M. Lang, V. Madhavan, H. Eisaki, S. Uchida, and J. C. Davis, "A four unit cell periodic pattern of quasi-particle states surrounding vortex cores in $Bi_2Sr_2CaCu_2O_{8+\delta}$.," *Science (New York, N.Y.)*, vol. 295, no. 5554, pp. 466–469, 2002, ISSN: 00368075. DOI: 10.1126/science.1066974. arXiv: 0201348 [cond-mat].

[28] V. B. Zabolotnyy, A. A. Kordyuk, D. Evtushinsky, V. N. Strocov, L. Patthey, T. Schmitt, D. Haug, C. T. Lin, V. Hinkov, B. Keimer, B. Büchner, and S. V. Borisenko, "Pseudogap in the chain states of $YBa_2Cu_3O_{6.6}$," *Physical Review B*, vol. 85, no. 6, pp. 1–7, 2012, ISSN: 10980121. DOI: 10.1103/PhysRevB.85.064507.

[29] S. Sachdev, "Quantum Criticality: competing ground states in low dimensions," *Science*, vol. 288, no. April, p. 19, 2000, ISSN: 00368075. DOI: 10.1126/science.288.5465.475. arXiv: 0009456 [cond-mat]. [Online]. Available: http://arxiv.org/abs/cond-mat/0009456.

[30] P. W. Anderson, "Hidden Fermi liquid: The secret of high-Tc cuprates," *Physical Review B*, vol. 78, no. 17, pp. 6–11, 2008, ISSN: 10980121. DOI: 10.1103/PhysRevB.78.174505.

[31] R.-H. He, M. Hashimoto, H. Karapetyan, J. D. Koralek, J. P. Hinton, J. P. Testaud, V. Nathan, Y. Yoshida, H. Yao, K. Tanaka, W. Meevasana, R. G. Moore, D. H. Lu, S.-K. Mo, M. Ishikado, H. Eisaki, Z. Hussain, T. P. Devereaux, S. A. Kivelson, J. Orenstein, A. Kapitulnik, and Z.-X. Shen, "From a single-band metal to a high-temperature superconductor via two thermal phase transitions.," *Science (New York, N.Y.)*, vol. 331, no. 6024, pp. 1579–83, Mar. 2011, ISSN: 1095-9203. DOI: 10.1126/science.1198415. [Online]. Available: http://www.ncbi.nlm.nih.gov/pubmed/21436447.

[32] R. Daou, J. Chang, D. Leboeuf, O. Cyr-Choinière, F. Laliberté, N. Doiron-Leyraud, B. J. Ramshaw, R. Liang, D. A. Bonn, W. N. Hardy, and L. Taillefer, "Broken rotational symmetry in the pseudogap phase of a high-T(c) superconductor.," *Nature*, vol. 463, no. 7280, pp. 519–22, Jan. 2010, ISSN: 1476-4687. DOI: 10.1038/

nature08716. [Online]. Available: http://www.ncbi.nlm.nih.gov/pubmed/20110997.

[33] Y. Kohsaka, C. Taylor, K. Fujita, A. Schmidt, C. Lupien, T. Hanaguri, M. Azuma, M. Takano, H. Eisaki, H. Takagi, S. Uchida, and J. C. Davis, "An intrinsic bond-centered electronic glass with unidirectional domains in underdoped cuprates.," *Science (New York, N.Y.)*, vol. 315, no. 5817, pp. 1380–5, Mar. 2007, ISSN: 1095-9203. DOI: 10.1126/science.1138584. [Online]. Available: http://www.ncbi.nlm.nih.gov/pubmed/17289939.

[34] M. Hashimoto, R.-H. He, K. Tanaka, J.-P. Testaud, W. Meevasana, R. G. Moore, D. Lu, H. Yao, Y. Yoshida, H. Eisaki, T. P. Devereaux, Z. Hussain, and Z.-X. Shen, "Particle-hole symmetry breaking in the pseudogap state of Bi2201," *Nature Physics*, vol. 6, no. 6, pp. 414–418, Apr. 2010, ISSN: 1745-2473. DOI: 10.1038/nphys1632. [Online]. Available: http://www.nature.com/doifinder/10.1038/nphys1632.

[35] J. Xia, E. Schemm, G. Deutscher, S. a. Kivelson, D. a. Bonn, W. N. Hardy, R. Liang, W. Siemons, G. Koster, M. M. Fejer, and A. Kapitulnik, "Polar Kerr-Effect Measurements of the High-Temperature $YBa_2Cu_3O_{6+x}$ Superconductor: Evidence for Broken Symmetry near the Pseudogap Temperature," *Physical Review Letters*, vol. 100, no. 12, p. 127 002, Mar. 2008, ISSN: 0031-9007. DOI: 10.1103/PhysRevLett.100.127002. [Online]. Available: http://link.aps.org/doi/10.1103/PhysRevLett.100.127002.

[36] A. Kaminski, S. Rosenkranz, H. M. Fretwell, J. C. Campuzano, Z. Li, H. Raffy, W. G. Cullen, H. You, C. G. Olson, C. M. Varma, and H. Höchst, "Spontaneous breaking of time-reversal symmetry in the pseudogap state of a high-T_c superconductor.," *Nature*, vol. 416, no. 6881, pp. 610–3, Apr. 2002, ISSN: 0028-0836. DOI: 10.1038/416610a. [Online]. Available: http://www.ncbi.nlm.nih.gov/pubmed/11948344.

[37] W. W. Warren, R. E. Walstedt, G. F. Brennert, R. J. Cava, R. Tycko, R. F. Bell, and G. Dabbagh, "Cu spin dynamics and superconducting precursor effects in planes above T_c in $YBa_2Cu_3O_6.7$," *Physical Review Letters*, vol. 62, no. 10, pp. 1193–1196, 1989, ISSN: 00319007. DOI: 10.1103/PhysRevLett.62.1193.

[38] J. Demsar, B. Podobnik, V. Kabanov, T. Wolf, and D. Mihailovic, "Superconducting Gap Δ_c, the Pseudogap Δ_p, and Pair Fluctuations above T_c in Overdoped $Y_{1-x}Ca_xBa_2Cu_3O_{7-\delta}$ from Femtosecond Time-Domain Spectroscopy," *Physical Review Letters*, vol. 82, no. 24, pp. 4918–4921, Jun. 1999, ISSN: 0031-9007. DOI: 10.1103/PhysRevLett.82.4918. [Online]. Available: http://link.aps.org/doi/10.1103/PhysRevLett.82.4918.

[39] W. Tabis, Y. Li, M. L. Tacon, L. Braicovich, A. Kreyssig, M. Minola, G. Dellea, E. Weschke, M. J. Veit, M. Ramazanoglu, A. I. Goldman, T. Schmitt, G. Ghiringhelli, N. Barišić, M. K. Chan, C. J. Dorow, G. Yu, X. Zhao, B. Keimer, and M. Greven, "Charge order and its connection with Fermi-liquid charge transport in a pristine high-T_c cuprate.," *Nature communications*, vol. 5, p. 5875, Jan. 2014, ISSN: 2041-1723. DOI: 10.1038/ncomms6875. [Online]. Available: http://www.ncbi.nlm.nih.gov/pubmed/25522689.

[40] M. Platé, J. D. F. Mottershead, I. S. Elfimov, D. C. Peets, R. Liang, D. A. Bonn, W. N. Hardy, S. Chiuzbaian, M. Falub, M. Shi, L. Patthey, and A. Damascelli, "Fermi surface and quasiparticle excitations of overdoped $Tl_2Ba_2CuO_{6+\delta}$," *Physical Review Letters*, vol. 95, no. 7, pp. 2–5, 2005, ISSN: 00319007. DOI: 10.1103/PhysRevLett.95.077001. arXiv: 0503117 [cond-mat].

[41] N. Mannella, W. L. Yang, X. J. Zhou, H. Zheng, J. F. Mitchell, J. Zaanen, T. P. Devereaux, N. Nagaosa, Z. Hussain, and Z.-X. Shen, "Nodal quasiparticle in pseudogapped colossal magnetoresistive manganites.," *Nature*, vol. 438, no. 7067, pp. 474–8, Nov. 2005, ISSN: 1476-4687. DOI: 10.1038/nature04273. [Online]. Available: http://www.ncbi.nlm.nih.gov/pubmed/16306987.

[42] R. Bindu, G. Adhikary, N. Sahadev, N. P. Lalla, and K. Maiti, "Pseudogap and charge ordering in a large-bandwidth electron-doped manganite," *Physical Review B*, vol. 84, no. 5, p. 052 407, Aug. 2011, ISSN: 1098-0121. DOI: 10.1103/PhysRevB.84.052407. [Online]. Available: http://link.aps.org/doi/10.1103/PhysRevB.84.052407.

[43] M. Hashimoto, E. a. Nowadnick, R.-H. He, I. M. Vishik, B. Moritz, Y. He, K. Tanaka, R. G. Moore, D. Lu, Y. Yoshida, M. Ishikado, T. Sasagawa, K. Fujita, S. Ishida, S. Uchida, H. Eisaki, Z. Hussain, T. P. Devereaux, and Z.-X. Shen, "Direct spectroscopic evidence for phase competition between the pseudogap and superconductivity in $Bi_2Sr_2CaCu_2O_{8+\delta}$," *Nature materials*, vol. 14, no. January, Nov. 2014, ISSN: 1476-1122. DOI: 10.1038/nmat4116. [Online]. Available: http://www.ncbi.nlm.nih.gov/pubmed/25362356.

[44] T. Kondo, R. Khasanov, T. Takeuchi, J. Schmalian, and A. Kaminski, "Competition between the pseudogap and superconductivity in the high-T_c copper oxides.," *Nature*, vol. 457, no. 7227, pp. 296–300, 2009, ISSN: 0028-0836. DOI: 10.1038/nature07644. arXiv: 0902.1342.

[45] G. Coslovich, C. Giannetti, F. Cilento, S. Dal Conte, T. Abebaw, D. Bossini, G. Ferrini, H. Eisaki, M. Greven, A. Damascelli, and F. Parmigiani, "Competition Between the Pseudogap and Superconducting States of $Bi_2Sr_2Ca_{0.92}Y_{0.08}Cu_2O_{8+\delta}$ Single Crystals Revealed by Ultrafast Broadband Optical Reflectivity," *Physical Review Letters*, vol. 110, no. 10, p. 107 003, Mar. 2013, ISSN: 0031-9007. DOI: 10.1103/PhysRevLett.110.107003. [Online]. Available: http://link.aps.org/doi/10.1103/PhysRevLett.110.107003.

[46] Y. Liu, Y. Toda, K. Shimatake, N. Momono, M. Oda, and M. Ido, "Direct Observation of the Coexistence of the Pseudogap and Superconducting Quasiparticles in $Bi_2Sr_2CaCu_2O_{8+y}$ by Time-Resolved Optical Spectroscopy," *Physical Review Letters*, vol. 101, no. 13, pp. 1–4, Sep. 2008, ISSN: 0031-9007. DOI: 10.1103/PhysRevLett.101.137003. [Online]. Available: http://link.aps.org/doi/10.1103/PhysRevLett.101.137003.

[47] A. Alexandrov and J. Ranninger, "Bipolaronic superconductivity," *Phys. Rev. B*, vol. 24, no. 3, pp. 1164–1169, Aug. 1981, ISSN: 0163-1829. DOI: 10.1103/PhysRevB.24.1164. [Online]. Available: http://link.aps.org/doi/10.1103/PhysRevB.24.1164.

[48] A. Alexandrov, "Bose-Einstein condensation of charged bosons in a magnetic field," *Phys. Rev. B*, vol. 48, no. 14, pp. 10 571–10 574, Oct. 1993, ISSN: 0163-1829. DOI: 10.1103/PhysRevB.48.10571. [Online]. Available: http://link.aps.org/doi/10.1103/PhysRevB.55.3173%20http://link.aps.org/doi/10.1103/PhysRevB.48.10571.

[49] A. S. Alexandrov and N. F. Mott, "Bipolarons," *Reports on Progress in Physics*, vol. 57, no. 12, pp. 1197–1288, Dec. 1994, ISSN: 0034-4885. DOI: 10.1088/0034-4885/57/12/001. [Online]. Available: http://stacks.iop.org/0034-4885/57/i=12/a=001?key=crossref.fb036173edeebf6e6c69f426da4abfd5.

[50] T. Mertelj, V. Kabanov, and D. Mihailovic, "Charged Particles on a Two-Dimensional Lattice Subject to Anisotropic Jahn-Teller Interactions," *Phys. Rev. Lett.*, vol. 94, no. 14, p. 147 003, Apr. 2005, ISSN: 0031-9007. DOI: 10.1103/PhysRevLett.94.147003. [Online]. Available: http://link.aps.org/doi/10.1103/PhysRevLett.94.147003.

[51] P. W. Anderson, "The Resonating Valence Bond State in La_2CuO_4 and Superconductivity," *Science*, vol. 235, no. 4793, pp. 1196–1198, Mar. 1987, ISSN: 0036-8075. DOI: 10.1126/science.235.4793.1196. [Online]. Available: http://www.sciencemag.org/cgi/doi/10.1126/science.235.4793.1196.

[52] S. A. Kivelson, D. S. Rokhsar, and J. P. Sethna, "Topology of the resonating valence-bond state: Solitons and high-Tc superconductivity," *Physical Review B*, vol. 35, no. 16, pp. 8865–8868, 1987, ISSN: 01631829. DOI: 10.1103/PhysRevB.35.8865.

[53] D. J. Scalapino, E. Loh, and J. E. Hirsch, "D-wave pairing near a spin-density-wave instability," *Physical Review B*, vol. 34, no. 11, pp. 8190–8192, 1986, ISSN: 01631829. DOI: 10.1103/PhysRevB.34.8190.

[54] K. Miyake, S. Schmitt-Rink, and C. M. Varma, "Spin-fluctuation-mediated even-parity pairing in heavy-fermion superconductors," *Physical Review B*, vol. 34, no. 9, pp. 6554–6556, 1986, ISSN: 01631829. DOI: 10.1103/PhysRevB.34.6554.

[55] C. Gadermaier, V. V. Kabanov, a. S. Alexandrov, L. Stojchevska, T. Mertelj, C. Manzoni, G. Cerullo, N. D. Zhigadlo, J. Karpinski, Y. Q. Cai, X. Yao, Y. Toda, M. Oda, S. Sugai, and D. Mihailovic, "Strain-Induced Enhancement of the Electron Energy Relaxation in Strongly Correlated Superconductors," *Physical Review X*, vol. 4, no. 1, p. 011 056, Mar. 2014, ISSN: 2160-3308. DOI: 10.1103/PhysRevX.4.011056. [Online]. Available: http://link.aps.org/doi/10.1103/PhysRevX.4.011056.

[56] C. Gadermaier, A. Alexandrov, V. Kabanov, P. Kusar, T. Mertelj, X. Yao, C. Manzoni, D. Brida, G. Cerullo, and D. Mihailovic, "Electron-Phonon Coupling in High-Temperature Cuprate Superconductors Determined from Electron Relaxation Rates," *Physical Review Letters*, vol. 105, no. 25, pp. 1–4, Dec. 2010, ISSN: 0031-9007. DOI: 10.1103/PhysRevLett.105.257001. [Online]. Available: http://link.aps.org/doi/10.1103/PhysRevLett.105.257001.

[57] L. Perfetti, P. a. Loukakos, M. Lisowski, U. Bovensiepen, H. Eisaki, and M. Wolf, "Ultrafast Electron Relaxation in Superconducting $Bi_2Sr_2CaCu_2O_{8+\delta}$ by Time-Resolved Photoelectron Spectroscopy," *Phys. Rev. Lett.*, vol. 99, no. 19, p. 197 001, Nov. 2007, ISSN: 0031-9007. DOI: 10.1103/PhysRevLett.99.197001. [Online]. Available: http://link.aps.org/doi/10.1103/PhysRevLett.99.197001.

[58] M. Oda, K. Hoya, R. Kubota, C. Manabe, N. Momono, T. Nakano, and M. Ido, "Strong pairing interactions in the underdoped region of $Bi_2Sr_2CaCu_2O_{8+\delta}$," *Physica C: Superconductivity*, vol. 281, no. 2-3, pp. 135–142, Aug. 1997, ISSN: 09214534. DOI: 10.1016/S0921-4534(97)00505-4. [Online]. Available: http://linkinghub.elsevier.com/retrieve/pii/S0921453497005054.

[59] Y. Toda, T. Mertelj, P. Kusar, T. Kurosawa, M. Oda, M. Ido, and D. Mihailovic, "Quasiparticle relaxation dynamics in underdoped $Bi_2Sr_2CaCu_2O_{8+\delta}$by two-color pump-probe spectroscopy," *Phys. Rev. B*, vol. 84, no. 17, pp. 1–8, Nov. 2011, ISSN: 1098-0121. DOI: 10.1103/PhysRevB.84.174516. [Online]. Available: http://link.aps.org/doi/10.1103/PhysRevB.84.174516.

[60] C. Giannetti, F. Cilento, S. D. Conte, G. Coslovich, G. Ferrini, H. Molegraaf, M. Raichle, R. Liang, H. Eisaki, M. Greven, A. Damascelli, D. van der Marel, and F. Parmigiani, "Revealing the high-energy electronic excitations underlying the onset of high-temperature superconductivity in cuprates," *Nature Communications*, vol. 2, no. may, p. 353, Jun. 2011, ISSN: 2041-1723. DOI: 10.1038/ncomms1354. [Online]. Available: http://www.nature.com/doifinder/10.1038/ncomms1354.

[61] N. Gedik, P. Blake, R. Spitzer, J. Orenstein, R. Liang, D. Bonn, and W. Hardy, "Single-quasiparticle stability and quasiparticle-pair decay in $YBa_2Cu_3O_6.5$," *Physical Review B*, vol. 70, no. 1, p. 014 504, Jul. 2004, ISSN: 1098-0121. DOI: 10.1103/PhysRevB.70.014504. [Online]. Available: http://link.aps.org/doi/10.1103/PhysRevB.70.014504.

[62] P. Kusar, J. Demsar, D. Mihailovic, and S. Sugai, "A systematic study of femtosecond quasiparticle relaxation processes in $La_{2-x}Sr_xCuO_4$," *Physical Review B*, vol. 72, no. 1, p. 014 544, Jul. 2005, ISSN: 1098-0121. DOI: 10.1103/PhysRevB.72.014544. [Online]. Available: http://link.aps.org/doi/10.1103/PhysRevB.72.014544.

[63] P. Gay, D. C. Smith, C. J. Stevens, C. Chen, and J. F. Ryan, "Femtosecond Dynamics of BSCCO-2212," *Journal of Low Temperature Physics*, vol. 117, pp. 1025–1029, 1999. DOI: 10.1023/A:1022561904373.

[64] V. V. Kabanov, J. Demsar, B. Podobnik, and D. Mihailovic, "Quasiparticle relaxation dynamics in superconductors with different gap structures: Theory and experiments on $YBa_2Cu_3O_{7-\delta}$," *Physical Review B*, vol. 59, no. 2, pp. 1497–1506, Jan. 1999, ISSN: 1098-0121. DOI: 10.1103/PhysRevB.59.1497. [Online]. Available: http://link.aps.org/doi/10.1103/PhysRevB.59.1497.

[65] P. B. Allen, "Theory of thermal relaxation of electrons in metals," *Physical Review Letters*, vol. 59, no. 13, pp. 1460–1463, Sep. 1987, ISSN: 0031-9007. DOI: 10.1103/PhysRevLett.59.1460. [Online]. Available: http://link.aps.org/doi/10.1103/PhysRevLett.59.1460.

[66] I. M. L. M. I. Kaganov and L. V. Tanatarov, *Zh. Eksp. Teor. Fiz.*, vol. 31, p. 232, 1956.

[67] J. P. Carbotte, "Properties of boson-exchange superconductors," *Reviews of Modern Physics*, vol. 62, no. 4, pp. 1027–1157, Oct. 1990, ISSN: 00346861. DOI: 10.1103/RevModPhys.62.1027. [Online]. Available: http://link.aps.org/doi/10.1103/RevModPhys.62.1027.

[68] W. McMillan, "Transition Temperature of Strong-Coupled Superconductors," *Physical Review*, vol. 167, no. 2, pp. 331–344, Mar. 1968, ISSN: 0031-899X. DOI: 10.1103/PhysRev.167.331. [Online]. Available: http://link.aps.org/doi/10.1103/PhysRev.167.331.

[69] E. E. M. Chia, D. Springer, S. K. Nair, X. Q. Zou, S. A. Cheong, C. Panagopoulos, T. Tamegai, H. Eisaki, S. Ishida, S. Uchida, A. J. Taylor, and J.-X. Zhu, "Doping dependence of the electron–phonon and electron–spin fluctuation interactions in the high- T c superconductor $Bi_2Sr_2CaCu2O_{8+\delta}$," *New Journal of Physics*, vol. 15, no. 10, p. 103 027, Oct. 2013, ISSN: 1367-2630. DOI: 10.1088/1367-2630/15/10/103027. [Online]. Available: http://stacks.iop.org/1367-2630/15/i=10/a=103027?key=crossref.b61d266557255315c2e980cf7a37fd43.

[70] V. V. Baranov and V. V. Kabanov, "Theory of electronic relaxation in a metal excited by an ultrashort optical pump," *Physical Review B*, vol. 89, no. 12, p. 125 102, Mar. 2014, ISSN: 1098-0121. DOI: 10.1103/PhysRevB.89.125102. [Online]. Available: http://link.aps.org/doi/10.1103/PhysRevB.89.125102.

[71] V. V. Kabanov and A. S. Alexandrov, "Electron relaxation in metals: Theory and exact analytical solutions," *Physical Review B*, vol. 78, pp. 1–8, 2008, ISSN: 10980121. DOI: 10.1103/PhysRevB.78.174514. arXiv: 0809.0818.

[72] K.-h. Lin, K.-J. Wang, C.-c. Chang, Y.-c. Wen, D.-h. Tsai, Y.-r. Wu, Y.-t. Hsieh, M.-j. Wang, B. Lv, P. C.-W. Chu, and M.-K. Wu, "Observation of pseudogap-like feature above Tc in LiFeAs and $(Ba_0.6K_0.4)Fe_2As_2$ by ultrafast optical measurement," *arXiv*, vol. 174502, p. 26, 2014, ISSN: 1550235X. DOI: 10.1103/PhysRevB.90.174502. arXiv: 1407.3539. [Online]. Available: http://arxiv.org/abs/1407.3539.

[73] J. Demsar, R. Hudej, J. Karpinski, V. Kabanov, and D. Mihailovic, "Quasiparticle dynamics and gap structure in $HgBa_2Ca_2Cu_3O_{8+\delta}$ investigated with femtosecond spectroscopy," *Physical Review B*, vol. 63, no. 5, pp. 1–7, Jan. 2001, ISSN: 0163-1829. DOI: 10.1103/PhysRevB.63.054519. [Online]. Available: http://link.aps.org/doi/10.1103/PhysRevB.63.054519.

[74] P. Gay, C. J. Stevens, D. C. Smith, C. Chen, and J. F. Ryan, "Anisotropy of non-equilibrium quasi-particle dynamics in single-crystal $YBa_2Cu_3O_{7-\delta}$," *Physica C: Superconductivity and its Applications*, vol. 341-348, pp. 2269–2270, 2000, ISSN: 09214534. DOI: 10.1016/S0921-4534(00)00977-1.

[75] L. Stojchevska, P. Kusar, T. Mertelj, V. Kabanov, X. Lin, G. Cao, Z. Xu, and D. Mihailovic, "Electron-phonon coupling and the charge gap of spin-density wave iron-pnictide materials from quasiparticle relaxation dynamics," *Phys. Rev. B*, vol. 82, no. 1, pp. 1–4, Jul. 2010, ISSN: 1098-0121. DOI: 10.1103/PhysRevB.82.012505. [Online]. Available: http://link.aps.org/doi/10.1103/PhysRevB.82.012505.

[76] L. Stojchevska, T. Mertelj, J.-H. Chu, I. R. Fisher, and D. Mihailovic, "Doping dependence of femtosecond quasiparticle relaxation dynamics in $Ba(Fe,Co)_2As_2$ single crystals: Evidence for normal-state nematic fluctuations," *Phys. Rev. B*, vol. 86, no. 2, p. 024 519, Jul. 2012, ISSN: 1098-0121. DOI: 10.1103/PhysRevB.86.024519. [Online]. Available: http://link.aps.org/doi/10.1103/PhysRevB.86.024519.

[77] Y. Toda, J. Sekiya, Y. H. Liu, N. Momono, M. Oda, and M. Ido, "Nonequilibrium Carrier Dynamics Studied in Underdoped Bi2212 by Polarized Optical Pump-Probe Spectroscopy," *Journal of Superconductivity and Novel Magnetism*, vol. 23, no. 5, pp. 871–872, Dec. 2009, ISSN: 1557-1939. DOI: 10.1007/s10948-009-0608-0. [Online]. Available: http://link.springer.com/10.1007/s10948-009-0608-0.

[78] W. Li, C. Zhang, X. Wang, J. Chakhalian, and M. Xiao, *Ultrafast spectroscopy of quasiparticle dynamics in cuprate superconductors*, Jul. 2014. DOI: 10.1016/j.jmmm.2014.06.056. arXiv: 1406.6207. [Online]. Available: http://linkinghub.elsevier.com/retrieve/pii/S0304885314005782.

[79] Y. Toda, T. Mertelj, P. Kusar, T. Kurosawa, M. Oda, M. Ido, and D. Mihailovic, "Quasiparticle relaxation dynamics in underdoped $Bi_2Sr_2CaCu_2O_{8+\delta}$ by two-color pump-probe spectroscopy," *Physical Review B*, vol. 84, no. 17, pp. 1–8, Nov. 2011, ISSN: 1098-0121. DOI: 10.1103/PhysRevB.84.174516. [Online]. Available: http://link.aps.org/doi/10.1103/PhysRevB.84.174516.

[80] S. Sakai, S. Blanc, M. Civelli, Y. Gallais, M. Cazayous, M.-a. Méasson, J. S. Wen, Z. J. Xu, G. D. Gu, G. Sangiovanni, Y. Motome, K. Held, A. Sacuto, A. Georges, and M. Imada, "Raman-Scattering Measurements and Theory of the Energy-Momentum Spectrum for Underdoped $Bi_2Sr_2CaCuO_{8+\delta}$ Superconductors: Evidence of an s-Wave Structure for the Pseudogap," *Physical Review Letters*, vol. 111, no. 10, p. 107 001, Sep. 2013, ISSN: 0031-9007. DOI: 10.1103/PhysRevLett.111.107001. [Online]. Available: http://link.aps.org/doi/10.1103/PhysRevLett.111.107001.

[81] R. Cortés, L. Rettig, Y. Yoshida, H. Eisaki, M. Wolf, and U. Bovensiepen, "Momentum-Resolved Ultrafast Electron Dynamics in Superconducting $Bi_2Sr_2CaCu_2O_{8+\delta}$," *Physical Review Letters*, vol. 107, no. 9, p. 097 002, Aug. 2011, ISSN: 0031-9007. DOI: 10.1103/PhysRevLett.107.097002. arXiv: 1011.1171. [Online]. Available: http://arxiv.org/abs/1011.1171%20http://link.aps.org/doi/10.1103/PhysRevLett.107.097002.

[82] P. Kusar, V. V. Kabanov, J. Demsar, T. Mertelj, S. Sugai, and D. Mihailovic, "Controlled Vaporization of the Superconducting Condensate in Cuprate Superconductors by Femtosecond Photoexcitation," *Physical Review Letters*, vol. 101, no. 22, pp. 1–4, Nov. 2008, ISSN: 0031-9007. DOI: 10.1103/PhysRevLett.101.227001. [Online]. Available: http://link.aps.org/doi/10.1103/PhysRevLett.101.227001.

[83] D. Mattis and J. Bardeen, "Theory of the Anomalous Skin Effect in Normal and Superconducting Metals," *Physical Review*, vol. 111, no. 2, 1958.

[84] A. Rothwarf and B. N. Taylor, "Measurement of recombination lifetimes in superconductors," *Physical Review Letters*, vol. 19, no. 1, pp. 27–30, 1967, ISSN: 00319007. DOI: 10.1103/PhysRevLett.19.27.

[85] V. V. Kabanov, J. Demsar, and D. Mihailovic, "Kinetics of a Superconductor Excited with a Femtosecond Optical Pulse," *Physical Review Letters*, vol. 95, no. 14, p. 147 002, Sep. 2005, ISSN: 0031-9007. DOI: 10.1103/PhysRevLett.95.147002. [Online]. Available: http://link.aps.org/doi/10.1103/PhysRevLett.95.147002.

[86] G. P. Segre, N. Gedik, J. Orenstein, D. A. Bonn, R. Liang, and W. N. Hardy, "Photoinduced changes of reflectivity in single crystals of $YBa_2Cu_3O_{6.5}$ (ortho II).," *Physical review letters*, vol. 88, no. Ortho II, p. 137 001, 2002, ISSN: 0031-9007. DOI: 10.1103/PhysRevLett.88.137001. arXiv: 0107325 [cond-mat].

[87] J. Demsar, R. Averitt, V. Kabanov, and D. Mihailovic, "Comment on "Photoinduced Changes of Reflectivity in Single Crystals of $YBa_2Cu_3O_{6.5}$ (Ortho II)"," *Physical Review Letters*, vol. 91, no. October, p. 169 701, 2003, ISSN: 0031-9007. DOI: 10.1103/PhysRevLett.91.169701. [Online]. Available: http://link.aps.org/doi/10.1103/PhysRevLett.91.169701.

[88] M. Beyer, D. Städter, M. Beck, H. Schäfer, V. V. Kabanov, G. Logvenov, I. Bozovic, G. Koren, and J. Demsar, "Photoinduced melting of superconductivity in the high-T_c superconductor $La_{2-x}Sr_xCuO_4$ probed by time-resolved optical and terahertz techniques," *Physical Review B*, vol. 83, pp. 1–8, 2011, ISSN: 10980121. DOI: 10.1103/PhysRevB.83.214515. arXiv: 1102.3012.

[89] P. Kusar, V. V. Kabanov, J. Demsar, T. Mertelj, S. Sugai, and D. Mihailovic, "Controlled Vaporization of the Superconducting Condensate in Cuprate Superconductors by Femtosecond Photoexcitation," *Phys. Rev. Lett.*, vol. 101, no. 22, pp. 1–4, Nov. 2008, ISSN: 0031-9007. DOI: 10.1103/PhysRevLett.101.227001. [Online]. Available: http://link.aps.org/doi/10.1103/PhysRevLett.101.227001.

[90] L. Stojchevska, P. Kusar, T. Mertelj, V. V. Kabanov, Y. Toda, X. Yao, and D. Mihailovic, "Mechanisms of nonthermal destruction of the superconducting state and melting of the charge-density-wave state by femtosecond laser pulses," *Physical Review B*, vol. 84, no. 18, p. 180 507, Nov. 2011, ISSN: 1098-0121. DOI: 10.1103/PhysRevB.84.180507. [Online]. Available: http://link.aps.org/doi/10.1103/PhysRevB.84.180507.

[91] V. Schmidt, P. Müller, and A. Ustinov, *The Physics of Superconductors: Introduction to Fundamentals and Applications*. Springer, 1997, ISBN: 9783540612438. [Online]. Available: http://books.google.si/books?id=8O8svNo%5C_tWoC.

[92] M. Tinkham, *Introduction to Superconductivity: Second Edition*, ser. Dover Books on Physics. Dover Publications, 2004, ISBN: 9780486435039. [Online]. Available: http://books.google.si/books?id=k6AO9nRYbioC.

[93] L. D. Landau, "On the Theory of Phase Transitions," *Zh. Eksp. Teor. Fiz.*, vol. 7, pp. 19–32, 1937. DOI: 10.1038/138840a0.

[94] V. L. Pokrovsky, *Landau and modern physics*, 2009. DOI: 10.3367/UFNr.0179.200911j.1237.

[95] L. D. Landau and E. M. Lifshitz, "Statistical Physics, Part 1," *Physics Today*, vol. 34, p. 74, 1981.

[96] A. Schmid, "A time dependent Ginzburg-Landau equation and its application to the problem of resistivity in the mixed state," *Physik der Kondensierten Materie*, vol. 5, pp. 302–317, 1966, ISSN: 14346028. DOI: 10.1007/BF02422669.

[97] E. Abrahams and T. Tsuneto, "Time variation of the ginzburg-landau order parameter," *Physical Review*, vol. 152, no. i, pp. 416–432, 1966, ISSN: 0031899X. DOI: 10.1103/PhysRev.152.416.

[98] N. Kopnin, "Introduction to Ginzburg-Landau and Gross-Pitaevskii Theories for Superconductivity and Superfluids," *Journal of low temperature physics*, vol. 129, no. 5/6, pp. 219–262, 2002.

[99] I. K. Schuller and K. E. Gray, "Time-dependent Ginzburg-Landau: From single particle to collective behavior," *Journal of Superconductivity and Novel Magnetism*, vol. 19, no. July, pp. 401–407, 2006, ISSN: 15571939. DOI: 10.1007/s10948-006-0179-2.

[100] I. S. Aranson and L. Kramer, "The world of the complex Ginzburg-Landau equation," *Reviews of Modern Physics*, vol. 74, no. January, pp. 99–143, 2002, ISSN: 00346861. DOI: 10.1103/RevModPhys.74.99. arXiv: 0106115.

[101] L. P. Pitaevskii and E. M. Lifshitz, *Physical Kinetics*, v. 10. Elsevier Science, 2012, ISBN: 9780080570495. [Online]. Available: http://books.google.si/books?id=DTHxPDfV0fQC.

[102] G. E. Volovik, "Defect formation in inhomogeneous second-order phase transition: theory and experiment," *Physica B: Condensed Matter*, vol. 280, pp. 122–127, 2000, ISSN: 09214526. DOI: 10.1016/S0921-4526(99)01512-4.

[103] P. Kusar, "Influence of irregularities and dimensonality on electron relaxation.," PhD thesis, University of Ljubljana, 2007.

[104] I. Coherent, *Operator's Manual Verdi V-8/V-10 Diode-Pumped Lasers*. Santa Clara, 2005, ISBN: 8003677890.

[105] C. E. Web and J. D. Jones, Eds., *Handbook of laser technology and applications. - Vol. 1*. Institute of Physics PublishingBristol and Philadelphia, 2004.

[106] R. Paschotta, Ed., *Encyclopedia of Laser Physics and Technology*. Wiley, 2008.

[107] *Operator's Manual: The Coherent Mira Seed Laser*. Coherent Inc, Santa Clara, 1996.

[108] *Operator's Manual: Vitara Modelocked Ti:S Laser*. Coherent Inc, Santa Clara, 2011.

[109] V. L. Ginzburg, "The scattering of light near points of phase transition in solids," *Soviet Physics Uspekhi*, vol. 5, no. 4, p. 649, 1963. [Online]. Available: http://stacks.iop.org/0038-5670/5/i=4/a=A09.

[110] R. Merlin, "Generating coherent THz phonons with light pulses," *Solid State Communications*, vol. 102, no. 2-3, pp. 207–220, Apr. 1997, ISSN: 00381098. DOI: 10.1016/S0038-1098(96)00721-1. [Online]. Available: http://linkinghub.elsevier.com/retrieve/pii/S0038109896007211.

[111] T. Stevens, J. Kuhl, and R. Merlin, "Coherent phonon generation and the two stimulated Raman tensors," *Physical Review B*, vol. 65, no. 14, p. 144 304, Mar. 2002, ISSN: 0163-1829. DOI: 10.1103/PhysRevB.65.144304. [Online]. Available: http://link.aps.org/doi/10.1103/PhysRevB.65.144304.

[112] H. Okamoto, T. Miyagoe, K. Kobayashi, H. Uemura, H. Nishioka, H. Matsuzaki, A. Sawa, and Y. Tokura, "Photoinduced transition from Mott insulator to metal in the undoped cuprates Nd_2CuO_4 and La_2CuO_4," *Physical Review B*, vol. 83, no. 12, p. 125 102, Mar. 2011, ISSN: 1098-0121. DOI: 10.1103/PhysRevB.83.125102. [Online]. Available: http://link.aps.org/doi/10.1103/PhysRevB.83.125102.

[113] J. Karpinski, H. Schwer, I. Mangelschots, K. Conder, A. Morawski, T. Lada, and A. Paszewin, "Crystals of Hg superconductors," *Nature*, vol. 371, no. 6499, pp. 661–661, 1994, ISSN: 0028-0836. DOI: 10.1038/371661a0.

[114] S. Hüfner, M. A. Hossain, A. Damascelli, and G. A. Sawatzky, "Two gaps make a high-temperature superconductor?" *Reports on Progress in Physics*, vol. 71, no. 6, p. 062 501, Jun. 2008, ISSN: 0034-4885. DOI: 10.1088/0034-4885/71/6/062501. [Online]. Available: http://stacks.iop.org/0034-4885/71/i=6/a=062501?key=crossref.99900432df925753967b8d6fcabdfaa3.

[115] P. A. Lee, N. Nagaosa, and X. G. Wen, "Doping a Mott insulator: Physics of high-temperature superconductivity," *Reviews of Modern Physics*, vol. 78, no. January, 2006, ISSN: 00346861. DOI: 10.1103/RevModPhys.78.17. arXiv: 0410445 [cond-mat].

[116] N. F. Mott, "Metal-Insulator Transition," *Rev. Mod. Phys.*, vol. 40, no. 4, pp. 677–683, Oct. 1968, ISSN: 0034-6861. DOI: 10.1103/RevModPhys.40.677. [Online]. Available: http://link.aps.org/doi/10.1103/RevModPhys.40.677.

[117] G. Ghiringhelli, M. Le Tacon, M. Minola, S. Blanco-Canosa, C. Mazzoli, N. B. Brookes, G. M. De Luca, A. Frano, D. G. Hawthorn, F. He, T. Loew, M. M. Sala, D. C. Peets, M. Salluzzo, E. Schierle, R. Sutarto, G. a. Sawatzky, E. Weschke, B. Keimer, and L. Braicovich, "Long-Range Incommensurate Charge Fluctuations in (Y,Nd)Ba2Cu3O6+x," *Science*, vol. 337, no. June, pp. 821–825, 2012, ISSN: 0036-8075. DOI: 10.1126/science.1223532.

[118] K. B. Efetov, H. Meier, and C. Pépin, "Pseudogap state near a quantum critical point," *Nat. Phys.*, vol. 9, no. 7, pp. 442–446, 2013, ISSN: 1745-2473. DOI: 10.1038/nphys2641. [Online]. Available: http://dx.doi.org/10.1038/nphys2641.

[119] P. A. Lee, "Amperean pairing and the pseudogap phase of cuprate superconductors," *Physical Review X*, vol. 4, no. April, pp. 1–13, 2014, ISSN: 21603308. DOI: 10.1103/PhysRevX.4.031017. arXiv: arXiv:1401.0519v4.

[120] P. Curty and H. Beck, "Pseudogap and Amplitude Fluctuations in High Temperature Superconductors," *arXiv preprint*, no. 0606807, 2006. arXiv: 0606807 [cond-mat]. [Online]. Available: http://arxiv.org/abs/cond-mat/0606807.

[121] T. P. Devereaux and R. Hackl, "Inelastic light scattering from correlated electrons," *Rev. Mod. Phys.*, vol. 79, no. 1, pp. 175–233, Jan. 2007, ISSN: 0034-6861. DOI: 10.1103/RevModPhys.79.175. [Online]. Available: http://link.aps.org/doi/10.1103/RevModPhys.79.175.

[122] T. Kondo, A. D. Palczewski, Y. Hamaya, T. Takeuchi, J. S. Wen, Z. J. Xu, G. Gu, and A. Kaminski, "Formation of gapless fermi arcs and fingerprints of order in the pseudogap state of cuprate superconductors," *Physical Review Letters*, vol. 111, no. October, pp. 1–5, 2013, ISSN: 00319007. DOI: 10.1103/PhysRevLett.111.157003. arXiv: 1208.3448.

[123] H.-B. Yang, J. D. Rameau, Z.-H. Pan, G. D. Gu, P. D. Johnson, H. Claus, D. G. Hinks, and T. E. Kidd, "Reconstructed Fermi Surface of Underdoped $Bi_2Sr_2CaCu_2O_{8+\delta}$ Cuprate Superconductors.," *Physical review letters*, vol. 107, no. July, p. 047 003, 2011, ISSN: 0031-9007. DOI: 10.1103/PhysRevLett.107.047003.

[124] T. J. Reber, N. C. Plumb, Z. Sun, Y. Cao, Q. Wang, K. McElroy, H. Iwasawa, M. Arita, J. S. Wen, Z. J. Xu, G. Gu, Y. Yoshida, H. Eisaki, Y. Aiura, and D. S. Dessau, "The origin and non-quasiparticle nature of Fermi arcs in $Bi_2Sr_2CaCu2O_{8+\delta}$," *Nature Physics*, vol. 8, no. July, pp. 606–610, 2012, ISSN: 1745-2473. DOI: 10.1038/nphys2352. arXiv: 1408.0441.

[125] J. W. Loram, J. L. Luo, J. R. Cooper, W. Y. Liang, and J. L. Tallon, "The condensation energy and pseudogap energy scale of Bi:2212 from the electronic specific heat," *Physica C: Superconductivity*, vol. 341-348, pp. 831–834, Nov. 2000, ISSN: 09214534. DOI: 10.1016/S0921-4534(00)00706-1. [Online]. Available: http://linkinghub.elsevier.com/retrieve/pii/S0921453400007061.

[126] M. J. Lawler, K. Fujita, J. Lee, A. R. Schmidt, Y. Kohsaka, C. K. Kim, H. Eisaki, S. Uchida, J. C. Davis, J. P. Sethna, and E.-A. Kim, "Intra-unit-cell electronic nematicity of the high-T_c copper-oxide pseudogap states.," *Nature*, vol. 466, no. 7304, pp. 347–51, Jul. 2010, ISSN: 1476-4687. DOI: 10.1038/nature09169. [Online]. Available: http://www.ncbi.nlm.nih.gov/pubmed/20631795.

[127] D. H. Torchinsky, F. Mahmood, A. T. Bollinger, I. Božović, and N. Gedik, "Fluctuating charge-density waves in a cuprate superconductor.," *Nature materials*, vol. 12, no. 5, pp. 387–91, May 2013, ISSN: 1476-1122. DOI: 10.1038/nmat3571. [Online]. Available: http://www.ncbi.nlm.nih.gov/pubmed/23435216.

[128] P. A. Miles, S. J. Kennedy, G. J. McIntyre, G. D. Gu, G. J. Russell, and N. Koshizuka, "Refinement of the incommensurate structure of high quality Bi-2212 single crystals from a neutron diffraction study," *Physica C: Superconductivity*, vol. 294, no. 3-4, pp. 275–288, 1998, ISSN: 09214534. DOI: 10.1016/S0921-4534(97)01682-1.

[129] M. Vershinin, S. Misra, S. Ono, Y. Abe, Y. Ando, and A. Yazdani, "Local ordering in the pseudogap state of the high-Tc superconductor $Bi_2Sr_2CaCu2O_{8+\delta}$.," *Science (New York, N.Y.)*, vol. 303, no. 5666, pp. 1995–8, Mar. 2004, ISSN: 1095-9203. DOI: 10.1126/science.1093384. [Online]. Available: http://www.ncbi.nlm.nih.gov/pubmed/14963336.

[130] I. Zeljkovic, E. J. Main, T. L. Williams, M. C. Boyer, K. Chatterjee, W. D. Wise, Y. Yin, M. Zech, A. Pivonka, T. Kondo, T. Takeuchi, H. Ikuta, J. Wen, Z. Xu, G. D. Gu, E. W. Hudson, and J. E. Hoffman, "Scanning tunnelling microscopy imaging of symmetry-breaking structural distortion in the bismuth-based cuprate superconductors.," *Nature materials*, vol. 11, no. 7, pp. 585–9, Jul. 2012, ISSN: 1476-1122. DOI: 10.1038/nmat3315. [Online]. Available: http://www.ncbi.nlm.nih.gov/pubmed/22561901.

[131] R. Yusupov, T. Mertelj, V. V. Kabanov, S. Brazovskii, P. Kusar, J.-H. Chu, I. R. Fisher, and D. Mihailovic, "Coherent dynamics of macroscopic electronic order through a symmetry breaking transition," *Nat. Phys.*, vol. 6, no. 9, pp. 681–684, Aug. 2010, ISSN: 1745-2473. DOI: 10.1038/nphys1738. [Online]. Available: http://www.nature.com/doifinder/10.1038/nphys1738.

[132] P. Kusar, I. Madan, M. Lu-Dac, T. Mertelj, V. V. Kabanov, and D. Mihailovic, "Coherent trajectory through the normal-to-superconducting transition reveals ultrafast vortex dynamics in a superconductor.," *arXiv preprint*, pp. 1–5, 2012. arXiv: 1207.2879.

[133] J. Demsar, L. Forró, H. Berger, and D. Mihailovic, "Femtosecond snapshots of gap-forming charge-density-wave correlations in quasi-two-dimensional dichalcogenides 1T-TaS_2 and 2H-$TaSe_2$," *Physical Review B*, vol. 66, no. 4, p. 041 101, Jun. 2002, ISSN: 0163-1829. DOI: 10.1103/PhysRevB.66.041101. [Online]. Available: http://link.aps.org/doi/10.1103/PhysRevB.66.041101.

[134] V. M. Krasnov, S.-O. Katterwe, and A. Rydh, "Signatures of the electronic nature of pairing in high-T_c superconductors obtained by non-equilibrium boson spectroscopy.," *Nature communications*, vol. 4, p. 2970, Jan. 2013, ISSN: 2041-1723. DOI: 10.1038/ncomms3970. [Online]. Available: http://www.pubmedcentral.nih.gov/articlerender.fcgi?artid=3905708&tool=pmcentrez&rendertype=abstract.

[135] I. M. Vishik, W. S. Lee, F. Schmitt, B. Moritz, T. Sasagawa, S. Uchida, K. Fujita, S. Ishida, C. Zhang, T. P. Devereaux, and Z. X. Shen, "Doping-Dependent Nodal Fermi Velocity of the High-Temperature Superconductor $Bi_2Sr_2CaCu2O_{8+\delta}$ Revealed Using High-Resolution Angle-Resolved Photoemission Spectroscopy," *Physical Review Letters*, vol. 104, no. 20, p. 207 002, May 2010, ISSN: 0031-9007. DOI: 10.1103/PhysRevLett.104.207002. [Online]. Available: http://link.aps.org/doi/10.1103/PhysRevLett.104.207002.

[136] A. Patashinski, V. Pokrovskii, and P. Shepherd, *Fluctuation theory of phase transitions: covering second-order phase transitions, scale and conformal invariance, algebras of fluctutating quantities, degenerate systems, critical dynamics, epsilon expansions, renormalization group, and applications*, ser. International series in natural philosophy. Pergamon Press, 1979, ISBN: 9780080216645.

[137] M. Quijada, D. Tanner, R. Kelley, M. Onellion, H. Berger, and G. Margaritondo, "Anisotropy in the ab-plane optical properties of $Bi_2Sr_2CaCu2O_8$ single-domain crystals," *Physical Review B*, vol. 60, no. 21, pp. 14 917–14 934, Dec. 1999, ISSN: 0163-1829. DOI: 10.1103/PhysRevB.60.14917. [Online]. Available: http://link.aps.org/doi/10.1103/PhysRevB.60.14917.

[138] G.-m. Zhao, M. B. Hunt, H. Keller, and K. A. Müller, "Evidence for polaronic supercarriers in the copper oxide superconductors $La_{2-x}Srx$CuO4," *Nature*, vol. 385, no. 6613, pp. 236–239, Jan. 1997, ISSN: 0028-0836. DOI: 10.1038/385236a0. [Online]. Available: http://www.nature.com/doifinder/10.1038/385236a0.

[139] G.-m. Zhao, K. Conder, H. Keller, and K. A. Müller, "Oxygen isotope effects in $La_{2-x}Srx$CuO4 : evidence for polaronic charge carriers and their condensation," *Journal of Physics: Condensed Matter*, vol. 10, no. 40, pp. 9055–9066, Oct. 1998, ISSN: 0953-8984. DOI: 10.1088/0953-8984/10/40/010. [Online]. Available: http://stacks.iop.org/0953-8984/10/i=40/a=010?key=crossref.6668039fc24de220f98aabdd73bc1131.

[140] D. Mihailovic, V. V. Kabanov, and K. A. Müller, "The attainable superconducting T_c in a model of phase coherence by percolating," *Europhysics Letters (EPL)*, vol. 57, no. 2, pp. 254–259, Jan. 2002, ISSN: 0295-5075. DOI: 10.1209/epl/i2002-00569-0. [Online]. Available: http://stacks.iop.org/0295-5075/57/i=2/a=254?key=crossref.6e45472a8a8ec9f0817c2bec897b80ab.

[141] Y. Kohsaka, C. Taylor, P. Wahl, A. Schmidt, J. Lee, K. Fujita, J. W. Alldredge, K. McElroy, J. Lee, H. Eisaki, S. Uchida, D.-H. Lee, and J. C. Davis, "How Cooper pairs vanish approaching the Mott insulator in $Bi_2Sr_2CaCu_2O_{8+\delta}$.," *Nature*, vol. 454, no. 7208, pp. 1072–8, Aug. 2008, ISSN: 1476-4687. DOI: 10.1038/nature07243. [Online]. Available: http://www.ncbi.nlm.nih.gov/pubmed/18756248.

[142] G. Coslovich, B. Huber, W.-S. Lee, Y.-D. Chuang, Y. Zhu, T. Sasagawa, Z. Hussain, H. A. Bechtel, M. C. Martin, Z.-X. Shen, R. W. Schoenlein, and R. A. Kaindl, "Ultrafast charge localization in a stripe-phase nickelate.," *Nature communications*, vol. 4, p. 2643, Jan. 2013, ISSN: 2041-1723. DOI: 10.1038/ncomms3643. [Online]. Available: http://www.pubmedcentral.nih.gov/articlerender.fcgi?artid=3826635&tool=pmcentrez&rendertype=abstract.

[143] C. L. Smallwood, W. Zhang, L. T. Miller, C. Jozwiak, H. Eisaki, D.-H. Lee, and A. Lanzara, "Time- and momentum-resolved gap dynamics in $Bi_2Sr_2CaCu2O_{8+\delta}$," *Physical Review B*, vol. 89, no. 11, p. 115126, Mar. 2014, ISSN: 1098-0121. DOI: 10.1103/PhysRevB.89.115126. [Online]. Available: http://link.aps.org/doi/10.1103/PhysRevB.89.115126.

[144] V. V. Kabanov, T. Mertelj, and D. Mihailovic, "Mesoscopic Phase Separation in the Model with Competing Jahn-Teller and Coulomb Interaction," *J. Supercond. Novel Magn*, vol. 19, no. 1-2, pp. 67–71, Sep. 2006, ISSN: 1557-1939. DOI: 10.1007/s10948-005-0096-9. [Online]. Available: http://link.springer.com/10.1007/s10948-005-0096-9.

[145] T. Mertelj, V. Kabanov, J. Mena, and D. Mihailovic, "Self-organization of charged particles on a two-dimensional lattice subject to anisotropic Jahn-Teller-type interaction and three-dimensional Coulomb repulsion," *Phys. Rev. B*, vol. 76, no. 5, p. 054523, Aug. 2007, ISSN: 1098-0121. DOI: 10.1103/PhysRevB.76.054523. [Online]. Available: http://link.aps.org/doi/10.1103/PhysRevB.76.054523.

[146] H. Keller, A. Bussmann-Holder, and K. A. Müller, "Jahn-Teller physics and high-Tc superconductivity," *Mater. Today*, vol. 11, no. 9, pp. 38–46, Sep. 2008, ISSN: 13697021. DOI: 10.1016/S1369-7021(08)70178-0. [Online]. Available: http://linkinghub.elsevier.com/retrieve/pii/S1369702108701780.

[147] S. Agrestini, N. L. Saini, G. Bianconi, and A. Bianconi, "The strain of CuO_2 lattice: the second variable for the phase diagram of cuprate perovskites," *Journal of Physics A: Mathematical and General*, vol. 36, no. 35, pp. 9133–9142, Sep. 2003, ISSN: 0305-4470. DOI: 10.1088/0305-4470/36/35/302. [Online]. Available: http://stacks.iop.org/0305-4470/36/i=35/a=302?key=crossref.c6d332512495c7abffcc2c0b4dc9ab92.

[148] A. Mishchenko and N. Nagaosa, "Electron-Phonon Coupling and a Polaron in the t-J Model: From the Weak to the Strong Coupling Regime," *Phys. Rev. Lett.*, vol. 93, no. 3, p. 036 402, Jul. 2004, ISSN: 0031-9007. DOI: 10.1103/PhysRevLett.93.036402. [Online]. Available: http://link.aps.org/doi/10.1103/PhysRevLett.93.036402.

[149] S. A. Kivelson, E. Fradkin, and V. J. Emery, "Electronic liquid-crystal phases of a doped Mott insulator," *Nature*, vol. 393, no. 6685, pp. 550–553, Jun. 1998, ISSN: 0028-0836. DOI: 10.1038/31177. [Online]. Available: http://www.nature.com/doifinder/10.1038/31177.

[150] Y. Toda, F. Kawanokami, T. Kurosawa, M. Oda, I. Madan, T. Mertelj, V. V. Kabanov, and D. Mihailovic, "Dynamics of broken symmetry nodal and anti-nodal excitations in $Bi_2Sr_2CaCu_2O_{8+\delta}$ probed by polarized femtosecond spectroscopy," no. Dm, pp. 1–5, Nov. 2013. arXiv: 1311.4719. [Online]. Available: http://arxiv.org/abs/1311.4719.

[151] D. Mihailović, C. M. Foster, K. Voss, and A. J. Heeger, "Application of the polaron-transport theory to $\sigma(\omega)$ in $Tl_2Ba_2Ca_{1-x}Gd_xCu_2O_8$, YBa_2," *Physical Review B*, vol. 42, no. 13, pp. 7989–7993, Nov. 1990, ISSN: 0163-1829. DOI: 10.1103/PhysRevB.42.7989. [Online]. Available: http://link.aps.org/doi/10.1103/PhysRevB.42.7989.

[152] A. Mourachkine, *High-Temperature Superconductivity in Cuprates: The Nonlinear Mechanism and Tunneling Measurements*, ser. Fundamental Theories of Physics. Springer Netherlands, 2006, ISBN: 9780306480638. [Online]. Available: https://books.google.si/books?id=3AAMCAAAQBAJ.

[153] P. Kusar, V. V. Kabanov, S. Sugai, J. Demšar, T. Mertelj, and D. Mihailović, "Dynamical Structural Instabilities in $La_1.9Sr_0.1CuO_4$ Under Intense Laser Photoexcitation," *Journal of Superconductivity and Novel Magnetism*, vol. 24, no. 1-2, pp. 421–425, Oct. 2010, ISSN: 1557-1939. DOI: 10.1007/s10948-010-0951-1. [Online]. Available: http://www.springerlink.com/index/10.1007/s10948-010-0951-1%20http://link.springer.com/10.1007/s10948-010-0951-1.

[154] B. Mansart, D. Boschetto, A. Savoia, F. Rullier-Albenque, F. Bouquet, E. Papalazarou, A. Forget, D. Colson, A. Rousse, and M. Marsi, "Ultrafast transient response and electron-phonon coupling in the iron-pnictide superconductor $Ba(Fe_{1-x}Co_x)_2As_2$," *Physical Review B*, vol. 82, no. 2, p. 024 513, Jul. 2010, ISSN: 1098-0121. DOI: 10.1103/PhysRevB.82.024513. [Online]. Available: http://link.aps.org/doi/10.1103/PhysRevB.82.024513.

[155] T. Mertelj, P. Kusar, V. V. Kabanov, P. Giraldo-Gallo, I. R. Fisher, and D. Mihailovic, "Incoherent Topological Defect Recombination Dynamics in $TbTe_3$," *Phys. Rev. Lett.*, vol. 110, no. 15, p. 156 401, Apr. 2013, ISSN: 0031-9007. DOI: 10.1103/PhysRevLett.110.156401. [Online]. Available: http://link.aps.org/doi/10.1103/PhysRevLett.110.156401.

[156] A. Junod, A. Erb, and C. Renner, "Specific heat of high temperature superconductors in high fields at T_c : from BCS to the Bose - Einstein condensation," *Physica C*, vol. 317-318, pp. 333–344, 1999.

[157] A. Alexandrov, W. Beere, V. Kabanov, and W. Liang, "Contrasting Effects of Magnetic Field on Thermodynamic and Resistive Transitions in High- Tc Cuprates," *Phys. Rev. Lett.*, vol. 79, no. 8, pp. 1551–1554, Aug. 1997, ISSN: 0031-9007. DOI: 10.1103/PhysRevLett.79.1551. [Online]. Available: http://link.aps.org/doi/10.1103/PhysRevLett.79.1551.

[158] A. Junod, M. Roulin, B. Revaz, and A. Erb, "Experimental survey of critical fluctuations in the specific heat of high-temperature superconductors," *Physica B Condens. Matter*, vol. 280, no. 1-4, pp. 214–219, May 2000, ISSN: 09214526. DOI: 10.1016/S0921-4526(99)01581-1. [Online]. Available: http://linkinghub.elsevier.com/retrieve/pii/S0921452699015811.

[159] V. L. Berezinskii, "Destruction of Long-range Order in One-dimensional and Two-dimensional Systems having a Continuous Symmetry Group I. Classical Systems," *JETP*, vol. 32, p. 493, 1971.

[160] ——, "Destruction of Long-range Order in One-dimensional and Two-dimensional Systems Possessing a Continuous Symmetry Group. II. Quantum Systems.," *JETP*, vol. 34, p. 610, 1972.

[161] J. M. Kosterlitz and D. J. Thouless, "Ordering, metastability and phase transitions in two-dimensional systems," *Journal of Physics C: Solid State Physics*, vol. 6, no. 7, pp. 1181–1203, Apr. 1973, ISSN: 0022-3719. DOI: 10.1088/0022-3719/6/7/010. [Online]. Available: http://stacks.iop.org/0022-3719/6/i=7/a=010?key=crossref.f2d443370878b9288c142e398ad429b1.

[162] V. J. Emery and S. A. Kivelson, "Importance of phase fluctuations in superconductors with small superfluid density," *Nature*, vol. 374, no. 6521, pp. 434–437, Mar. 1995, ISSN: 0028-0836. DOI: 10.1038/374434a0. [Online]. Available: http://www.nature.com/doifinder/10.1038/374434a0.

[163] V. J. Emery, S. A. Kivelson, and O. Zachar, "Pairing and phase coherence in high temperature superconductors," *Physica C: Superconductivity*, vol. 282-287, pp. 174–177, Aug. 1997, ISSN: 09214534. DOI: 10.1016/S0921-4534(97)00255-4. [Online]. Available: http://linkinghub.elsevier.com/retrieve/pii/S0921453497002554.

[164] V. J. Emery and S. A. Kivelson, "Crossovers and phase coherence in cuprate superconductors," *Journal of Physics and Chemistry of Solids*, vol. 59, no. 10-12, pp. 1705–1710, Oct. 1998, ISSN: 00223697. DOI: 10.1016/S0022-3697(98)00087-0.

[165] E. Silva, S. Sarti, R. Fastampa, and M. Giura, "Excess conductivity of overdoped $Bi_2Sr_2CaCu2O_{8+x}$ crystals well above Tc," *Physical Review B*, vol. 64, no. 14, p. 144 508, Sep. 2001, ISSN: 0163-1829. DOI: 10.1103/PhysRevB.64.144508. [Online]. Available: http://link.aps.org/doi/10.1103/PhysRevB.64.144508.

[166] M. Truccato, A. Agostino, G. Rinaudo, S. Cagliero, and M. Panetta, "Possible dominance of the Maki–Thompson process in the fluctuation conductivity of Bi-2212 superconducting whiskers," *Journal of Physics: Condensed Matter*, vol. 18, no. 35, pp. 8295–8312, Sep. 2006, ISSN: 0953-8984. DOI: 10.1088/0953-8984/18/35/015. [Online]. Available: http://stacks.iop.org/0953-8984/18/i=35/a=015?key=crossref.3c8506ad040a132f7db622d75e325593.

[167] A. Ghosh and A. Basu, "Fluctuation-induced conductivity in quenched and furnace-cooled $Bi_2Sr_2CaCu_2O_{8+\delta}$: Aslamazov-Larkin or short-wavelength fluctuations," *Physical Review B*, vol. 59, no. 17, pp. 11 193–11 196, May 1999, ISSN: 0163-1829. DOI: 10.1103/PhysRevB.59.11193. [Online]. Available: http://link.aps.org/doi/10.1103/PhysRevB.59.11193.

[168] G. Balestrino, A. Crisan, D. Livanov, S. Manokhin, and E. Milani, "Fluctuation magnetoconductivity of BSCCO-2212 films in parallel magnetic field," *Physica C: Superconductivity*, vol. 355, no. 1-2, pp. 135–139, Jun. 2001, ISSN: 09214534. DOI: 10.1016/S0921-4534(00)01771-8. [Online]. Available: http://linkinghub.elsevier.com/retrieve/pii/S0921453400017718.

[169] S. Bhatia and C. Dhard, "Excess conductivity and pair-breaking effects in $YBa_2Cu_3O_7$ and $Bi_2Sr_2Ca_{1-x}Y_xCu_2O_{8+\delta}$ systems," *Physical Review B*, vol. 49, no. 17, pp. 12 206–12 215, May 1994, ISSN: 0163-1829. DOI: 10.1103/PhysRevB.49.12206. [Online]. Available: http://link.aps.org/doi/10.1103/PhysRevB.49.12206.

[170] L. Li, Y. Wang, S. Komiya, S. Ono, Y. Ando, G. D. Gu, and N. P. Ong, "Diamagnetism and Cooper pairing above T_c in cuprates," *Phys. Rev. B*, vol. 81, no. 5, pp. 1–9, Feb. 2010, ISSN: 1098-0121. DOI: 10.1103/PhysRevB.81.054510. [Online]. Available: http://link.aps.org/doi/10.1103/PhysRevB.81.054510.

[171] Y. Wang, L. Li, M. Naughton, G. Gu, S. Uchida, and N. Ong, "Field-Enhanced Diamagnetism in the Pseudogap State of the Cuprate $Bi_2Sr_2CaCu2O_{8+\delta}$ Superconductor in an Intense Magnetic Field," *Physical Review Letters*, vol. 95, no. 24, p. 247 002, Dec. 2005, ISSN: 0031-9007. DOI: 10.1103/PhysRevLett.95.247002. [Online]. Available: http://link.aps.org/doi/10.1103/PhysRevLett.95.247002.

[172] J. L. Tallon, J. G. Storey, and J. W. Loram, "Fluctuations and critical temperature reduction in cuprate superconductors," *Physical Review B*, vol. 83, no. 9, p. 092 502, Mar. 2011, ISSN: 1098-0121. DOI: 10.1103/PhysRevB.83.092502. [Online]. Available: http://link.aps.org/doi/10.1103/PhysRevB.83.092502.

[173] T. Kondo, Y. Hamaya, A. D. Palczewski, T. Takeuchi, J. S. Wen, Z. J. Xu, G. Gu, J. Schmalian, and A. Kaminski, "Disentangling Cooper-pair formation above the transition temperature from the pseudogap state in the cuprates," *Nat. Phys.*, vol. 7, no. 1, pp. 21–25, Dec. 2010, ISSN: 1745-2473. DOI: 10.1038/nphys1851. [Online]. Available: http://www.nature.com/doifinder/10.1038/nphys1851.

[174] F. Rullier-Albenque, H. Alloul, and G. Rikken, "High-field studies of superconducting fluctuations in high-T_c cuprates: Evidence for a small gap distinct from the large pseudogap," *Phys. Rev. B*, vol. 84, no. 1, p. 014 522, Jul. 2011, ISSN: 1098-0121. DOI: 10.1103/PhysRevB.84.014522. [Online]. Available: http://link.aps.org/doi/10.1103/PhysRevB.84.014522.

[175] Y. Chen and C. Ting, "Magnetic-field-induced spin-density wave in high-temperature superconductors," *Phys. Rev. B*, vol. 65, no. 18, p. 180 513, May 2002, ISSN: 0163-1829. DOI: 10.1103/PhysRevB.65.180513. [Online]. Available: http://link.aps.org/doi/10.1103/PhysRevB.65.180513.

[176] J. Orenstein, J. Corson, S. Oh, and J. Eckstein, "Superconducting fluctuations in $Bi_2Sr_2Ca_{1-x}Dy_xCu_2O_{8+\delta}$ as seen by terahertz spectroscopy," *Annalen der Physik*, vol. 15, no. 7-8, pp. 596–605, Jul. 2006, ISSN: 0003-3804. DOI: 10.1002/andp.200510202. [Online]. Available: http://doi.wiley.com/10.1002/andp.200510202.

[177] J. Corson, R. Mallozzi, and J. Orenstein, "Vanishing of phase coherence in underdoped $Bi_2Sr_2CaCuO_{8+\delta}$," *Nature*, vol. 398, pp. 221–223, 1999. DOI: 10.1038/18402. [Online]. Available: http://www.nature.com/nature/journal/v398/n6724/abs/398221a0.html.

[178] D. Fisher, M. Fisher, and D. Huse, "Thermal fluctuations, quenched disorder, phase transitions, and transport in type-II superconductors," *Phys. Rev. B*, vol. 43, no. 1, pp. 130–159, Jan. 1991, ISSN: 0163-1829. DOI: 10.1103/PhysRevB.43.130. [Online]. Available: http://link.aps.org/doi/10.1103/PhysRevB.43.130.

[179] C. van der Beek, S. Colson, M. Indenbom, and M. Konczykowski, "Supercooling of the Disordered Vortex Lattice in $Bi_2Sr_2CaCu2O_{8+\delta}$," *Physical Review Letters*, vol. 84, no. 18, pp. 4196–4199, May 2000, ISSN: 0031-9007. DOI: 10.1103/PhysRevLett.84.4196. [Online]. Available: http://www.ncbi.nlm.nih.gov/pubmed/10990644%20http://link.aps.org/doi/10.1103/PhysRevLett.84.4196.

[180] I. Schuller and K. E. Gray, "Experimental Observation of the Relaxation Time of the Order Parameter in Superconductors," *Phys. Rev. Lett.*, vol. 36, pp. 429–432, 8 Feb. 1976. DOI: 10.1103/PhysRevLett.36.429. [Online]. Available: http://link.aps.org/doi/10.1103/PhysRevLett.36.429.

[181] A. S. Alexandrov, "High-temperature superconductivity: the explanation," *Phys. Scr.*, vol. 83, no. 3, p. 038 301, Mar. 2011, ISSN: 0031-8949. DOI: 10.1088/0031-8949/83/03/038301. [Online]. Available: http://stacks.iop.org/1402-4896/83/i=3/a=038301?key=crossref.dcfa91f3a5984bab0e09ca996329b764.

[182] ——, "Theory of high-temperature superconductivity in doped polar insulators," *Europhys. Lett.*, vol. 95, no. 2, p. 27 004, Jul. 2011, ISSN: 0295-5075. DOI: 10.1209/0295-5075/95/27004. [Online]. Available: http://stacks.iop.org/0295-5075/95/i=2/a=27004?key=crossref.39805131f2b46c40fd34dd14ff969958.

[183] V. Z. Kresin and S. A. Wolf, "Inhomogeneous Superconducting State and Intrinsic T_c : Near Room Temperature Superconductivity in the Cuprates," *Journal of Superconductivity and Novel Magnetism*, vol. 25, no. 2, pp. 175–180, Sep. 2011, ISSN: 1557-1939. DOI: 10.1007/s10948-011-1308-0. [Online]. Available: http://link.springer.com/10.1007/s10948-011-1308-0.

[184] R. Yusupov, T. Mertelj, V. V. Kabanov, S. Brazovskii, P. Kusar, J.-H. Chu, I. R. Fisher, and D. Mihailovic, "Coherent dynamics of macroscopic electronic order through a symmetry breaking transition," *Nat. Phys.*, vol. 6, no. 9, pp. 681–684, Aug. 2010, ISSN: 1745-2473. DOI: 10.1038/nphys1738. [Online]. Available: http://www.nature.com/doifinder/10.1038/nphys1738.

[185] K. M. Lang, V. Madhavan, J. E. Hoffman, E. W. Hudson, H. Eisaki, S. Uchida, and J. C. Davis, "Imaging the granular structure of high-T_c superconductivity in underdoped $Bi_2Sr_2CaCu_2O_{8+\delta}$.," *Nature*, vol. 415, no. 6870, pp. 412–416, 2002, ISSN: 00280836. DOI: 10.1038/415412a. arXiv: 0112232 [cond-mat].

[186] E. V. Antipov, A. M. Abakumov, and S. N. Putilin, "Chemistry and structure of Hg-based superconducting Cu mixed oxides," *Superconductor Science and Technology*, vol. 15, no. 7, J. Tauber, Ed., R31–R49, Jul. 2002, ISSN: 0953-2048. DOI: 10.1088/0953-2048/15/7/201. [Online]. Available: http://www.aanda.org/10.1051/0004-6361/201321621%20http://stacks.iop.org/0953-2048/15/i=7/a=201?key=crossref.a22ce907bdd30d99ebfadf4a0f2438d4.

[187] T. Matsuzaki, N. Momono, M. Oda, and M. Ido, "Electronic Specific Heat of $La_{2-x}Srx$CuO4: Pseudogap Formation and Reduction of the Superconducting Condensation Energy," *Journal of the Physics Society Japan*, vol. 73, no. 8, pp. 2232–2238, Aug. 2004, ISSN: 0031-9015. DOI: 10.1143/JPSJ.73.2232. [Online]. Available: http://jpsj.ipap.jp/link?JPSJ/73/2232/.

[188] N. Barišić, S. Badoux, M. K. Chan, C. Dorow, W. Tabis, B. Vignolle, G. Yu, J. Béard, X. Zhao, C. Proust, and M. Greven, "Universal quantum oscillations in the underdoped cuprate superconductors," *Nature Physics*, vol. 9, no. 12, pp. 761–764, Nov. 2013, ISSN: 1745-2473. DOI: 10.1038/nphys2792. [Online]. Available: http://www.nature.com/doifinder/10.1038/nphys2792.

[189] S. I. Mirzaei, D. Stricker, J. N. Hancock, C. Berthod, A. Georges, E. van Heumen, M. K. Chan, X. Zhao, Y. Li, M. Greven, N. Barišić, and D. van der Marel, "Spectroscopic evidence for Fermi liquid-like energy and temperature dependence of the relaxation rate in the pseudogap phase of the cuprates.," *Proceedings of the National Academy of Sciences of the United States of America*, vol. 110, no. 15, pp. 5774–8,

2013, ISSN: 1091-6490. DOI: 10.1073/pnas.1218846110. arXiv: 1207.6704. [Online]. Available: http://www.pubmedcentral.nih.gov/articlerender.fcgi?artid=3625325&tool=pmcentrez&rendertype=abstract.

[190] P. A. R. Ade, N. Aghanim, C. Armitage-Caplan, M. Arnaud, M. Ashdown, F. Atrio-Barandela, J. Aumont, C. Baccigalupi, A. J. Banday, R. B. Barreiro, J. G. Bartlett, N. Bartolo, E. Battaner, R. Battye, K. Benabed, A. Benoît, A. Benoit-Lévy, J.-P. Bernard, M. Bersanelli, P. Bielewicz, J. Bobin, J. J. Bock, A. Bonaldi, L. Bonavera, J. R. Bond, J. Borrill, F. R. Bouchet, M. Bridges, M. Bucher, C. Burigana, R. C. Butler, J.-F. Cardoso, A. Catalano, A. Challinor, A. Chamballu, L.-Y. Chiang, H. C. Chiang, P. R. Christensen, S. Church, D. L. Clements, S. Colombi, L. P. L. Colombo, F. Couchot, A. Coulais, B. P. Crill, A. Curto, F. Cuttaia, L. Danese, R. D. Davies, R. J. Davis, P. de Bernardis, A. de Rosa, G. de Zotti, J. Delabrouille, J.-M. Delouis, F.-X. Désert, J. M. Diego, H. Dole, S. Donzelli, O. Doré, M. Douspis, A. Ducout, J. Dunkley, X. Dupac, G. Efstathiou, T. A. Enßlin, H. K. Eriksen, J. Fergusson, F. Finelli, O. Forni, M. Frailis, E. Franceschi, S. Galeotta, K. Ganga, M. Giard, G. Giardino, Y. Giraud-Héraud, J. González-Nuevo, K. M. Górski, S. Gratton, A. Gregorio, A. Gruppuso, F. K. Hansen, D. Hanson, D. Harrison, S. Henrot-Versillé, C. Hernández-Monteagudo, D. Herranz, S. R. Hildebrandt, E. Hivon, M. Hobson, W. A. Holmes, A. Hornstrup, W. Hovest, K. M. Huffenberger, T. R. Jaffe, A. H. Jaffe, W. C. Jones, M. Juvela, E. Keihänen, R. Keskitalo, T. S. Kisner, J. Knoche, L. Knox, M. Kunz, H. Kurki-Suonio, G. Lagache, A. Lähteenmäki, J.-M. Lamarre, A. Lasenby, R. J. Laureijs, C. R. Lawrence, J. P. Leahy, R. Leonardi, J. Lesgourgues, M. Liguori, P. B. Lilje, M. Linden-Vørnle, M. López-Caniego, P. M. Lubin, J. F. Macías-Pérez, B. Maffei, D. Maino, N. Mandolesi, M. Maris, D. J. Marshall, P. G. Martin, E. Martínez-González, S. Masi, S. Matarrese, F. Matthai, P. Mazzotta, J. D. McEwen, A. Melchiorri, L. Mendes, A. Mennella, M. Migliaccio, S. Mitra, M.-A. Miville-Deschênes, A. Moneti, L. Montier, G. Morgante, D. Mortlock, A. Moss, D. Munshi, P. Naselsky, P. Natoli, C. B. Netterfield, H. U. Nørgaard-Nielsen, F. Noviello, D. Novikov, I. Novikov, S. Osborne, C. A. Oxborrow, F. Paci, L. Pagano, F. Pajot, D. Paoletti, F. Pasian, G. Patanchon, H. V. Peiris, O. Perdereau, L. Perotto, F. Perrotta, F. Piacentini, M. Piat, E. Pierpaoli, D. Pietrobon, S. Plaszczynski, E. Pointecouteau, G. Polenta, N. Ponthieu, L. Popa, T. Poutanen, G. W. Pratt, G. Prézeau, S. Prunet, J.-L. Puget, J. P. Rachen, C. Räth, R. Rebolo, M. Remazeilles, C. Renault, S. Ricciardi, T. Riller, C. Ringeval, I. Ristorcelli, G. Rocha, C. Rosset, G. Roudier, M. Rowan-Robinson, B. Rusholme, M. Sandri, D. Santos, G. Savini, D. Scott, M. D. Seiffert, E. P. S. Shellard, L. D. Spencer, J.-L. Starck, V. Stolyarov, R. Stompor, R. Sudiwala, F. Sureau, D. Sutton, A.-S. Suur-Uski, J.-F. Sygnet, J. A. Tauber, D. Tavagnacco, L. Terenzi, L. Toffolatti, M. Tomasi, M. Tristram, M. Tucci, J. Tuovinen, L. Valenziano, J. Valiviita, B. Van Tent, J. Varis, P. Vielva, F. Villa, N. Vittorio, L. A. Wade, B. D. Wandelt, D. Yvon, A. Zacchei, and A. Zonca, "Dependence of the gap parameter on the number of CuO2 layers in a unit cell of optimally doped BSCCO, TBCCO, HBCCO and HSCCO," *Astronomy and Astrophysics*, vol. 571, J. Tauber, Ed., A25, Nov. 2014. arXiv: 0111342 [cond-mat]. [Online]. Available: http://www.aanda.org/10.1051/0004-6361/201321621.

Bibliography

Publications Related to the Thesis

Journal Articles

1. I. Madan, T. Kurosawa, Y. Toda, M. Oda, T. Mertelj, P. Kusar, D. Mihailovic. Separating pairing from quantum phase coherence dynamics above the superconducting transition by femtosecond spectroscopy. Scientific reports, **4**, (2015).

2. Y. Toda, F. Kawanokami, T. Kurosawa, M. Oda, I. Madan, T. Mertelj, V. V. Kabanov, and D. Mihailovic. Rotational symmetry breaking in $Bi_2Sr_2CaCu_2O_{8+\delta}$ probed by polarized femtosecond spectroscopy. Phys. Rev. B, **90**, (2014).

3. I. Madan, T. Kurosawa, Y. Toda, M. Oda, T. Mertelj, and D. Mihailovic. Evidence for carrier localization in the pseudogap state of cuprate superconductors from coherent quench experiments. Nature Communications **6**, (2015)

Conference Paper

1. I. Madan, J. Karpinski, T. Mertelj, D. Mihailovic. Pump-probe reflectivity study of $HgBa_2CuO_{4+\delta}$ cuprate superconductor. 6th Jožef Stefan International Postgraduate School Students' Conference, (2014)

...